PICOSECOND SEMICONDUCTOR SWITCHING DEVICES

Walter Margulis

A Thesis submitted for the Degree of Doctor of Philosophy in the University of London and for the Diploma of Membership of Imperial College

Department of Physics
Imperial College, London

August, 1981

Abstract

Picosecond semiconductor switching devices activated by mode-locked laser pulses have been studied and used in ultrafast voltage pulse generation. The properties of different semiconductors (Si, GaAs, GaP) were investigated under a range of experimental conditions. The risetime and recovery time of the devices were measured using correlation methods and oscilloscopes.

High voltage pulses were obtained from a Si switch and the picosecond synchronization to the activating laser pulse allowed greatly reducing the jitter of streak cameras. Jitter as low as $\pm$ 15ps was consistently obtained at a writing speed of 2×10^{10} cm/s. A gold photocathode streak camera used in UV picosecond pulse studies was also driven with Si switches.

Both semi-insulating GaAs and GaP devices were used to generate trains of picosecond high voltage pulses which activated a Pockel's cell modulating system, mode-locking a flashlamp pumped dye laser. Trains with 100% modulation and pulse durations of $\sim$ 30ps were recorded, at a wavelength region $\sim$ 430-535nm. A similar arrangement was employed to generate subnanosecond trains of pulses with a XeCl discharge laser and the results were analysed with the help of a simple model.

Acknowledgements

My PhD programme has been a happy and enriching experience on the personal level. This was due to a great extent to the friendship of the members of the laser group at Imperial College, and first of all I want to express my gratitude to all those involved.

I would also like to thank in particular Prof. D.J. Bradley for his supervision, useful discussions and constructive pressure;

Wilson Sibbett for the tireless guidance, support, patience and all the invaluable advice provided throughout the work;

my friend Grace Reksten for rendering unforgettable the thousands of shared hours in the lab and office, for the constant positive attitude towards research, and above all for what she taught me in Physics and otherwise;

Alan Cormier for the consistent struggle to beat the (laser) system described in chapter 6;

my colleagues Mark Holbrook, Joe Wilson, Dave Welford, Jorge Tocho and Thomas Varghese with whom experiments were carried out and useful discussion held;

Bill Sleat for the advice with streak-cameras, and

Pete Dobson from the Solid-State Physics group for the support and enthusiasm.

I want to express my gratitude also to the members of the group of Suzanne Laval (S. Laval, Catherine Bru, Alain Koster, Mireille Rousseau and Nicole Paraire) at the Institut D'Electronique Fondamentale at Orsay, France, for the important suggestions given, the use of facilities, and also for the warmth with which I was recieved during the long writing up period.

I am also indebted to Janie Coghill for having skillfully typed the thesis and done its layout, and to the Brazilian people, who finantially supported me through the CNPq (Conselho Nacional de Desenvolvimento Cientifico e Tecnologico, Brasil).

Finally I want to thank Iona for the infinte companionship and love, and dedicate this thesis to her, with a very big and happy smile.

Firing! Three, Two, One ....

CONTENTS

CHAPTER 1

GENERAL INTRODUCTION

Twenty years after its invention, the laser has been extensively developed and exploited in many different applications in science, engineering, medicine and others. One of the most interesting areas of research which evolved during these two decades consists of the use of high intensity laser pulses of picosecond durations obtained with the technique of mode-locking. Very important physical processes are known to happen in this ultrashort time scale, such as the initial stages of photosynthesis and energy transfer mechanisms in biological systems. Furthermore, several important phenomena, including excitation and relaxation processes, the evolution of chemical reactions, and others can be examined in detail with ultrashort light pulses and the techniques which were developed simultaneously.

Another field of science which has expanded significantly in recent years is electronics. In particular, with the invention and development of integrated circuits and their use in large and small computers, the need arose for faster solid-state elements capable of performing electronic operations in a faction of a nanosecond. Because of the commercial interest and immediate applications envisaged, a great effort is at present being made towards the development of faster devices. At the same time, due to the enormous potential capabilities of telecommunications by lasers, techniques and materials are being extensively studied in order to allow the manipulation, transmission and detection of light signals. In such systems ultrafast modulation techniques of the laser light are clearly of great importance. Typical modulation systems rely on conventional high frequency oscillators, where

voltage pulse durations of a few nanoseconds (and at best $\sim$ 100ps) are obtained. For the detection of ultrashort light pulses the fastest photodiodes available have typical response times of $\sim$ 50ps, and therefore such detectors must be improved to allow the measurement of light signals with picosecond resolution.

The advances in non-linear optics which followed the generation of high intensity ultrashort duration laser pulses include the use of electro-optical components such as Pockel's cells and Kerr cells, where the presence of an intense electric field induces a change in the refractive index of the non-linear medium. Since these effects happen very rapidly, they have been used in ultrafast light gates, and to fully exploit the capability of such devices, very short risetime electrical signals are needed. Ultrafast risetime voltages are also necessary for the opto-electronic instruments which are employed to characterize picosecond light pulses, such as sampling oscilloscopes and streak cameras. Low voltage signals of short duration are used in sampling heads, which at present have a time resolution of $\sim$ 25ps, and it would be clearly advantageous to reduce this limit to $\lesssim$ 1ps. High voltage pulses of ultrafast risetime are required for the deflection system of streak cameras. Although such instruments have at present a time resolution $\lesssim$ 1ps, new streak tubes are being developed to allow studies in the subpicosecond range. Besides the margin for improvement in terms of synchronization between the deflection and the light event under observation in the commercially available streak cameras, faster sweep speeds will soon be required.

It is therefore apparent that much can be gained if the picosecond techniques developed with mode-locked lasers can be used in the generation of ultrafast electrical signals.

This thesis describes work done on semiconductor devices that, when illuminated by ultrashort laser pulses, switch electrical signals with picosecond risetimes. The solid-state switches were used to activate Pockel's cells and to synchronize streak cameras, and properties of different semiconductors were investigated under a range of experimenttal conditions. It is shown that they embody a simple and useful tool in the study of fundamental properties of the crystals employed, such as photoconductivity and electronic transport processes. Furthermore, a comparison between their performance to that of conventional elements in terms of speed, high voltage capability, and synchronization of the switching action to the laser pulse is carried out wherever possible, and the advantages and difficulties of using the semiconductor devices is underlined.

Picosecond techniques are now a well established field of research but it is nevertheless convenient to introduce the terminology employed throughout the thesis with a brief review of the methods of generation and measurement of ultrashort laser pulses. In this context, emphasis is only given to the aspects which are directly related to the work that is described in greater detail later in the thesis, and is far from being a comprehensive review of the subject.

Although the work carried out was not restricted to high voltage devices, the major applications demonstrated exploit the use of high amplitude fast risetime signals. Therefore the review on semiconductor switching devices describing the other relevant results published in the literature which was also included, serves not only to introduce the specific subject matter of this thesis, but mainly to exemplify the variety of materials employed, studies which are carried out and the techniques already developed.

The characterization and the construction of the devices used in the experiments is described in some length, and several examples of measurements that can be performed to greater detail are also included. The major applications demonstrated include the synchronization of streak cameras with picosecond precision, and the active mode-locking of a dye laser and of an excimer laser using ultrashort duration voltage pulses from semiconductor switching devices.

CHAPTER 2

INTRODUCTION TO PICOSECOND LASER TECHNIQUES

2.1 Lasers

Laser oscillators consist of an amplifying medium inside an optical cavity. The amplification of light occurs as the photons returning to the gain medium stimulate further emission of photons. The optical flux builds up, and the fraction of the radiation leaving the system (usually through one of the mirrors) consists the laser output.

To emit and amplify light, the gain medium has to be pumped by an independent source of energy, which can be optical, electrical, chemical, or of other nature. The characteristics of the laser are to a great extent determined by the pumping means and the material providing optical gain, which can be a solid, liquid or a gas. In some cases it is possible to supply energy continuously to the amplifier, and sometimes it is desirable or necessary to store a relatively large amount of energy and then quickly discharge it on the gain medium. As a consequence, some laser systems can be operated continuously (CW lasers), and others generate short duration pulses of light (single-shot lasers), of durations ranging from nanoseconds to miliseconds. Some single shot lasers can be operated at high repetition rates (up to $\sim 10^5$ KHz), and there are systems that can only be fired once every several minutes, or even hours.

It is usual to place additional elements inside the cavity formed by the mirrors, introducing losses of a particular kind. These elements are for instance modulators, apertures and filters and they help in defining the spatial, spectral and temporal properties of the laser

beam, i.e., in determining the shape, range of frequencies and time evolution of the light output. Some of these elements are described in detail later in this chapter.

Laser emission occurs between two energy states, and optical gain can only exist when the excitation source is able to create a situation where the number of atoms or molecules in the excited state is larger than that of the state of lower energy (population inversion). This is accomplished by different mechanisms, depending on the properties of the active medium.

Of particular importance to this work are flashlamp pumped dye lasers and Nd:glass lasers, which are briefly described in the following sub-sections.

2.1.1 Dye Lasers

The complex energy level configuration of organic dye molecules can be approximately described by a four level system [1]. The molecule is excited to a higher electronic state, quickly looses the excess vibrational energy by collisions with the solvent ($\tau \sim$ ps), and remains on the upper laser level for a few nanoseconds. With the emission of a photon, the molecule is taken to one of the several vibrational - rotational states which constitute the lower laser level, and collisions with the solvent finally return it to the ground state. Because of the great number of closely spaced rotational lines associated with the electronic S_0, S_1 laser levels, the energy of the laser photons released with the radiative decay can take a wide range of values, and the laser can be tuned within a large bandwidth [2]. Due to the relatively short lifetime of the excited state, dye lasers reach threshold easily but do not sustain population inversion for long periods, and so the laser

pulse profile closely follows that of the pump light.

Dye lasers are optically excited, either by a flashlamp or by another laser system, which is often a Ruby, Nitrogen, excimer, argon ion, krypton ion or a frequency doubled neodymium laser. Except for the important case of continuous wave excitation, picosecond pulses are usually generated with flashlamp pumped lasers, where a large amount ($\sim$ KJ) of electrical energy is quickly deposited on one or a few linear flashlamps (risetime $\sim$ 1μs), and the optical gain exceeds the losses for $\sim$ 1-2μs [3].

Because of its large stimulated emission cross section, tunability, stability and relative low price, the Rhodamine 6G dye is frequently employed, being disolved in either water or alcohol. It can be tuned from $\sim$ 570nm (yellow) to $\sim$ 630nm (red), and typical optical energies obtained with a flashlamp system are $\sim 10^{S}$mJ. However, other dyes are also available, covering the whole visible light region of the spectrum, as well as some of the near ultra-violet and near infra-red [1].

2.1.2 Neodymium lasers

The other class of laser systems which is very often employed to produce picosecond pulses in the mode-locked neodymium laser [4]. Neodymium atoms dope a solid host which is usually a glass or Yitrium Aluminium Garnate (YAG), and Nd^{3+} ions are formed, exhibiting an energy level structure which allows fluorescent emission at 1.06μm. Nd lasers also operate as 4 level systems, but the long lifetime of the upper laser level ($\tau \sim$ ms) means that the population inversion can be maintained for longer periods. As a consequence, the laser can store large amounts of optical energy, and is capable of producing high power light pulses.

Nd:glass lasers have a relatively large spectral width (compared with atomic gas or Nd:YAG lasers), and when mode-locked, are capable of generating pulses of few picoseconds duration [5]. Typically, energies of ∿ 1mJ can be obtained in a single ∿ 5ps pulse with conventional flash-lamp pumped Nd:glass systems, and the mode-locked train can consist of ∿ 10-100 pulses.

The Nd rod is usually pumped with a helical flashlamp, since the requirement of fast risetime is not stringent. In order to accelerate the dissipation of heat, and particularly due to the poor thermal conductivity of the glass, a cooling jacket with flowing water is provided [6]. However, heating of the rod imposes a serious limitation on the repetition rate of the laser, which can be ∿ 1 shot per minute, or less. Also, non-linear effects on the refractive index of the laser rod are very important because of the high powers available. Besides the spatial, spectral and temporal deterioration of the pulses due to phenomena such as self-phase modulation and self-focussing, there is a considerable risk of permanently damaging the solid host with self-focussing of the light beam [4].

The capability of efficient amplification of short duration laser pulses by a series of light amplifiers consitutues a very important asset of such systems, and for this reason Nd lasers are a major candidate in laser fusion studies.

2.2 Mode-locking

A laser with a cavity length L defines a set of longitudinal modes of oscillation (as in any standing wave system). If losses and diffraction effects at the mirrors can be neglected, the number of modes

n present is given by

$$n\lambda/2 = L.$$

Since $\lambda = c/\nu$, the separation between these modes in frequency is

$$\Delta\nu_m = c/2L,$$

corresponding to a wavelength separation of $\Delta\lambda_m \simeq \lambda^2/2L$. The laser spectral width is usually much larger than $\Delta\nu_m$, and therefore thousands of longitudinal modes are permitted to oscillate. In a Rhodamine 6G dye laser (where $\Delta\lambda_L \sim 5$nm at $\sim 0.6\mu$m) with a 1m cavity length, approximately 5×10^3 modes are supported, while for a Nd:glass laser (with $\Delta\lambda_L \sim 10$nm at $\sim 1.06\mu$m), $\sim 3 \times 10^3$ modes can exist [7].

It is possible to have a single longitudinal mode oscillator, either by using very short cavity lengths, or alternatively by introducing filters in the cavity to reduce the bandwidth of the laser. This can be accomplished in practice by using a few Fabry-Perot interferometers or other dispersive elements, and single mode gas, semiconductor and dye lasers are currently used, in for instance, high resolution spectroscopy[8].

It is also possible to lock the otherwise unrelated phase of all the axial modes of the laser, which in this case is said to be mode-locked [9]. The output of a mode-locked laser consists of a succession of short duration light pulses, exactly separated by the cavity roundtrip time. The individual pulse durations depend on the number of modes existent, and on how close to the ideal mode-locked situation the laser is operated. In general, flashlamp pumped dye lasers and Nd:glass lasers reliably produce pulses as short as a few picoseconds. When all the modes are perfectly phase-locked, the duration of the pulses and the bandwidth of the radiation are related through the uncertainty principle ($\Delta\nu\Delta t \sim \hbar$), and the pulses are said to be bandwidth (or Fourier transform) limited.

To understand the mechanisms leading to the generation of such ultrashort pulses, it is possible to examine the system either in the frequency domain or in its Fourier transform, the time domain. It is much easier to visualize the physical aspects of the later. The additional element introduced in the laser cavity allowing the locking of the axial modes is an active or a passive loss modulator. Active modulators require an external signal (either optical or more often electrical) to alter its transmission function at a frequency equal to the inverse of the roundtrip time of the cavity. Passive modulators usually consist of a non-linear filter (dye) which absorbs light at the laser wavelength and saturates at high intensities, so that its transmission approaches 100% for very intense pulses. Passive mode-locking usually produces shorter pulsewidths, although adequate saturable absorbers are often not available to mode-lock the laser, because of the wavelength, recovery time and absorption cross-section requirements. In these cases, active modulators can be employed.

Different mechanisms are responsible for the generation of ultrashort pulses, depending on the characteristics of the gain medium and on the modulator. A comprehensive description of passively mode-locked flashlamp pumped ruby and neodymium lasers can be found in [10] and on references therein. It suffices here to relate the different stages of the process: the laser reaches threshold following a long build-up of the flashlamp ($\sim 100^{s}\mu s$), and a period follows when the radiation in the cavity suffers linear amplification at the gain medium and linear losses at the saturable absorber. The output is relatively weak, and consists of a nearly periodic noise structure, with spikes of a fraction of a picosecond duration (at laser threshold) to a few picoseconds (at the end of the process). When the most intense spikes are able to saturate the absorber, the combined action of the mode-locking

dye and the depletion of the gain medium can lead, in a large percentage of cases, to the preferential amplification of a single spike, at expense of the others. The photon flux is then concentrated into a single pulse which travels in space between the mirrors, and measures $\sim$ 1-3mm. A fraction of the energy leaves the cavity every time the pulse reaches the output coupler, and the laser output then consists of a succession (or the so-called train) of pulses, separated by the cavity double transit time of the single pulse which is generated.

Passively mode-locked flashlamp pumped dye lasers have also been extensively reviewed [11, 12, 13]. In this case threshold is reached much more quickly than in Nd lasers. Because the recovery time of the saturable absorber is relatively long ($\sim 100^{s}$ ps), after a few passes the laser output consists of a burst of noise of duration $\sim 100^{s}$ ps. With further amplification, the combination of the two shortening mechanisms of saturation of the gain in the laser medium (when the population inversion is severely depleted by the front part of the pulse, so that the trailing edge does not experience as much gain), and saturation of the absorber (when the front part of the pulse is absorbed and saturates the mode-locking dye and is therefore attenuated) leads to the formation of a picosecond pulse $\sim$ 30 roundtrips after threshold.

Both R6G dye and Nd:glass mode-locked lasers have been employed in the activation of semiconductor switching devices, as described later in the thesis, and further details about pulse evolution and the mode-locking dyes are postponed until then.

2.3 Non-Linear Optics Components

Mode-locked lasers allowed a fast development of non-linear optics, because the high intensity light pulses available greatly enhanced effects that were too weak to be detected otherwise. The non-linear phenomena exploited allowed the manipulation of the laser output and at the same time the investigation of fundamental processes in the interaction of radiation with matter. Non-linear optics is a complex subject, which has a relatively extensive specialized literature (see for instance [14] and [15]). Out of the several techniques which are currently used in laser technology, two are of particular importance for the work carried out, namely the second harmonic generation in crystals, and the rotation of light polarization with the Pockel's effect.

The second harmonic generation was the first of the non-linear effects that were reported following the invention of the laser [16]. The output beam of a ruby laser was directed to a quartz crystal and a very weak signal at the double of the frequency of the input radiation was detected with a photomultiplier. After this pioneer experiment, the conversion efficiency of the two-photon process was increased by several orders of magnitude with the phase matching technique.

The second harmonic is produced when two photons of the fundamental radiation combine in the non-linear crystal, and therefore the generation efficiency depends on the square of the light intensity. If the second harmonic (2ω) and fundamental (ω) waves experience a different refractive index as they travel in the medium, they become out of step and the interference that results transfers the energy from the 2ω wave back to the ω wave after an even number of "coherence lengths". Consequently, the conversion process is in general very inefficient. However, it is possible to cut the birefringent crystal at an angle such that the

ordinary refractive index for the fundamental is equal to the extraordinary refractive index for the second harmonic component, and the 2ω light adds constructively throughout the thickness of the specimen. In this case, the "phase-matching" condition is said to be satisfied, and the conversion efficiency is appreciably enhanced.

Since the refractive indices are frequency angle and temperature dependent, for a given laser wavelength it is possible to tune the crystal into phase matching either by adjusting the directions at which it is cut, or by varying its temperature. For the same reasons, lasers with a broad bandwidth and with a large beam divergence produce the second harmonic frequency with lower efficiency. In practice, commercially available crystals (ADP, KDP, $LiNbO_3$) can show conversion efficiencies of up to $\sim$ 50%, although this value is usually somewhat lower ($\sim$10-20% for flashlamp pumped dye and Nd laser systems, respectively).

The other non-linear phenomenum which is widely used in conjunction with mode-locked lasers was discovered in the nineteenth century, and is called the Pockel's effect [17]. It consists of a change in the refractive index of the non-linear medium due to the application of an electric field. A linearly polarized light beam entering a crystal which exhibits the Pockel's effect can be described in terms of two orthogonal components which experience different refractive indices, depending on E. The phase difference between the two components after having travelled through the "Pockel's cell" of length L is proportional to the voltage applied (V = EL). It is therefore possible to rotate the polarization of the light beam by adjusting the amplitude of the voltage across the crystal, and the voltages necessary for 45° and 90° rotation are denoted by $V_{\lambda/4}$ and $V_{\lambda/2}$, respectively. The half-wave voltage $V_{\lambda/2}$ is proportional to the laser wavelength.

The Pockel's effect takes place very quickly, i.e., the response of the medium to the electric field happens in $\sim$ ps. Therefore, an ultrafast light gate can be materialized when such element is placed between crossed polarizers. Initially no voltage is applied to the cell and the second polarizer rejects all the incoming light. As the Pockel's cell is activated by a voltage pulse of amplitude $V_{\lambda/2}$, the polarization of the light beam is rotated and becomes parallel to the preferential direction of the second polarizer, being transmitted. As the voltage applied drops to zero, the transmission of the light gate is also reduced to zero. Such a set-up is widely employed in selecting one or a few light pulses from a mode-locked train, and the duration of the voltage pulse applied across the Pockel's cell is often a few nanoseconds. Unfortunately, commercially available elements have typical risetimes of $\sim 100^{s}$ ps, and half-wave voltages of several kilovolts (for visible radiation), due to the relatively large crystal thicknesses necessary to produce an appreciable Pockel's effect.

2.4 Methods of Measurement

The development of mode-locked lasers required an extension of the techniques available for measuring optical phenomena in the picosecond time scale. Several methods of measurement were demonstrated, and in this section some of these techniques are outlined. Particular emphasis is given to streak camera systems, which have been used in the applications described in chapters 5, 6 and 7.

2.4.1 Indirect Methods

There are several indirect methods of measurement of ultrashort pulses, and time resolutions as good as < 0.1ps have been achieved [18].

In most cases (e.g., SHG and TPF) they rely on a multiphoton process which takes place when two or more light pulse components overlap on a non-linear medium. The records obtained provide information about the length of the pulse (and consequently about its time duration), but its intensity profile is not displayed directly. From the measurement, one obtains a correlation function of the electric field associated with the light pulse, the order of the correlation function depending on the particular technique employed.

The first of the non-linear methods of measurement proposed and demonstrated was the second harmonic generation (SHG) technique [19, 20, 21, 22]. The laser pulse is divided into two components at an interferometer, one arm of which has an adjustable position. The two beams are then directed to a SHG crystal where they may or may not temporally overlap, depending on the light paths. The second harmonic signal detected is maximum when the two components arrive simultaneously at the crystal and decreases as one is delayed in relation to the other. In order to obtain the complete auto-correlation curve, the delay has to be adjusted to several different values, and this is a severe drawback in the case of single-shot lasers, because of the pulse fluctuations from shot-to-shot and the amount of time required. On the other hand, due to its relative simplicity, low cost and good time resolution, the SHG technique is widely used for the diagnostic of pulses from CW mode-locked laser systems.

The complete intensity correlation function can be obtained on a single shot from the two-photon fluorescence (TPF) method of measurement [23, 24, 25]. In the most common experimental arrangement, the laser pulses are split into two identical components which overlap at the centre of a cell containing a substance that only fluoresces

when two or more photons are absorbed. The record obtained from the side of the cell (e.g. by photography [26] or by using photoelectric detection [27])yields information about the pulse duration, but great care has to be taken about the signal to background ratio. It has been shown that a free running laser yields a contrast ratio of 3:2, compared to 3:1 for a perfectly mode-locked laser [28]. Besides being fairly insensitive to the amount of energy in the pulses as compared to the background energy [24, 25], TPF measurements depend critically on the alignment of the two light components overlapping at the cell [24]. However, because of its simplicity, this technique has been extensively used in characterizing picosecond pulses from single-shot lasers.

Both the SHG and the TPF measurements provide the intensity auto-correlation function [9, 29] defined as

$$G^2(\tau) = \frac{\int_{-\infty}^{\infty} I(t)\ I\ (t-\tau)dt}{\int_{-\infty}^{\infty} I^2(t)dt}$$

which is always symetrical, regardless of the pulse shape. As a consequence, the intensity profile of the pulse can not be determined unambiguously nor its precise duration. Also, due to the relatively high intensities necessary to induce two-photon processes, TPF and SHG techniques are not suitable for studying non-laser events.

Another indirect method for ultrashort pulse measurement is the ultrafast gate using the optical Kerr effect. An intense polarized light pulse induces birefringence in a Kerr medium [30], which is placed between crossed polarizers. A weaker pulse arrives at different delays in relation to the pump (gating) pulse, and probes the transmission of the medium [31]. When CS_2 is used, such system can have a time resolution of $\sim$ 2ps, and it has been employed in several measurements [29]. It can be shown [32] that such technique yields the third order correlation

function if the gating and probing pulses have the same wavelength, or fourth order if the second harmonic of one of the components is used. By pumping the Kerr medium from the side so that the gating and probe beams are perpendicular, it is possible to improve the signal-to-noise ratio of the measurement, and this technique has been used in several experiments [33].

Other indirect methods of measurement of ultrashort pulses have been demonstrated, and correlation functions of up to the fifth order have been obtained [34]. From all these, it is worth mentioning the TPC method suggested by Lee and Jayaraman [35], which consisted of the photoconductive counterpart of the TPF. The fluorescing dye cell is replaced by a semiconductor which has its conductivity altered when the two light components temporally overlap. The pulse durations can be inferred from the photoconductivity measurements, and the time resolution of the system used was $\sim$ 2ps. More details of this arrangement are given later (section 3.3.4), because of its relation with the work described in this thesis.

2.4.2 Direct techniques

Direct measurements of ultrashort pulse durations and their shape consist of obtaining a plot of the evolution of the pulse as a function of time. There are at least two systems which provide such measurements, namely the photodiode - oscilloscope and the streak camera.

2.4.2.1 Oscilloscope Measurements

The simplest way to investigate light pulses from a mode-locked laser is by converting the optical information into an electrical signal, and displaying it on a fast oscilloscope. Such instruments can have a

bandwidth of a few GHz, corresponding to risetimes of $\sim$ 100ps [36]. The conversion of the light signal to an electrical signal is done at a photodiode, making use of photoelectric or photoconductive processes. Photodiodes are capable of delivering voltage which are proportional to the intensity of the light, and are extremely valuable for examining slowly varying events, such as unmode-locked laser pulses. For ultrashort pulse measurements, the bandwidth of commercially available photodiodes has considerably improved recently, and risetimes of $\sim$ 30ps (50ps FWHM) have been demonstrated [37].

For CW mode-locked laser applications, since the light events are repetitive, sampling systems can be used where the time evolving pulse is sampled at different points at a high rate ($\sim 10^5$Hz). Conventional sampling heads can have a time resolution of 25ps [38].

From the above figures it is clear that at present, oscilloscope-photodiode systems are not capable of yielding direct measurements of light pulses on a picosecond or subpicosecond time scale. The direct diagnostic of mode-locked laser pulses and the study of ultrafast non-laser events requires another measurement technique, such as the electron-optical chronoscopy. However, non-conventional sampling systems with an overall time resolution of $\sim$ 10 ps have been developed with the use of ultrafast semiconductor switches [39, 40]. Because such devices are closely related to the work described in later chapters, this application is discussed in more detail in chapter 3. It suffices to point out here that it is likely that ultrafast amorphous semiconductor devices will replace both photodiodes and the conventional fast electrical sampling circuitry, allowing the direct study of recurrent light pulses with time resolutions approaching $\sim$ 1 ps.

2.4.2.2 Electron-Optical Chronoscopy

2.4.2.2.1 Streak Cameras

The idea of using electron-optical chronoscopy to study ultra-fast light events was proposed by Zavoisky and Fanchenko [41] even before the invention of lasers. The basic elements of a conventional streak tube [42, 43, 44] are a photocathode, a mesh, accelerating and focussing electrodes, deflection plates and a phosphor screen. The operation of the streak camera can be described as follows: the light pulse to be studied is directed to an input slit, which is imaged on the photocathode by focussing lens. The number of photoelectrons produced at each instant is proportional to the intensity of the light falling on the photocathode, so that the information about the evolution in time of the optical event is carried by the photocurrent. The photoelectrons are accelerated and focussed on to the output screen, and the streaking occurs by applying a fast voltage ramp to the deflection plates. The passage of the electrons between the plates is synchronized with the sweep ramp, so that photoelectrons arriving at different instants experience different deflecting fields, and the time information is presented as a spatial image of the phosphor screen. Streak records consist of transversely swept images of the slit, so that the intensity of the light falling on the cathode at each instant is reproduced at a different position on the output phosphor, and the time evolution of the event can be examined directly. A d.c. bias applied to the deflection plates throughout the operation of the camera ensures that the sweep

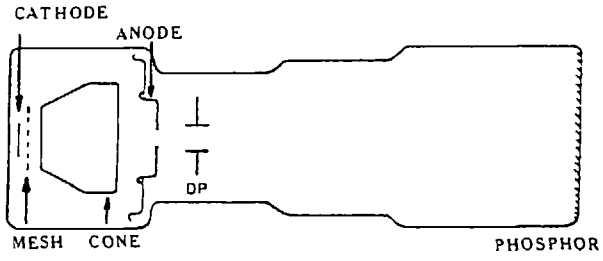

streak camera

covers the full screen size, and deflects photoelectrons emited before the start of the voltage ramp away from the output phosphor. Typically a 2.5KV bias is used, and the amplitude of the ramp is 5KV, applied so that the difference of potential between the deflection plates changes from +2.5KV to -2.5KV. In the work described later (chapters 5 and 6) the voltage pulses were supplied to one of the plates, so that only asymetric deflection was investigated. The duration of the sweep is $\sim 10^{-9}$s for picosecond time resolution, and ultrafast switching components are necessary for such high writing speeds. In practice the voltage switched often has slow start and end, and is only linear on the central (and faster portion). Therefore, in order to ensure that the time evolution is represented linearly on the output screen, only the central part of the ramp (typically from + 750V to -750V) is actually used, being sufficient for a full screen size sweep.

The large photocurrents associated with ultrashort light pulses give rise to space-charge effects, causing loss of spatial and temporal information. In order to minimize these effects, it is necessary to couple an image intensifier to single-shot streak cameras. In this case, the sensitivity of the instrument is greatly increased and weaker light events can be examined, so that the photocurrents in the tube are reduced. Modern intensifiers are fiber-optics coupled to the streak tube and the output records are often displayed directly on an optical multichannel analiser, simplifying the interpretation of the results, otherwise obtained by photography, which require densitometry.

The theoretical limit for the time resolution of electron-optical streak cameras is $\sim 10^{-14}$s[41], but at present the experimental systems have a resolution of $\sim$ 1ps [45]. Because it is often necessary to operate the streak camera near this limit, it is important to consider the minimum pulsewidth that can be recorded on the phosphor screen,

which depends on three factors : (1) the actual light pulse duration, t_p. (2) The time necessary to sweep through a resolution element on the phosphor screen, t_s. (3) The transit time spread of the photoelectrons, t_d. The combination of the three factors is a good approximation given by

$$t_r = \sqrt{t_d^2 + t_p^2 + t_s^2}, \qquad (2.1)$$

for assumed Gaussian pulse shapes.

The minimum time required to scan a line pair on the screen (also called technical or streak-limited resolution) depends on the sweep (or writing) speed v, and on the spatial resolution under dynamic conditions, and is given by

$$t_s = 1/v.n \qquad (2.2)$$

where n is measured in number of line pairs per centimetre. Typical values for Photochron II systems are $v = 10^{10}$ cm s^{-1} and n = 10 lp mm^{-1}, yielding t_s = 1ps.

The resolution of streak cameras is also limited by the difference of transit time that photoelectrons exhibit for travelling from the photocathode to the deflection plates. This time dispersion depends on the energy distribution near the photocathode, and the transit time spread is greatly reduced by quickly accelerating the photoelectrons with an intense electric field [41]. The introduction of a fine mesh near the photocathode provides the necessary field strengths [46], and this is adopted in most streak tubes (although a proximity focussed image converter was also developed, where the mesh is replaced by a microchannel plate [47, 48]). The expression that relates the time dispersion to the initial energy distribution and the electric field is [49]

$$t_d = \frac{2.34 \times 10^{-8} \sqrt{\Delta\varepsilon}}{E} \qquad (2.3)$$

where $\Delta\varepsilon$ is expressed in electron-volts, E in volts per centimetre and t_d in seconds. Typical values are, $\Delta\varepsilon \sim 1eV$, $E \sim 20KVcm^{-1}$, and in this case $t_d = 1.2ps$.

From expressions (2.1), (2.2) and (2.3) it is seen that the resolution of the streak camera depends not only on the operating conditions of the instrument (such as writing speed and electric field at the photocathode), but also on the particular wavelength of the radiation studied. Nevertheless, the camera instrumental resolution t_c is usually defined as

$$t_c = \sqrt{t_s^2 + t_d^2} \qquad (2.4)$$

Since the shortest laser pulses obtained are < 100fs [50], efforts are being made to improve the resolution of streak cameras, so that t_c becomes smaller than the pulse durations and the streak records accurately represent the pulse evolution. At present, the best time resolution reported for a streak-camera system was $t_c = 700fs$ [45], and new streak tubes of resolution $\sim$ 200-300fs are being developed [51].

2.4.2.2.2 Framing Cameras

Streak cameras are potentially capable of recording the temporal evolution of light events, maintaining the spatial information in one dimension (which is displayed along the slit). This feature can be used, for instance, in time resolved spectroscopic studies, where the spectral information is spread along the slit by a dispersive element, such as a grating. However, two dimensional pictures can also be obtained if the streak tube is operated in the framing mode.

A typical framing tube [52] is very similar to the streak tube, except that it is provided with two additional pairs of deflection plates and an aperture. The input slit is not used and the light event

is focussed directly on the photocathode. The photoelectrons are accelerated, swept by the deflection plates DF, and an aperture defines the time window of the seep. An identical voltage ramp is applied to the compensating plates in the opposite direction, so that the sweeping action is cancelled, and the two dimensional image appearing on the screen is not blurred. The record obtained in this way is a two dimensional photograph and the exposure time is defined by the writing speed of the ramp applied to the deflection plates. More than one frame can be obtained by applying a staircase-like voltage to the third pair of plates, which is perpendicular to the other two. They deflect the frames sideways, and provided the steps of voltage have sufficient amplitude, consecutive frames do not overlap on the screen. Because of synchronization difficulties framing cameras are usually operated at slow writing speeds (driven by recurrent sinosoidal voltages) and therefore the exposure of each frame is $\gtrsim$ 100ps-1ns.

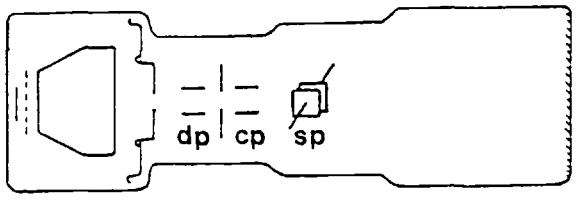

framing camera

Other framing cameras have also been demonstrated, some very simple [53] as for instance the proximity focussed tube (consisting of a photocathode and a phosphor screen), others quite complex with several deflection plates and compensating systems [54].

2.4.2.2.3 Synchroscan

One of the most successful applications of streak cameras in their use in conjunction with CW mode-locked lasers in a recurrent mode of operation [7]. The voltage ramp is applied to the deflection plates in synchronism with the roundtrip of the laser, so that consecutive

streak records superpose on the phosphor screen for a large number of pulses. The traces obtained in this manner have a very high signal-to-noise ratio, and accurate measurements can be carried out for low intensity light levels. Synchroscan is therefore very convenient to measure light phenomena in a picosecond time scale when the sample must not be illuminated by intense beams. Although it was first demonstrated in conjunction with a single-shot laser [55], it is with CW systems that most experiments have been performed, because it is relatively easy to synchronize the light pulses with the sweep ramp [56, 57, 58]. A high voltage sine wave is generated at exactly the frequency of the laser (or its multiple), and the most linear part is used for the deflection. The linearity of the sweep obtained is typically $\sim$ 4%, but writing speeds are limited to $\sim 5 \times 10^{9} cms^{-1}$. The best time resolution reported was $\sim$2.5ps [59].

References - Chapter 2

[1] Dye Lasers; ed. F.P. Schäfer, Springer-Verlag, Berlin (1973)

[2] F.P. Schäfer, W. Schmidt, J. Volze; Appl. Phys. Lett. 9, 306 (1966)

[3] E.G. Arthurs, D.J. Bradley, A.G. Roddie; Appl. Phys. Lett., 20 125 (1972)

[4] W. Koechner; Solid-State Laser Engineering, Springer-Verlag, NY (1976)

[5] A.J. DeMaria, D.A. Sletser, H. Heynan; Appl. Phys. Lett., 8, 174 (1966)

[6] R.B. Chesler, J.E. Geusic; Section B2 in Laser Handbook 1, ed. by F.T. Arecchi and E.D. Shultz-Dubois, North-Holland, Amsterdam (1972) p. 325.

[7] W. Sibbett; PhD Thesis, The Queen's Univ. of Belfast (1973)

[8] G.M. Gale; Opt. Commun., 7, 86 (1973)

[9] See for instance D.J. Bradley, G.H.C. New; Proc. of the IEEE, p. 313 (1974)

[10] G.H.C. New; Proc. IEEE 67, 380 (1979)

[11] J.R. Taylor; I .D Thesis, The Queen's Univ. of Belfast (1974)

[12] W.H. Lowdermile; Section B1 in Laser Handbook 3, ed. by M.L. Stitch, North-Holland, Amsterdam (1979) p. 361

[13] D.J. Bradley; Chapter 2 in Ultrashort Light Pulses, ed. by S.L. Shapiro, Topics in Appl. Phys. vol 18, Springer-Verlag, Berlin, (1977).

[14] D. Hon; Section B2 in Laser Handbook 3, ed. by M.L. Stitch, North-Holland, Amsterdam (1979)p. 423.

[15] D.H. Auston; Chapter 4 in Ultrashort Light Pulses, ed. by S.L.Shapiro Topics in Appl. Phys. Vol 18, Springer-Verlag, Berlin, (1977)

[16] P.A. Franken, A.E. Hill, C.W. Peters, G. Weinreich; Phys. Rev. Lett 7, 118 (1961).

[17] M. Born, E. Wolf;Principles of Optics, Pergamon Press, Oxford (1975)

[18] J.C. Diels, J. Menders, H. Sallaba; in Picosecond Phenomena II, ed. by R.M. Hochstrasser, W. Kaiser, C.V. Shank, Springer-Verlag, Berlin, p.41 (1980).

[19] J.A. Armstrong; Appl. Phys. Lett., 10, 16 (1967)

[20] H.P. Weber; J. Appl. Phys., 38, 2231 (1967)

[21] M. Maier, W. Kaiser, J.A. Giordamaine; Phys. Rev. Lett., 17, 1275 (1966)

[22] Spectra-Physics 409 Rapid Scanning Autocorrelator Technical Specification.

[23] J.A. Giordmaine, P.M. Rentzepis, S.L. Shapiro, K.W. Wecht; Appl. Phys. Lett., 11, 216 (1967)

[24] A.J. DeMaria, W.H. Glenn, M.J. Brienza, M.E. Mack; Proc. IEEE 57, 2 (1969)

[25] D. Von der Linde; IEEE J. Quantum. Elect.;, QE8, 328 (1972)

[26] D.J. Bradley, G.H.C. New, S.J. Caughey; Phys. Lett 30A, 78 (1969)

[27] S.L. Shapiro, M.A. Duguay; Phys. Lett., 28A, 698 (1968)

[28] H.P. Weber; Phys. Lett., 27A. 321 (1968)

[29] E.P. Ippen, C.V. Shank; Chapter 3 in Ultrashort Light Pulses, ed by S.L. Shapiro, Topics in Appl. Phys. vol 18, Springer-Verlag, Berlin (1977).

[30] G. Mayer, F. Gires; Compt. Rend de l'Academie des Sciences 258, 2039 (1964)

[31] M. Duguay, J.W Hansen; Appl. Phys. Lett., 15, 192 (1969)

[32] M.A. Duguay, A.T. Mattick; Appl. Opt. 10, 2162 (1971)

[33] See for instance M.M. Malley, P.M. Rentzepis; Chem.Phys. Lett., 3, 534 (1969)

[34] D.H. Auston; Appl. Phys. Lett., 18, 249 (1971)

[35] Chi H. Lee, S. Jayaraman; Opto-Electronics 6, 115 (1974)

[36] See for instance A. Antonetti, M.M. Malley, G. Mourou, A. Orzag; Opt. Commun., 23, 435 (1977)

[37] Spectra-Physics 403B Photodiode Technical Specification

[38] Tektronics S4 sampling-head Technical specification

[39] A.J. Low; PhD Thesis, Univ. of Cambridge (1978)

[40] D.H. Auston, A.M. Johnson, P.R. Smith, J.C. Bean; Appl. Phys. Lett., 37, 371 (1980)

[41] E.K. Zavoisky, S.D. Fanchenko; Appl. Optics 4, 1155 (1965), and refs. therein.

[42] Hadland Photonics Ltd., 775-799 Streak Camera Technical Brochure

[43] See for instance M. Ya. Schelev, M.C. Richardson, A.J. Alcock; Appl. Phys. Lett 18, 354 (1971)

[44] Hamamatzu Temporaldisperser C979 Technical Brochure

[45] D.J. Bradley, W. Sibbett; Appl. Phys. Lett., 27, 382 (1975)

[46] D.J. Bradley, B. Liddy, W.E. Sleat; Opt. Commun., 2, 391 (1971)

[47] A.Lieber; in Picosecond Phenomena, ed. by C.V. Shank, E.P. Ippen, S.L. Shapiro-Springer-Verlag, Berlin, p. 178 (1978)

[48] A.J. Lieber, R.F. Benjamin, H.D. Sutphin, C.B. Webb; Nucl. Inst. Meth 27, 87 (1975)

[49] V.V. Korobkin, A.A. Malyutin, M.Ya. Schelev; J. Photog. Sci. 17, 179 (1969)

[50] R.L. Fork, B.I. Greene, C.V. Shank; Appl. Phys. Lett., 38, 671 (1981)

[51] D.J. Bradley, K.W. Jones, W. Sibbett; High Speed Photog. and Photonics, ed. S. Hyodo- Jap. Soc. Precision Eng. Tokyo, p.517 (1979)

[52] Hadland Photonics Ltd., Framing Camera Technical Brochure

[53] G. Clément, G. Eschard, J.P. Hazan, R. Polaert; in Proc. 9th Int. Cong. High Speed Phot; ed by W.G. Hyzer, W.G. Chace-Colorado, USA (1970)p. 499

[54] R. Kalibjan; Rev. Sci. Inst. 49, 891 (1978)

[55] R. Haddland, K. Helbrough, A.E. Houston; Proc. 11th Intern. Cong. High Speed Photog., ed. P.J. Rolls, Chapman and Hall, London p. 107 (1974)

[56] W. Sibbett, J.R. Taylor, D. Welford; IEEE J. Quantum Elect. QE17, 500 (1981) and refs. therein.

[57] M.C. Adams, W. Sibbett, D.J. Bradley; Opt. Commun., 26, 273 (1978)

[58] D.J. Bradley, M.B. Holbrook, W.E. Sleat; IEEE J. Quantum Elect. QE17, 658 (1981)

[59] M.C. Adams; PhD Thesis, Imperial College, Univ. of London (1979)

CHAPTER THREE

SEMICONDUCTOR SWITCHES

3.1 Introduction

With the development of mode-locked lasers, optical pulses of picosecond durations and several gigawatts peak power became available. These intense pulses were used as sources of energy to investigate the absorption and fluorescence characteristics of a wide range of samples such as semiconductors [1], dyes [2], gases [3] and others, and methods were developed to study such transient phenomena with picosecond precision and resolution [4]. Optical pulses were also used to induce non-liniar effects in crystals [5] which were examined in this ultrafast time-scale, and techniques were created to manipulate light pulses in terms of their spatial, temporal and spectral properties.

In spite of the enormous technological interest, ultrafast electronics did not develop to such an extent, since high speed electronic elements have typical response times of $\gtrsim$ 100ps and very few watts peak power capability. The direct transformation of the energy of mode-locked light pulses into high amplitude, picosecond electrical signals by means of optical rectification was demonstrated [6, 7]. However, a much simpler, more versatile and efficient technique to make use of the energy carried by the mode-locked laser light to generate voltage pulses was devised by Auston in 1975 [8] with semiconductor switches. These devices have now been used in the switching of high voltage pulses of $\sim$ MW peak power with picosecond risetimes, capable of activating Pockel's and Kerr cells and synchronizing streak cameras, in the generation and detection of transient photocurrents with temporal resolution < 10ps, and several other applications. Picosecond semiconductor switching devices (Auston switches) quickly became an area

of active research because of the enormous interest and potential capabilities of the technique, and constitute the subject matter of this thesis. In this chapter, the most relevant results published in the literature are reviewed.

3.2 Description

The simplest energy level structure for electrons in a semiconductor crystal consists of a valence band and a conduction band separated by an energy gap. For a pure (intrinsic) semiconductor at room temperature, the number of electrons in the conduction band is small. The valence band is then full, and the resistivity of the crystal is large.

Electrons in the valence band can gain enough energy through interaction with photons from an external excitation source to be promoted to the conduction band. In this case they leave an empty state in the valence band which is called a 'hole'. Electrons in the conduction band and holes in the valence band can move freely through the crystal. In the presence of an external electric field, these photoinduced carriers are responsible for current flow. A single photon can promote an electron from the valence to the conduction band if its energy exceeds the energy gap. Multiphoton processes, although usually much less efficient, can also lead to the generation of free carriers.

The time taken for electrons to absorb energy and become free is very short ($\sim 10^{-14}$s). For intense light sources, the large numbers of photoinduced carriers can change the conductivity of the semiconductor crystal by several orders of magnitude. Therefore photoconductivity is an ultrafast effect, through which the conductance of a semiconductor

can be significantly altered.

Picosecond semiconductor switches are simple photoconductive devices. They basically consist of a piece of high resistivity semiconductor which is electrically connected to a transmission line, between a power supply (input) and a load (output). Initially the semiconductor slab exhibits a very high (dark) impedance, which prevents voltage from reaching the output, and the switch is said to be in its "off" state. However, when the slab is illuminated by an intense ultrashort laser pulse, the impedance of the semiconductor is significantly reduced, due to the creation of electron-hole pairs. The device is then said to be switched "on", since the continuity of the transmission line is established, and voltage is transmitted to the load.

For efficient switching to take place, the impedance of the device must become much lower than the characteristic impedance of the line, which is typically 50Ω. This defines a minimum amount of optical energy necessary to fully activate the switch. An expression relating the "on" impedance to the incident light pulse energy is derived in section 3.4.

The fast switching speed is based on the extremely short times during which photoinduced carriers are created. Therefore, the ultrashort duration of the light pulses used to activate the switches is a major requirement for picosecond risetimes. Other factors, such as the bandwidth of the electronic configuration, and the thermalization time of the carriers can also affect the maximum attainable speeds, as discussed later.

Most of the experiments described in this thesis deal with picosecond pulses as the excitation source for the semiconductor switches.

When continuous or quasi-continuous light sources are used, long duration voltage pulses are obtained and the devices operate in a steady-state mode. In this case too, the basic properties of the semiconductor crystals can be studied, such as transport mechanisms and steady-state photoconductivity.

When illuminated by intense light pulses generated by mode-locked pulsed lasers, semiconductor devices have the capability of switching high voltages, where the pulses generated have ultrafast risetimes and are in picosecond synchronism with the activating light pulses.

The relatively easy construction of semiconductor switching devices allows the fabrication of "home-made" prototypes. For their simplicity and low cost, the results that can be obtained are very encouraging. Furthermore, the use of various materials activated by a range of mode-locked lasers has already been demonstrated. Picosecond solid-state switches are versatile devices that have many practical applications, and a study of their operation can also assist in the understanding of some of the basic properties of semiconductors.

3.3 Semiconductors

In order to describe the basic features and possible applications of solid-state switching devices in further detail, it is useful to individually examine the different semiconductors that have been or can be used in particular configurations. Parameters such as resistivity, recombination time and energy gap are important for a clear understanding of the performance of the switches. In this section some of the properties of the semiconductors used are outlined and the limitations of the different materials that have been studies are also discussed.

3.3.1 Silicon

The most widely used semiconductor is silicon. For over three decades and particularly with the advent of integrated circuits and microprocessors Si technology has been extensively developed. Nearly intrinsic (i.e. high purity) silicon is commercially available at relatively low cost, and these crystals exhibit resistivities as high as $\sim 10^4 - 10^5 \Omega$cm.

Picosecond switches were first demonstrated by Auston [8] in 1975 using this semiconductor. His device consisted of a piece of high resistivity Si ($\rho \sim 10^4 \Omega$cm) on which a microstrip transmission line structure was formed. A uniform Al coating covered the bottom surface of the semiconductor chip which was maintained at earth potential. Two Al strip electrodes were prepared on the top surface, separated by a small gap. The input electrode was connected to a d.c. power supply ($\sim$ 20V), and the output taken to an oscilloscope via 50Ω coaxial cables. The high dark impedance across the gap initially prevented the transmission of the voltage signal ($T \lesssim 5\%$). Auston's switch was activated by a single $\sim$ 5ps duration light pulse of 0.53μm wavelength obtained by frequency doubling the output of a mode-locked Nd:glass laser. Due to the photoinduced electron-hole pairs, the impedance of the device was reduced to a few ohms or less, and the voltage applied was efficiently transmitted ($T \gtrsim 95\%$) with picosecond risetime.

The recombination time of carriers in nearly intrinsic Si is long ($\tau_r \sim$ 1-10μs). Therefore the Si switch generated a voltage pulse of duration typically $\sim 10^5$-10^6 times greater than its risetime. Therefore the shape of the electrical pulse on a picosecond and nanosecond time scale closely approached a step function. This is an advantage for some applications, such as in streak camera synchronization for single

pulse operation (c.f. Chapter 5). Sometimes, however, it is desirable to generate voltage pulses of ultrashort duration. In these cases an independent means, other than recombination, must be provided to terminate the switching action. Auston made use of the wavelength dependent penetration depth of Si.

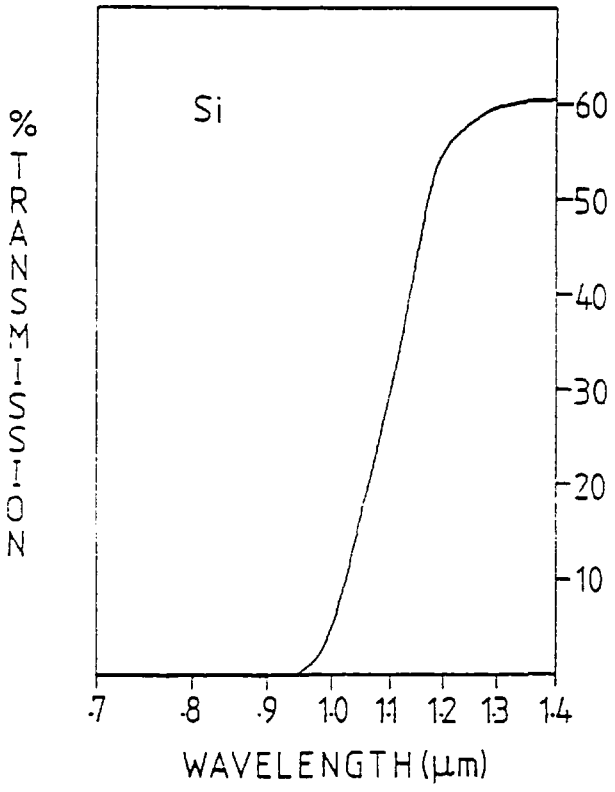

FIG 3.1 Optical transmission of 0.5mm thick silicon crystal for different wavelengths

In figure 3.1 the transmission of a 0.5mm thick Si crystal is shown for different wavelengths. Photons of 0.53μm wavelength (2.34eV) used to activate the switch are strongly absorbed in silicon, with an absorption constant $\alpha=8 \times 10^3 cm^{-1}$ [9]. Therefore the activating light pulse created electron-hole pairs on a very thin ($\sim$ 2.5μm) surface layer of the semiconductor. Green light did not reach the bulk of the crystal and the "switch on" process was mainly due to surface conductivity. However, the fundamental radiation of the Nd:glass laser has a wavelength (1.06μm) which closely approaches the band edge of Si ($\sim$1.05μm [10]). The absorption depth in this case is much longer ($\alpha = 7cm^{-1}$) and therefore, when the infrared light pulse of 1.06μm illuminated the device, carriers were created throughout the thickness of the semiconductor. Bulk conductivity was then responsible for a low resistance electrical path between the input electrode on the top surface and the ground plane on

the bottom surface of the semiconductor slab. The switch was in this case shorted to earth by the infrared pulse.

Auston provided a mode-locked laser pulse of 0.53μm to switch the device on, and a delayed one of 1.06μm wavelength to short it to ground The voltage pulse generated had a duration which was primarily determined by the delay between the two light pulses. The shorting, like the switch-on process, relied on the creation of carriers by photons and because of the ultrashort duration of the mode-locked pulses used, picosecond rise and fall times were obtained. Auston demonstrated that square voltage pulses of an adjustable duration in the range of many nanoseconds to a few picoseconds could be generated by this type of semiconductor switch.

The requirement of two light pulses having different wavelengths to switch the Si devices on and off is rather inconvenient, and this shortcoming was overcome by the coplanar structure [11, 12]. A third electrode was preapred on the top surface of the semiconductor, and grounded. The terminating action was accomplished by shorting the input to earth via a high conductance layer formed on the top surface of the switch by the second light pulse. In this case both mode-locked pulses could have the same penetration depth and consequently a single wavelength could be used. Several combinations of lasers and semi-conductors could be employed to generate picosecond voltage pulses by this method, since the coicidence of photon energy and energy gap that occured for Nd:glass and Si was no longer necessary.

It was pointed out in [8] that a coaxial line initially at voltage V discharging through a switch would also give rise to a square voltage pulse. This is usually known as the discharge line configuration and is widely used in pulse shaping networks. A schematic diagram of

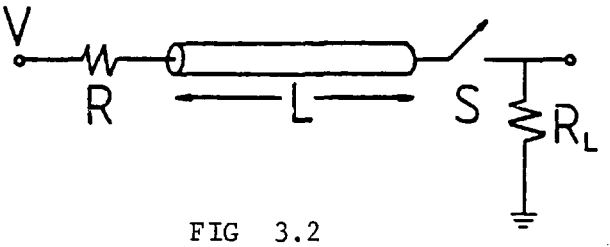

FIG 3.2

such an arrangement can be seen in figure 3.2. The d.c. voltage V charging the line can be described as a standing wave which is the sum of two components of amplitude V/2 travelling in opposite directions. Initially the two components are totally reflected at the extremes of the line, defined by the charging resistor R and the switch S. When the device is activated, only the component travelling forward reaches the output cable. The other one has to be reflected at the charging resistor before it starts propagating towards the output. In this way a square voltage pulse is switched, having an amplitude V/2 and a duration τ which is equal to the double transit time of the electromagnetic wave travelling down the line. If L is the length of the charged line and c_n is the speed of propagation, $\tau = 2L/c_n$.

In this configuration the second light pulse previously used to switch the device off is no longer necessary, since the voltage applied to the switch drops to zero when the line has fully discharged (assuming that the charging time through the resistor R is very long). Due to the picosecond risetime of the semiconductor device, the square voltage pulses can have very sharp edges. By adjusting the length of the charged line, square pulses of durations $\sim 10^1$-10^6ps can be obtained in practice. This arrangement is particularly useful for long recovery time switching because a single light pulse can be used to generate a square voltage pulse of arbitrary duration. The ripple present on the voltage pulse switched with the discharge line configuration is usually very small. Its major disadvantage is that the maximum amplitude obtained is limited to half of the d.c. voltage applied to the device.

The use of crystalline Si in the construction of picosecond switches is attractive not only because of its availability and low price. The energy gap of Si is relatively low (~1.1eV) and therefore the wavelength of most of the mode-locked lasers is shorter than the absorption edge of this semiconductor. As a consequence, a single photon has enough energy to promote an electron from the valence to the conduction band. This means that most mode-locked lasers can be used to activate Si devices. Furthermore the mobility* of conduction electrons is high ($\mu_e \sim 2 \times 10^3 cm^2 V^{-1} s^{-1}$) and as discussed in section 3-4, this leads to high switching efficiencies. The long recombination time of nearly intrinsic Si renders its use attractive when long as well as short duration voltage pulses are to be switched.

However, the repetition rate at which high purity Si switches can be operated is low ($\lesssim$ 1MHz). Because of the slow recombination of carriers a low resistance electrical path remains between the input and output electrodes for a relatively long period of time following the ultrashort irradiation pulse. This happens in all of the configurations described above, and therefore nearly intrinsic Si switches are not suitable for applications requiring high repetition rates.

The resistivity of high purity Si crystals commercially available does not exceed $\sim 10^5 \Omega cm$, and therefore the impedance of these devices is relatively low ($\lesssim 10^6 \Omega$). As a consequence, an applied d.c. bias gives rise to considerable leakage current flow across the gap between electrodes. The power dissipated as heat in the slab significantly decreases the resistivity of the crystal due to thermal creation of carriers. The dark impedance of the device then continues to drop, more current flows, and this leads to more heat, until eventually the switch is no longer

*The mobility of a carrier is defined as the velocity it gains per unit electric field applied, i.e., $\underline{v} = \mu \underline{E}$

capable of holding off the applied voltage. This effect is of particular importance for high voltage applications. Thermal problems prevent the use of nearly intrinsic Si at room temperature when the voltage pulses to be switched exceed $\sim 10^2$V. This feature is further discussed in section 5.3.

3.3.2 Gallium Arsenide

The alternative of a III-V semiconductor instead of Si in the construction of picosecond switching devices was demonstrated by Lee [13]. Commercially available semi-insulating chromium doped GaAs can exhibit resistivities as high as $\sim 10^8 \Omega$cm. The amount of chromium doping the crystals is chosen to exactly compensate for the impurities that are undesirably introduced during the fabrication, and these are therefore called compensated crystals. The semi-insulating (S.I.) GaAs devices can have very high dark impedance, which implies good insulation between the power supply and the output prior to the switching action. Also, the leakage current when a d.c. bias is applied is very small and consequently thermal stability is much better than for Si. High voltage can be applied continuously without excessive heat generation of carriers. This important feature is exploited in the application of GaAs devices described in Chapter 7.

The most striking difference between GaAs and Si switches is the recovery time. While nearly intrinsic Si devices generate voltage pulses lasting for microseconds, semi-insulating GaAs switches have recovery times of $\sim$ 100ps. Photoinduced carriers recombine very quickly, and as a consequence the repetition rate at which the devices can be operated is very high. The low resistance path created between input and output electrodes rapidly disappears, and the device is then ready for another

switching action. The recombination time of carriers in GaAs can be determined by correlation methods using semiconductor switches, as shown in Chapter 4. A number of experiments have been carried out to measure its value [14, 15, 16] and the results obtained showed recombination times of $\sim$ 50-150ps.

Soon after the demonstration of Si switches, Lawton and Scavannec [17] reported the use of semi-insulating Cr-doped GaAs as an ultrafast photodetector. Their device was activated by a mode-locked CW dye laser and was capable of easily resolving consecutive pulses in the train. The width of the voltage pulses displayed on a sampling oscilloscope was $\sim$ 100ps. It was pointed out that the photodetector could be used as an ultrafast optical switch, providing complete isolation of the gating signal. When the device is used as a photodetector however, it should be operated in a linear mode, and in order to avoid saturation only low intensity light pulses should illuminate the gap. In contrast, if the device is used as a switch, higher light energies are necessary for efficient switching. In this case the number of optically excited carriers must be high enough to reduce the impedance of the device to a negligible value.

The energy gap of GaAs at room temperature is Eg = 1.4eV, corresponding to an absorption edge of $\lambda \simeq 0.9\mu m$. Commonly used mode-locked Rhodamine 6G dye lasers and frequency doubled Nd lasers are capable of efficiently generating electron-hole pairs in a single photon process, while switching with the fundamental radiation of Nd lasers relies on multiphoton excitation (neglecting impurity states).

The most important carriers of current in GaAs switching devices are electrons. When the electric field applied across the gap of the switch is limited to $E \lesssim 3KVcm^{-1}$, electrons in the conduction band

exhibit very high and approximately constant mobility ($\mu_e \sim 1000^s cm^2 V^{-1}s^{-1}$). The mobility of holes in the valence band is much lower ($\mu_h \lesssim 400 cm^2 V^{-1}s^{-1}$). For weak electric fields, efficient switching is achieved with light pulses of relatively modest energies. Also, for a given illumination of the device, the voltage switched follows the voltage applied. As the voltage applied is increased, the output voltage also increases.

It was found, however, that in many cases as the field across the gap exceeded $\sim 3KVcm^{-1}$, the voltage switched decreased as the applied voltage was increased. This interesting transport phenomenum was first observed for GaAs switching devices by Lee [13]. The switch shows negative differential resistivity, and this is the same effect as used in Gunn diodes. In order to understand the physical process taking place, it is necessary to study the band structure of GaAs in further detail.

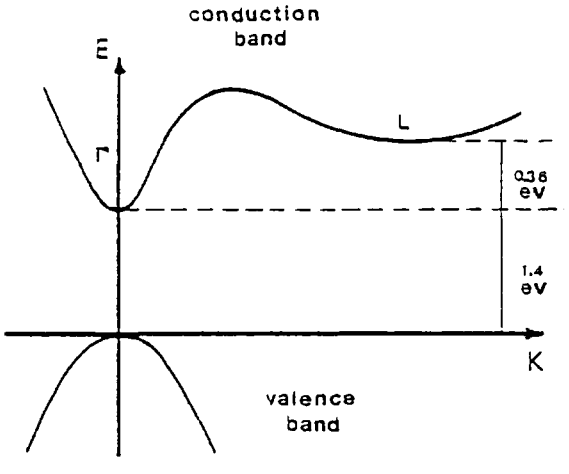

FIG 3.3 Schematic diagram of the band structure of GaAs in K-space

Figure 3.3 shows a simplified schematic diagram of the energy bands in the K-space. The conduction band has in fact more than one minimum in energy. Initially at room temperature, the population of the conduction band is negligible, and the switch exhibits high impedance. When photons of sufficient energy excite electrons from the valence to the conduction band, the conductivity of the slab increases. Transitions involving photons of energy $1.4eV \lesssim \varepsilon \lesssim 1.7eV$ take electrons to the central valley Γ of the conduction band. These so called direct transitions involve relatively little momentum

exchange with the lattice. Conduction electrons in the Γ valley exhibit high mobility.

Negative differential resistivity arises in GaAs because the mobility of electrons in the upper valley (L) is lower than in the central valley (Γ) of the conduction band. Different mechanisms can be responsible for populating the upper valley. Electrons can, for instance, be excited from the valence band, absorbing a photon of energy greater than the sum of the energy gap and the separation between valleys. The electrons promoted to the conduction band in this way have an excess energy, i.e. they are "hot electrons". When exchange of momentum also takes place (by phonon coupling with the lattice), the transitions are called indirect and can take electrons to the upper valley L of the conduction band. These electrons have high effective mass* and present low mobility. However, they are not in thermal equilibrium with the semiconductor, and therefore quickly loose the excess energy (∿ps). If no external mechanism is present to maintain high populations in the upper valley L, these electrons quickly thermalize to the central valley Γ of the conduction band, until they recombine.

Following the activation of the switch and thermalization, electrons populate mainly valley Γ and exhibit high mobility. Their interaction with an external electric field happens very quickly ($\tau \lesssim 10^{-13}$ [18]). If the accelerating field is strong enough, the electrons can reach high speeds between successive collisions. When the kynetic energy gained exceeds ∿ 0.36eV, scattering to the upper valley can take place and this process is very efficient for electric fields $\gtrsim 3\text{KVcm}^{-1}$. This transfer of

*Although subjected to quantum-mechanical forces, the average behaviour of an electron in a semiconductor can still be described by Newton's law it its mass is replaced by an effective mass which takes into account all the interaction with the crystal, and is defined as $m^* = \hbar^2(d^2\varepsilon/dK^2)$.

conduction electrons from valley Γ to L, competes with thermalization, which brings electrons down from valley L to Γ. However, significant depletion of population from the lower valley occurs, since the time taken for electrons to gain the excess ~ 0.36 eV is comparable with the thermalization time, but the density of states available in the L valley is much greater than in the Γ valley. The total conductance of the device is then significantly reduced. It is easy to see that this problem is even more serious for higher electric fields.

Submicron switching devices of different lengths have been used to study the transport properties of GaAs [19]. The gap of these switches was such that the transit time between electrodes was either smaller, comparable, or much larger than the thermalization time. Different wavelengths were also employed, creating electrons near the bottom of the central valley Γ, or in the upper valley L of the conduction band. The conductance of the devices was systematically studied, and a significant change in the mobility of hot electrons was infered to explain the results obtained.

Intervalley scattering is an interesting phenomenom which finds numerous applications, such as in Gunn oscillators [20] and in negative differential resistivity devices [21]. In most cases, however, it is desirable to obtain high switching efficiencies, and electrons transfer to the lower mobility valley is an inconvenience. In particular, when high voltage devices are used, the electric fields applied usually exceed the threshold for intervalley scattering. In these cases, for efficient switching to take place, the low mobility of hot electrons has to be compensated by a large number density of carriers. High energy light pulses are then necessary to fully saturate the devices.

A final but important feature of GaAs switches is that they can be

activated by mode-locked semiconductor lasers. Preliminary studies using $\sim$ 20ps duration light pulses from a GaAlAs laser [22] were carried out and electrical signals of few milivolts amplitude were generated, showing risetimes of $\sim$ 60ps. The possibility of incorporating GaAs switching devices in integrated optic systems therefore seems feasible and is potentially very promising.

3.3.3 Gallium Phosphide

Gallium phosphide is an additional crystaline semiconductor which has been used in solid-state switching devices. It is a III-V compound which exhibits in many cases similar properties to GaAs. GaP has an energy gap of 2.35 eV and is an indirect semiconductor (see for instance [23]), since the phonon-assisted transitions take electrons from the top of the valence band to the bottom of the conduction band with $\Delta K \neq 0$. As in GaAs, the conduction band has more than one minimium, but in GaP the electrons in the upper valley of the conduction band (lying 0.51eV above the minimum) exhibit a higher mobility than those lying in the lower valley. Consequently, as the electric field across the gap is increased and electrons begin to populate the upper valley, the conductivity also increases. Therefore, unlike GaAs, GaP should not exhibit negative differential resistivity. The evaluation of the performance of GaP switches for various electric field strengths in discussed in greater detail in section 4.6 and the results confirm that the voltage switched increases monotonically with the voltage applied, for electric fields up to at least $10KVcm^{-1}$.

The large energy gap of GaP requires the use of relatively short wavelength light ($\lambda \lesssim 0.53\mu m$) for single-photon activation of the switch. The fundamental radiation of Rhodamine 6G dye, ruby, Nd and

GaAlAs lasers is not energetic enough to directly promote an electron from the valence to the conduction band by single-photon excitation. However, the energy of the 0.53μm wavelength second harmonic radiation of Nd lasers is nearly coincident with the energy gap of GaP, and this coincidence can be used in the study of fundamental properties of the semiconductor [24], such as band structure and exciton states [25].

The long penetration depth of 0.53μm radiation (∿ 0.2mm) renders bulk conductivity dominant over surface conductivity. When the penetration depth is long, the risetime of the switch can be slightly slower, due to the propagation time of light inside the semiconductor [26], but this effect is almost always negligible. On the other hand, bulk conductivity can be an advantage, since unwanted imperfections on the top surface of the crystal are also usually unavoidable.

If light is absorbed on a thin semiconductor layer high temperatures can be produced. Very intense picosecond pulses can even render the top surface of the crystal liquid for a short time [27], or permanently amorphous [28]. When the electric field across the gap is strong, and in particular, if the light pulse illuminating the device is spatially non-uniform, heating can lead to surface electrical breakdown. When the penetration depth is long, however, heating effects on the top surface are less severe, and this is the case for GaP devices activated by 0.53μm radiation.

The semi-insulating GaP crystals (Cr-doped or undoped) which are commercially available can have resistivities as high as $10^9 \Omega$cm. Therefore the dark impedance of GaP switches is extremely high. Typically when devices of 25μm gap length were prepared on chips 3mm wide and 0.5mm thick, the impedances measured always exceeded 20MΩ. For longer gap lengths, even higher values were obtained. Also, because of the large

energy gap of GaP, the population of thermally excited carriers in the conduction band at room temperature is very small. As a consequence, the dark current in semi-insulating GaP is usually negligible, and the thermal stability of the switches is excellent.

Because of the fast recombination time of optically excited carriers, GaP switching devices are capable of resolving consecutive light pulses from a mode-locked laser train. Therefore they can be used as photodetectors of very simple and cheap construction. DC bias can be used, and the risetimes obtained are comparable with the duration of the activating light pulses, which can be ∿ps. In order to determine the actual recovery time of GaP devices an electrical correlation scheme was used, c.f. section 4.5.3.

The mobility of electrons and holes is approximately the same in GaP, and is a relatively low value, ∿ $120 cm^2 V^{-1} s^{-1}$. Therefore the absence of negative differential resistivity in GaP is somewhat overshadowed, since comparatively intense mode-locked laser pulses have to be used for efficient switching to take place.

3.3.4 Other Crystalline Semiconductors

3.3.4.1 Indium Phosphide

InP is the only other binary III-V semiconductor which has so far been used as a picosecond optoelectronic switch [29]. Semi-insulating InP is commercially available, and crystals with resistivity as high as $2.5 \times 10^8 \Omega cm$ have been employed. The samples used were Fe-doped, and the gap of the device was very short (∿ 3μm). As shown later in section 3.4, for a given illumination intensity, the "on impedance" of the

switch is proportional in the square of the gap length. By fabricating an extremely short device, Leonberger and Moulton were capable of obtaining reasonably high conductances ($\sim 2 \times 10^{-2}$mho) with only ~40pJ light pulses. A good semiconductor metal junction was ensured by providing the electrodes with semitransparent regions on either side of the gap, which were also illuminated.

The recombination time of optically excited carriers in InP was estimated to be ~ 50ps. Fast recovery photodetectors can, therefore, be made with this semiconductor. A significant result obtained was the demonstrated capability of activating InP switches with mode-locked GaAlAs lasers, since the energy gap of InP is ~ 1.34eV at room temperature [10]. As for semi-insulating GaAs, the possibility of using InP in integrated electroopical devices for laser telecommunication is very attractive.

As an application, InP switches were used to sample a 68.9MHz sine wave, activated by a laser at 275MHz and 40dB signal-to-noise ratio switching levels were obtained. Due to the fast recombination time of photocarriers, the devices can be activated by multiplexed light pulses, thereby yielding very high sampling rates.

3.3.4.2 Indium Gallium Arsenide

Recently, a ternary compound $In_{0.53}Ga_{0.47}As$ was employed as a fast photoconductive detector sensitive to radiation to wavelengths ~ 1.7μm [30]. The device was fabricated with p-type semiconductor and relied on electron sweep-out to terminate the high conductivity state resulting from irradiation. Because the gap was only 15μm long, and the peak drift velocity of electrons is high ($\sim 2.1 \times 10^{7}$cms^{-1}) at fields of ~ 3.5KVcm^{-1}, the electrical signals obtained had a relatively short

duration of 70ps FWHM.

3.3.4.3 Cadmium Sulphur Selenide

The only II-VI compound which has so far been used in picosecond switching devices was $CdS_{0.5}Se_{0.5}$ [31]. The search for new materials was motivated by the poor thermal stability of Si, and the undesired negative differential resistivity that most III-V compounds exhibit for high electric fields.

The crystals used were compensated and had a resistivity $\rho \sim 10^7 \Omega cm$. The solid solution employed had an energy gap of 2.0eV. Carrier relaxation mechanisms in $CdS_{0.5}Se_{0.5}$ switches were investigated [32], with picosecond laser pulses of 0.53μm and of 1.06μm wavelength. For the infrared pulses the penetration depth is long and bulk recombination is dominant, while for the green light, surface recombination is more important. At low light intensities ($\lesssim 3MWcm^{-2}$), for both wavelengths slow decay was observed ($\sim$ 20ms). At high excitation levels ($\sim 0.8GWcm^{-2}$), the decay of the voltage pulses switched consisted of a fast component ($\sim$ 20ns) followed by a slow component which lasted for several miliseconds. At high carrier densities red light was emitted by the crystal. The fast recombination was attributed to stimulated radiative processes taking place through a similar mechanism as had been reported earlier for CdS [33].

The absence of negative differential resistivity was not shown experimentally. However, the response of the switch for different light intensities was plotted on a log-log scale, and the voltage output was shown to increase linearly for at least four decades for 0.53μm excitation, with a slope 0.8. When 1.06μm light pulses were used, the slope was initially $\sim$ 2.0 and then saturated for high intensities. The slope 2.0

was attributed to two-photon carrier generation in the sample since it indicated that the conductance of the switch varies with the square of the light intensity illuminating the device.

As mentioned in chapter 2, a $CdS_{0.5}Se_{0.5}$ switch was used by Lee and Jayaraman to measure ultrashort optical pulses [34]. The technique was based on the two-photon conductivity (TPC) [35], which is similar to the two-photon fluorescence (TPF) described in chapter 2. The conductivity of the semiconductor depended on the square of the light intensity. This square law was used to measure the second order intensity correlation function of the picosecond light pulses. A triangular arrangement, similar to that commonly used in two-photon-fluorescence experiments was employed. The mode-locked pulse was split into two components which overlapped at the semiconductor. By slightly varying the light paths of the two components for consecutive laser shots, the second order autocorrelation of the light pulse was mapped out. This method to measure picosecond light pulse durations has the advantages that the alignement is much less critical than for TPF and no densitometry is required. A later version of the device [36] included a stack of seven small switches. They were mounted in such a way as to sample the autocorrelation curve at seven different points for a single laser shot. Contrast ratios of 2.8-1 were obtained experimentally, and pulses of $\sim$ 10ps duration were measured.

By using a device in a charged line configuration voltage pulses durations as short as $\sim$ 1ns were obtained with $CdS_{0.5}Se_{0.5}$. However the repetition rate of the switch was rather poor. Also, since the total mobility is relatively low ($\sim 4 \times 10^{2} cm^{2} V^{-1} cm^{-1}$), the $CdS_{0.5}Se_{0.5}$ devices are not very sensitive.

3.3.5 Amorphous Semiconductors

When the recombination time of carriers is extremely short, the switch can be used in the photoconductive mode as a picosecond light detector. If the energy of the light pulses illuminating the gap is kept low, the device shows a linear response. Such a high speed photodectector using a thin film of amorphous silicon was demonstrated by Auston [37]. The devices constructed were very similar to those described for crystalline Si in [8]. A $\sim$0.5μm thick film of α-Si was deposited on fused silica, and had a resistivity of 10^7Ωcm. Microstrip transmission line structures were fabricated on the α-Si, and gap lengths of 20-50μm exhibited dark impedances of $\sim 10^9\Omega$. The devices were d.c. biased to up 200V and the output of the devices was connected to a sampling oscilloscope. The photodetectors were tested by Auston with a CW Rhodamine 6G dye laser synchronously pumped by a mode-locked Ar^+ laser. The energy of the dye laser photons ($\sim$ 2ev) was higher than the absorption threshold of the semiconductor film (1.6eV).

The electrical pulses displayed on the 25ps risetime oscilloscope showed FWHM durations of 40ps, clearly limited by the instrument. Since then electronic correlation studies [38,39] performed with similarly prepared switches showed decay times $\lesssim$30ps. Ultrahigh-vacuum deposited (UHV) α-SI devices were also fabricated, and a comparison with the chemical vapour deposited α-Si switches showed that higher density of defects could be achieved by the UHV technique. Even faster relaxation times were then measured ($\tau \lesssim$ 4ps).

Amorphous silicon devices have already been shown to be capable of detecting ultrashort light pulses, generating FWHM voltage signals of $\sim$ 11ps [38]. This is a significant improvement over the response time of the fastest photodiodes currently available, which is typically $\sim$ 50ps. Even faster devices can be anticipated for the near future, with response times which approach the time duration of the light pulses.

Therefore, due to their simplicity, low price and remarkable performance, α-Si devices are very promising as ultrafast light detectors.

In order to maintain the ultrafast rise and fall times of the voltage pulses throughout the detection system, broad-bandwidth transmission lines and sampling heads are needed [40]. Conventional oscilloscopes do not exhibit the risetimes required. However, α-Si devices can be used as sampling gates. The gate opening time is given by the duration of the "on-state" of the device, which can be ∿ 5ps. This technique was illustrated by the electrical correlation measurements. A system incorporating an oscilloscope and such a sampling gate was used to measure the response time of fast unknown materials [39]. High signal-to-background ratio was obtained, and the jitter was minimal. The system is also attractive for its high sampling rate capability, due to the short recombination time of the α-Si gate.

The studies carried out by Auston and co-workers for α-Si have been extended to the measurement of physical properties of the semiconductor. The mobility of carriers and transport processes have been investigated [41], and the initial (transient) mobility found was ∿ 1-10$cm^2V^{-1}s^{-1}$, which is significantly lower than in crystalline samples. This value did not change appreciably for samples prepared by chemical vapour or ultra-high vacuum deposition, but was found to be considerably higher in radiation damaged α-Si [42]. The relaxation rate strongly depended on the density of defects.

High voltage α-Si switches have not been demonstrated because the high density of defects means that the carriers recombine very quickly, before reaching the output electrode. As a consequence, small gaps have to be used for relatively efficient collection of photocarriers. Furthermore, the mobility of electrons is low, so the use of α-Si switches

will be probably restricted to low voltage applications.

Although other amorphous materials have not been used so far, it is expected that the techniques described by Auston for α-Si will be employed for other semiconductors as well, in the near future.

3.4 Switching Efficiency

It is useful to have an analytical expression for the switching efficiency in terms of different parameters which characterize the laser, the semiconductor, and the experimental set-up. The exact behaviour of the switches can only be described by a complicated formula which takes into account effects due to the electrodes, penetration depth, non-homogeneity of the light pulse and of the field across the gap, and so on. Theoretical models describing the performance of the switches when compared to systematic experimental data, can lead to a better understanding of fundamental physical processes in semiconductors. Picosecond switching devices are a useful tool in the study of photoconductivity, metal-semiconductor junctions, transport of charge and relaxation mechanisms in different materials. The relevant experimental parameters involved, however, must be known to a reasonable degree of accuracy. These studies involve a great deal of time and effort, and fall outside the scope of this thesis. What follows is a simple expression which describes approximately the performance of the devices, and explains qualitatively the experimental results obtained during the work. When used to provide quantitative information, it usually predicted values which agreed with those measured to within the experimental errors.

For a high resistivity semiconductor irradiated by a mode-locked

laser, the fraction of thermally excited carriers is very small, compared to the total numbers of carriers created by light absorption. Therefore, in order to determine the conductance of the gap it is necessary to calculate the number density of photoinduced carriers. Recombination is initially not taken into account, and it is assumed for simplicity that all free electrons contribute equally to the conductivity. Multiple reflections between layers of atoms is also neglected.

The conductivity of the semiconductor is given by

$$\sigma = e(n_e\mu_e + n_p\mu_p)$$

where n_e, n_p, μ_e and μ_p are the number densities and mobilities of electrons and holes, respectively, and e the electronic charge. Assuming that the number of electrons promoted to the conduction band is equal to the number of holes in the valence band,

$$n_e = n_p = n,$$

and therefore

$$\sigma = e(\mu_n + \mu_p)n.$$

When a light pulse of energy ε illuminates the gap, part of the energy is absorbed by the crystal and part is reflected. In the case of normal incidence, the coefficient of light transmission from air into the semiconductor is given by Fresnel's relation

$$T = \frac{4n_r}{(1+n_r)^2}$$

where n_r is the refractive index of the material [43]. Therefore the total number of photons of energy $h\nu$ that actually enter the crystal is

$$I_o = \frac{4n_r}{(1+n_r)^2} \frac{\varepsilon}{h\nu} . \qquad (1)$$

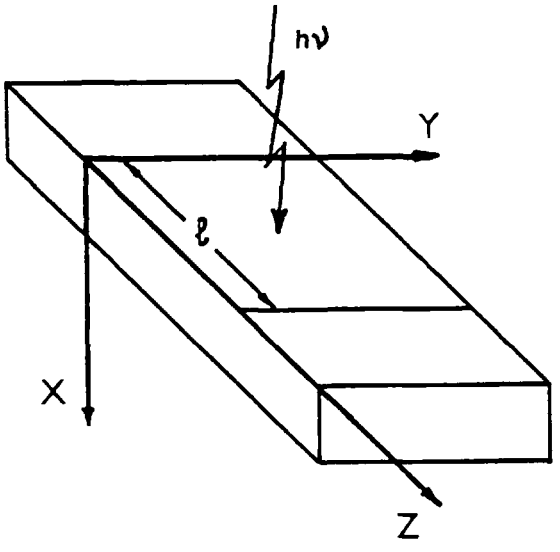

FIG 3.4

Referring to figure 3.4, let $i(x,y,z)$ represent the photon distribution inside the semiconductor slab. The x axis corresponds to depth, y to width and z to length. If saturable absorption of light by the crystal can be neglected, then

$$i(x,y,z) = i(x)p(y,z)$$

Assuming that the numbers of photons absorbed at depth x is proportional to the number of photons available at depth x, and calling $i_o(y,z)$ the distribution at the top surface of the semiconductor,

$$i(x,y,z) = i_o(y,z)e^{-x/\alpha}$$

where α is a absorption constant. The normalization is expressed as

$$I_o = \int\int i_o(y,z)dydz$$

integrated over the gap area.

Different processes are responsible for the absorption of light by the sample. The creation of electron-hole pairs is the most important one when the photon energy exceeds the energy gap of the semiconductor. In this case the quantum efficiency is approximately unity, and the absorption of each photon can be attributed to the creation of an electron-hole pair. For unity quantum efficiency, the number of carriers created in a layer of thickness dx at depth x, is equal to the number of photons absorbed as the light pulse passes through that layer.

$$n(x) = \frac{-di(x)}{dx} = \frac{i_o}{\alpha} e^{-x/\alpha}$$

If y and z dependence is made explicit,

$$n(x,y,z) = \frac{i_o(y,z)}{\alpha} \quad e^{-x/\alpha}$$

The conductivity of any element of the crystal between the electrodes can therefore be expressed as

$$\sigma(x,y,z) = \frac{e(\mu_e + \mu_p)}{\alpha} i_o(y,z)e^{-x/\alpha}$$

The spatial intensity distribution $I_o(y,z)$ of the light pulse illuminating the gap is usually non-uniform. However, if the gap is much smaller than the size of the beam, the simplifying approximation of uniform beam intensity can be made. In practice the light pulse is often considerably larger than the gap, to ensure proper activation of the switch. In this case

$$I_o = \int\int i_o(y,z)\, dydz = i_o\, w\ell$$

Hence from (1)

$$i_o = \frac{4n_r}{(1+n_r)^2} \frac{\varepsilon}{h\nu} \frac{1}{w\ell}$$

Finally, the total conductance across the gap is given by

$$G = \frac{w}{\ell} \int \sigma(x)\, dx,$$

and therefore, assuming that no light is transmitted through the whole thickness of the slab (i.e $0 \leq x \leq \infty$),

$$G = \frac{4n_r}{(1+n_r)^2} \frac{e(\mu_e + \mu_p)}{\ell^2} \frac{\varepsilon}{h\nu} = \frac{1}{Z} \qquad (2)$$

This expression gives the conductance (and impedance) of the switch when illuminated by a picosecond pulse, before recombination starts to take place. The choice of a particular semiconductor determines the refractive index and the mobility of carriers, the choice of mode-locked

laser defines the wavelength and the total energy of the activating pulse, and the gap length is chosen when fabricating the device. As expected, higher pulse energy and carrier mobility lead to higher conductance. The impedance of the gap depends on the square of the gap length. Therefore it is advantageous to have devices with the distance between electrodes as short as possible, for efficient switching to occur.

For the discharge line arrangement shown in figure 3.2, the amplitude V_m of the voltage pulse measured at the 50Ω oscilloscope (load) is given by:

$$V_m = V_a \times \frac{50}{100+G^{-1}} \qquad (3)$$

where the electrodes are assumed ideal. Therefore the conductance can be determined experimentally, and expression (2) can be used to provide information about the mobility of carriers in the semiconductor. Conversely, if the mobility is known, the switch can be used to measure the energy content of the light pulse. Since the capacitance of the switching devices is small ($\sim 10^{-2}$ -10^{-1} pF), the impedance is almost entirely resistive, and $Z = 1/G \simeq R$.

The switching efficiency η can be defined as the ratio between the voltage actually switched by the semiconductor device and the maximum that could be obtained for the particular configuration employed. For the discharge line configuration, expression (3) gives

$$\eta = \frac{V_m}{V_a/2} = \frac{100}{100 + Z} \qquad (4)$$

If the impedance Z becomes negligible compared to 100Ω, the efficiency is unity and the voltage measured at the load equals half of the voltage applied. For the travelling wave arrangement, since the bias is pulsed,

$$\eta \equiv \frac{V_m}{V_a} = \frac{50}{50 + Z} \qquad (5)$$

where the impedance of the oscilloscope (load) is still assumed to be 50Ω. In this case, the impedance Z of the device should become much smaller than 50Ω, since for this configuration twice as much current can flow across the switch, and therefore more carriers are required for the same switching efficiency. Expressions (2), (4) and (5) relate the different parameters involved in the activation of the device to the efficiency of the process.

Using equation (2), it is worthwhile to calculate the energy necessary to activate a Si switch with 1.06μm radiation. For a 1mm gap length, and with the values $n_r = 3.6$, $\mu_e + \mu_p = 2 \times 10^3 cm^2 V^{-1} s^{-1}$ and $h\nu/e = 1.17V$,

$$\varepsilon G^{-1} = 9\mu J \times \Omega$$

If a resistance of 5Ω or less is to be obtained,

$$\varepsilon \gtrsim 2\mu J.$$

In practice the energy of the light pulse used should be at least ten times greater to ensure fully covering the gap area with a laser pulse of reasonable uniform intensity distribution and to saturate the device.

Finally, it should be pointed out that for fast recombination time semiconductors, care must be taken when measuring the voltage switched. For single shot oscilloscopes with risetimes $\sim 100^s$ps, the voltage pulses displayed have lower amplitude than the voltage pulses actually switched by for instance semi-insulating GaAs, GaP and InP devices. The voltage pulses then appear integrated, and this fact should be taken into account when the conductance of the device and the

switching efficiency are determined.

3.5 High Voltage Switching

It was soon realized that in order to fully exploit the potential capabilities of picosecond semiconductor switching devices, the range of voltages switched should be extended. Large amplitude electrical signals of picosecond risetime find numerous applications in ultrafast pulse technology and some of these applications are described in detail in chapters 5, 6 and 7. In this section, a summary of the other results obtained with picosecond high voltage devices reported in the literature is presented.

The first kilovolt semiconductor switch demonstrated by Le Fur and Auston [44]. A nearly intrinsic Si device was activated by a single 0.53μm wavelength light pulse. A bias of 1.5KV was used, but it had to be pulsed, in order to prevent electrical breakdown across the 0.7mm gap. The voltage pulse applied lasted for 25ns. Unlike the discharge line, with this travelling wave arrangement up to the full bias amplitude can be switched and thus a 1.5KV pulse was produced with picosecond risetime. It was applied to a microstrip transmission line formed on a crystal of $LiTaO_3$ used as a Pockel's cell. A linearly polarized light pulse was diffused and illuminated entirely one of the side faces of the crystal.

Initially all the light transmitted by the crystal was rejected by an analysing polarizer. As the voltage pulse propagated along the microstrip, the polarization of the diffuse light pulse was rotated by the Pockel's cell. Some light passed then through the analysing polarizer, and was recorded on film. The light pulse was delayed, and

a sequence of photographs was taken for different delays, one for each laser shot. In this way the propagation of the high voltage pulse along the Pockel's cell could be studied. Each record showed a bright region, which corresponded to the part of the crystal where voltage was already applied, and a dark one, where no voltage was yet present. The transition between the dark and bright regions represented the risetime of the Pockel's cell, which was determined to be ∿ 25ps. This value is an upper limit for the risetime of the voltage pulses switched by the Si device.

The results obtained by Le Fur and Auston proved that:

1. Semiconductor switching devices were capable of handling high voltages.
2. The kilovolt pulse switched had picosecond risetime.
3. The high voltage pulse could be used to activate ultrafast electro-optical components, such as Pockel's cells.
4. The overall risetime of the system was still of ∿ picoseconds.

The experiment also showed that thermal effects in crystalline Si were overcome by a pulsed bias lasting for few nanoseconds.

The undesirable thermal effects observed for Si are greatly reduced for semi-insulating GaAs. Lee[13] used this semiconductor biased to up to 5KV d.c. However, the highest voltage switched was ∿600V, due to the reduction in switching efficiency for intense electric fields. Since then, up to ∿ 4KV voltage pulses have been switched by d.c. biased GaAs devices, activated by energetic Nd:Yag laser pulses of 1.06μm [45]. Voltages as high as 5KV have been obtained with travelling pulse biased GaAs switches activated by a flashlamp pumped R6G dye laser.

The d.c. hold off capability of other semi-insulating III-V

compounds is also high, and therefore pulsed bias is usually not required. As an illustration, high voltage switching by a GaP device is demonstrated in figure 3.5. A d.c. bias of 2.8KV was applied to the 2mm gap switch.

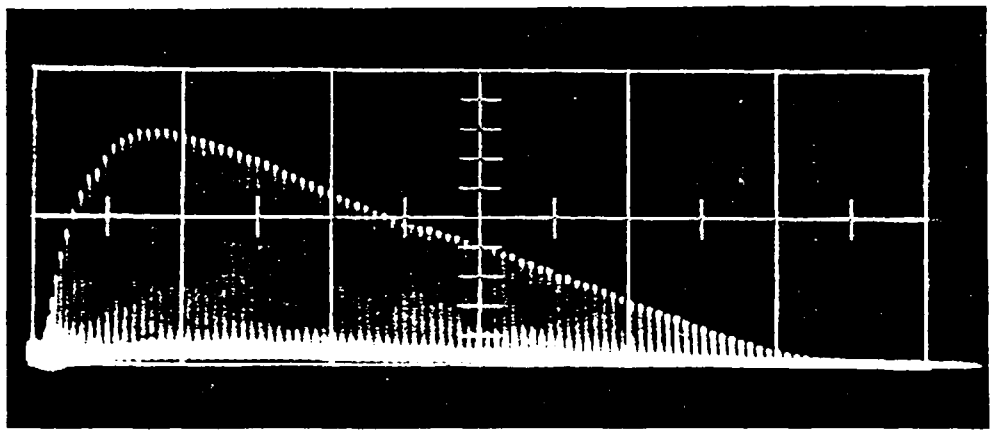

FIG 3.5 Oscillogram showing the response of a GaP switch to a mode-locked train of pulses of 0.53μm wavelength. The voltage and time scales are 1KV/div and 100ns/div, respectively.

The device was illuminated by the second harmonic of a mode-locked Nd: phosphate glass laser. The individual pulses of the train can be clearly resolved, which confirms the fast recovery time of the GaP switch. The peak voltage in the oscillogram shown is ∿1.4KV, which is the maximum that can be switched for the particular configuration used. Typically a 2mm gap GaP device will hold-off a d.c. bias voltage of ∿3KV, but if the bias is pulsed for a few nanoseconds, much higher voltages can be applied. Also the full amplitude can be switched, compared to just half in a charged line configuration, as pointed out earlier. Using a 7ns duration bias, up to 5KV picosecond voltage pulses were switched with a 2mm gap device [46].

In order to apply d.c. high voltages to the solid-state switching devices, the configuration described by Auston is no longer appropriate. Thin semiconductor substrates are not capable of holding off several kilovolts, since breakdown develops through the slab, between the input electrode and the ground plane. It has been demonstrated [13] that an insulating substrate should be introduced between the thin semiconductor chip and the ground plane. The switch

then exhibited high voltage hold off, and the 50Ω microstrip transmission line structure could be maintained. This configuration was adopted in all the high voltage experiments, and also in most of the low voltage applications described in the following chapters.

A coaxial structure has also been demonstrated. A section of the center electrode of a conventional HN connector was replaced by a cylindrical semiconductor piece. A window was provided on the connector body, through which light illuminated the chip. The risetimes of these coaxial devices were shown to be comparable to the risetimes measured for the microstrip switches. Up to 10KV voltages have been held off for a few nanoseconds, and efficiently switched by coaxial Si devices [47].

It is apparent from the preceeding section that the gap between the input and output electrodes of the switch should be as short as possible for high switching efficiencies. However, short lengths have associated high electric fields across the gap, leading in many cases to electrical breakdown. This is a serious problem, particularly when high voltages are required, or very weak laser pulses are available. In order to maintain the electric field below the threshold value for electric breakdown, long gaps have to be used for high voltage applications. The switching efficiency is then low, and energetic laser pulses are required to activate the devices. Conversely, if weak activating light pulses are used, the gap lengths have to be short, and only low voltages can then be applied. The threshold for electric breakdown will again determine the minimum gap length that can be used. Typical values range from a few millimeters for high voltage devices, to a few microns for applications in conjunction with CW mode-locked lasers.

Heat is the major cause for premature breakdown in nearly intrinsic Si devices. Thermal problems, however, are greatly reduced at cryogenic temperatures, c.f. section 5.3. At room temperatures thermal carrier generation can be avoided to a great extent by pulsing the voltage bias for a short time. In some cases a short duration bias pulse is not a serious limitation. In Chapter 5, a system is discussed in which the bias of a Si switch lasts for only $\lesssim$ 10ns and the breakdown spark does not have time to develop. It has been demonstrated, however, that Si switches with $\sim$ mm gap lengths can hold off a few kilovolts for several microseconds [45]. After this time the resistivity of the slab is considerably reduced by thermally excited carriers. It was observed that the risetime of the long voltage pulse applied to the device should be slower than the dielectric relaxation time, which is $\sim$ 10-40ns for Si [48]. The synchronization of microsecond long voltage pulses with the arrival of the light at the switch can be easily achieved. Also, the amplitude of the bias can be very stable. Systems incorporating Si switches with μs duration bias can exhibit excellent performance [49].

Recently picosecond switching devices have been extensively used in conjunction with Kerr and Pockel's cells. The optical transmission of a Kerr cell has been examined [50] and the risetime of commercial Pockel's cells have been measured [45, 47]. A high voltage GaAs switch was also used to drive a Pockel's cell in an active pulse shaping technique [51]. The light pulse sliced had a risetime of 40ps and FWHM duration of 70ps. A high voltage Si device was employed to drive three Pockel's cells in series [48]. The arrangement had picosecond synchronization and showed a contrast ratio of 10^9. It was used to suppress low light intensity preceeding the main laser pulse for a laser fusion system. Other experiments reporting the use of high

voltage picosecond switches to activate Pockel's cells [52, 53] will be discussed in detail in chapter 7.

3.6 Conclusion

The most important parameters of different semiconductors that have so far been demonstrated in picosecond switching device construction are summarized in table 3.1. The resistivities quoted are typical values at room temperature of samples obtained commercially, or as reported in the literature. The recovery times are approximate because they depend on many factors, such as doping of the crystal and light intensities used. The mobility of carriers quoted for GaAs and InP is significantly reduced for high electric fields.

It is now apparent that almost any crystalline semiconductor showing high resistivity can be used in picosecond switching devices. Depending on the particular application for which the devices are intended, other parameters, such as recombination time and energy gap became important. The choice of materials will have constraints imposed by the mode-locked laser used to activate the switch, since the energy of the laser pulse determines a minimum mobility of carriers for efficient switching to take place, as discussed in section 3.4. Also, the wavelength of the light pulses defines a maximum energy gap, in the choice of semiconductor. Finally, but not least important, availability and price of the materials have to be taken into consideration.

The extension of picosecond switching techniques to high voltage devices greatly widened the possible applications of semiconductor switches. Their compatibility with several different laser systems, and the intrinsic picosecond synchronization between light and voltage is

exploited in the chapters that follow. Before then, however, an evaluation of some characteristics of the switches, and a description of their construction is presented in chapter 4.

TABLE 3.1

SEMICONDUCTOR	ε_{gap}(eV)	ρ(Ωcm)	τ	$\mu(cm^2V^{-1}s^{-1})$
intrinsic Si	1.1	$\sim 10^4$	$\sim$ 10μs	$\sim$ 2000
s.i. GaAs	1.4	$\sim 10^7$	$\sim$ 100ps	$\sim$ 7000
s.i. GaP	2.3	$\sim 10^9$	$\sim$ 100ps	$\sim$ 300
s.i. InP	1.3	$\sim 10^7$	$\sim$ 50ps	
s.i. $CdS_{0.5}Se_{0.5}$	2.0	$\sim 10^7$	∿20ns to 20ms	$\sim$ 400

References - Chapter 3

[1] D.H. Auston, S. McAfee, C.V. Shank, E.P. Ippen, O. Teschke; Solid State Electronics 21, 147 (1978).

[2] W. Sibbett, J.R. Taylor, D. Welford; IEEE J. Quantum Elect. QE17, 500(1981).

[3] S. L. Shapiro, R.C. Hyer, A.J. Campillo; Phys. Rev. Lett., 33, 513 (1974).

[4] See for instance Ultrashort Light Pulses, Topics in Appl. Phys. Vol 18, ed. by S.L. Shapiro, Springer-Verlag, NY (1977).

[5] D.H. Auston, ibid, chapter 4.

[6] M. Bass, P.A. Franken, J.F. Ward, G. Weinreich; Phys. Rev. Lett., 9, 466 (1962)

[7] D.H. Auston, A.M. Glass; Appl. Phys. Lett., 28, 398 (1972).

[8] D.H. Auston; Appl. Phys. Lett., 26, 101 (1975)

[9] A. Antonetti, A. Mingus, M.M. Malley, G. Mourou; Opt. Commun., 23, 435 (1977).

[10] R. Bube; Photoconductivity of Solids, John Wiley and Sons, NY (1960)

[11] W. Platte; Elect. Lett., 12, 437 (1976)

[12] R. Castagné, S. Laval, R. Laval; Elect. Lett., 12, 438 (1976)

[13] Chi H. Lee; Appl. Phys. Lett., 30, 84 (1977)

[14] S. Jayaraman, Chi H. Lee; Appl. Phys. Lett., 20, 392 (1972)

[15] V. K. Mathur, S. Rogers; Appl. Phys. Lett., 31, 765 (1977)

[16] Chi H. Lee, A. Antonetti, G. Mourou; Opt. Commun., 21, 158 (1977)

[17] R.A. Lawton, A. Scavannec; Elect. Letters, 11, 74 (1975)

[18] N.Holonyak Jr., M.H. Lee; in Semiconductors and Semimetals vol 14 ed. by R.K. Willardson, A.C. Beer, Academic Press, NY (1967) p.5.

[19] S. Laval, C. Bru, R. Castagné, R. Arnodo; 1980 International Conf. on GaAs and Related Compounds, Vienna, Austria.

[20] J.B. Gunn; Solid State Commun., 1, 88 (1963)

[21] B.K. Ridley, T.B. Watkins; Proc. Phys. Soc., 78, 293 (1961)

[22] D.J. Bradley, M.B. Holbrook, W.E. Sleat; IEEE J. Quantum Elect. QE17, 658 (1981)

[23] H. Mathieu, P. Merle, E.L. Ameziane, B. Archilla, J. Camassell, G. Poibland; Phys. Rev B 19, 2209 (1979)

[24] E.J. Johnson; Chapter 6 in Semiconductors and Semimetals Vol 3, Optical Properties of III-V Compounds, Edited by R.K. Willardson and A.C. Beer, Academic Press, NY (1967)

[25] J.O. Dimmock; Chapter 7 in Semiconductor and Semimetals Vol 3 Optical Properties of III-V Compounds, Edited by R.K. Willardson and A.C. Beer, Academic Press, NY (1967).

[26] V.K. Mathur, Chi H. Lee; J.Appl. Phys. 51, 1634 (1980)

[27] K. Murakami, K. Gamo, S. Namba, M. Kawabe, Y. Aoyagi; Appl. Phys. Lett., 35, 628 (1979)

[28] P.L. Liu, R. Yen, N. Bloembergen, R.T. Hodgson; Appl. Phys. Lett., 34, 864 (1979)

[29] F.J. Leonberger, P.F. Moulton; Appl. Phys. Lett., 35, 712 (1979)

[30] J. Degani, R.F. Leheny, R.E. Nahory, M.A. Pollack, J.P. Heritage, J.C. DeWinter; Appl. Phys. Lett., 38, 27 (1981)

[31] P.S. Mak, V.K. Mathur, Chi. H. Lee; Optics Commun., 32, 485 (1980)

[32] V.K. Mathur, P.S. Mak, Chi. H. Lee; J. Appl. Phys. 51, 4889 (1980)

[33] I.M. Catalano, A. Cingolani, A. Minafro; Phys. Rev B 9, 707 (1974)

[34] Chi H. Lee, S. Jayaraman; Opto-Electronics 6, 115 (1974).

[35] C.K.N. Patel; Appl. Phys. Lett 18, 25 (1971)

[36] Chi H. Lee, P.S. Mak; p93 in Picosecond Phenomena II, Chemical Physics 14, ed. by R.M. Hochstrasser, W. Kaiser, C.V. Shank, Springer-Verlag NY (1980).

[37] D.H. Auston, P.Lavallard, N.Sol, D. Kaplan; Appl. Phys. Lett 36, 66 (1980)

[38] D.H. Auston, A.M. Johnson, P.R. Smith, J.C. Bean; Appl. Phys. Lett., 37, 371 (1980).

[39] D.H. Auston, P.R. Smith, A.M. Johnson, W.M. Augustyniak; p.71 in Picosecond Phenomena II-Chemical Physics 14, ed. by R.M. Hochstrasser, W. Kaiser, C.V. Shank, Springer-Verlag NY (1980).

[40] P.R. Smith, D.H. Auston, A.M. Johnson; Rev. Sci. Instrum., 52 138 (1981)

[41] A.M. Johnson, D.H. Auston, P.R. Smith, J.C. Bean, J.P. Harbison, D. Kaplan; p. 285, ibid.

[42] P.R. Smith, D.H. Auston, A.M. Johnson, W.M. Augustyniak; Appl. Phys. Lett., 38,47 (1981)

[43] J.D. Jackson; Classical Electrodynamics, 2nd ed, p. 281, J. Wiley and Sons, NY (1975).

[44] P. LeFur, D.H. Auston; Appl. Phys. Lett., 28, 21 (1976)

[45] G. Mourou, W. Knox; Appl. Phys. Lett., 35, 492 (1979).

[46] W. Margulis, W. Sibbett; Opt. Commun., 37, 224 (1981).

[47] A. Antonetti, M.M. Malley, G. Mourou, A. Orszag; Optics Commun., 23, 435 (1977)

[48] G. Mourou, J. Bunkenburg, W. Seka; Optics Commun., 34, 252 (1980)

[49] G. Mourou, W. Knox; Appl. Phys. Lett., 36, 623 (1980)

[50] M. Stavola, J. Agostinelli, M. Sceats; Appl.Optics 18, 4101 (1979)

[51] J. Agostinelli, G. Mourou, C.W. Gabel; Appl. Phys. Lett., 35, 731 (1979)

[52] W. Margulis, W. Sibbett, J.R. Taylor; Optics Commun., 35, 153 (1980)

[53] G. Reksten, T. Varghese, W. Margulis; Appl. Phys. Lett., 39, 129 (1981)

CHAPTER 4

CONSTRUCTION AND EVALUATION

4.1 Introduction

There are two ways of tackling the problems posed by the construction of the semiconductor switches: either by carefully studying all the possible limitations and difficulties that might occur in their application, and deciding a priori on the best configuration, so that the switches actually constructed are as near to the ideal as possible; or alternatively, choosing a configuration which is not perfect, but allows a series of experiments to be readily carried out, and trying to optimize the design of the devices only when serious limitations are encountered. The choice of approach will depend on the objective one has. If it is desired to reach the best possible performance with a particular semiconductor switch, so as to be able to study the intrinsic limitations imposed by e.g. the choice of semiconductor, the geometry, the activating laser pulse, and others, the first approach should be chosen. If, on the other hand, the major interest is to exemplify different applications of solid-state switching devices, and in particular, with a limited time period in mind, then a more pragmatic attitude must prevail.

The switches were fabricated following a very simple procedure, and the configuration was chosen as to allow maximum versatility in their construction. The reasons leading to this approach are not only the interest in different applications and the limited time available, but also the ignorance of important facts which would otherwise have prevented the construction of a nearly ideal device. For instance, the

perfect semiconductor switch should have ohmic contacts, and to fabricate ohmic semiconductor-metal junctions is not a trivial problem. Also, as often happens, most major difficulties were only discovered much after the experimental work had started.

Evaluating the performance of the switches can be best done in the actual experiments. However, it is of interest in many cases to determine physically important parameters, such as the recombination time of carriers in a particular semiconductor. In these instances, a separate measurement was carried out.

In the following sections of this chapter, the fabrication of the switches is described. An evaluation of the switching performance, and some physical aspects of the photoconduction mechanisms involved in the creation of carriers are also discussed.

4.2 Microstrip Configuration

As mentioned in section 3.5, the configuration which was adopted in nearly all experiments described in this thesis was originally proposed by Lee [1]. A piece of semiconductor was mounted on an insulating substrate interrupting a 50Ω transmission line. The substrate used was double-sided printed circuit board (PCB), which is cheap, easily available, easy to handle, allows a rapid and reproducible fabrication of a 50Ω microstrip, can hold-off several kilovolts, and allows direct soldering of the input and output coaxial cables to the transmission line, so that the impedance mismatch introduced is minimal. The main disadvantage of PCB is that dispersion losses of very high frequency Fourier components of the voltage pulses switched is higher than for thinner substrates. In other words, the risetime of the voltage

pulses obtained at the semiconductor becomes longer as the signal propagates along the microstrip. However, the length of the transmission line that existed between the semiconductor chip and the output cable was typically $\lesssim$ 1cm, so picosecond risetimes were still obtained.

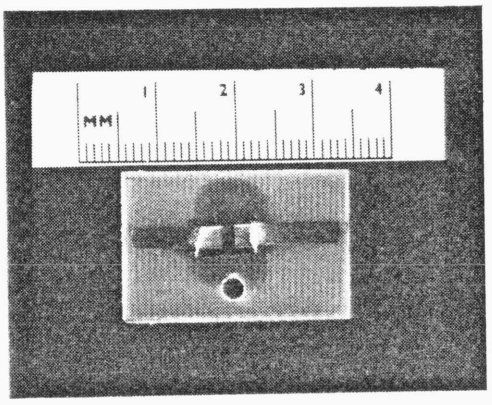

FIG 4.1

An example of a semiconductor switch can be seen in figure 4.1. The device shown has a chip of nearly intrinsic Si, and the gap length is 1mm. A similar switch was used in the application described in chapter 5.

4.2.1 Impedance Matching

In order to obtain ultrafast risetimes it is important to match the impedance of the switch to that of the input and output cables, which was 50Ω. There are a number of expressions relating the different parameters of a microstrip, such as width of the line W, thickness of the dielectric substrate h, dielectric constant ε_r, thickness of the conductive strip t, and the impedance Z_o. The most accurate relations are obtained semi-empirically due to the complexity of the theory of microstrips [2, 3, 4]. The formulas which were used to determine the appropriate width of the strip conductor that should be used for a 50Ω impedance were obtained from the review on design of microstrip lines by Bahl and Trivedi [5].

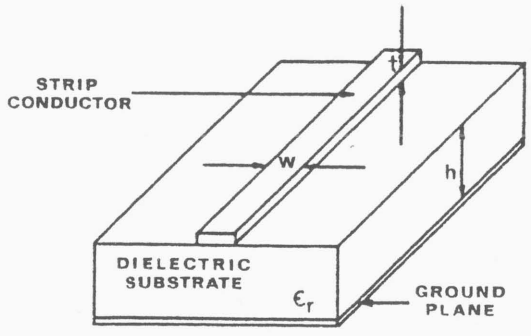

The dielectric constant of the double-sided printed circuit board was 4.8, and the thickness of the dielectric substrate was 1.64mm. The ratio between the width of the line and the thickness of the insulator is given by

$$W/h = \frac{8 \exp(A)}{\exp(2A)-2} \qquad (1)$$

where

$$A = \frac{Z_o}{60}\sqrt{\frac{\varepsilon_r + 1}{2}} + \frac{\varepsilon_r - 1}{\varepsilon_r + 1}\,(0.23+0.11/\varepsilon_r).$$

Conversely, for a given ratio W/h, the impedance of the line can be calculated with the expression

$$Z_o = \frac{120\pi\sqrt{\varepsilon_{eff}}}{W/h+1.393+0.667\ln(W/h+1.444)} \qquad (2)$$

where ε_{eff} is an effective dielectric constant which is lower than the relative dielectric constant ε_r of the material, and takes into account the degree of confinement of the electromagnetic field inside the substrate. ε_{eff} is related to ε_r by

$$\varepsilon_{eff} = \frac{\varepsilon_r+1}{2} + \frac{\varepsilon_r-1}{2}\,(1 + 12\,h/W)^{-\frac{1}{2}}$$

In order to obtain an impedance of 50Ω, from equation (1) A = 1.58, W/h = 1.79, and therefore the width of the strip conductor should be 2.94mm.

Both the finite thickness of the strip conductor and dispersion in the line were neglected in the above calculation, and it is worthwhile to evaluate how serious these approximations are. For PCB, the effective width of the line W_e can be calculated if the thickness of the conductor (t) is known, according to the expression:

$$\frac{W_e}{h} = \frac{W}{h} + \frac{t}{\pi h}\left(1 + \ell n \frac{2h}{t}\right)$$

For a copper thickness of 0.1mm, the effective width is 3.08mm, which from (2) corresponds to an impedance of 49Ω. More considerable is the mismatch existent at the semiconductor chip. If a relatively thick crystal is used, the impedance of the transmission line will no longer be 50Ω, even if the semiconductor is fully activated by the light pulse. The effect of the thickness of a Si crystal on the impedance of the line can be calculated, assuming that it is illuminated by an intense pulse of 1.06μm radiation, such that the entire bulk of the semiconductor becomes conducting. For a 0.5mm thick slab, W_e = 3.4mm, and the corresponding impedance of the line is then 46Ω. Therefore, even in this case, the effect of the thickness of the slab is relatively small, and can be neglected in a first approximation.

The problems caused by dispersion are much more serious. The electrical signal which propagates along the transmission line can be expressed in terms of its Fourier components, and for high frequencies the dispersion becomes significant. Expresssions for the effective dielectric constant and for the impedance of the line as a function of the frequency f are also given in [5]:

$$\varepsilon_{eff}(f) = \varepsilon_r - \frac{\varepsilon_r - \varepsilon_{eff}}{1+G(f/f_p)^2} \qquad (3)$$

where $f_p = \frac{Z_o}{8\pi h}$, $G = 0.6+0.009\ Z_o$, and f is expressed in GHz and h in cm,

and

$$Z_o(f) = \frac{377h}{W_{eff}(f)\sqrt{\varepsilon_{eff}(f)}} \qquad (4)$$

where the effective width of the line is given by

$$W_{eff}(f) = W + \frac{W_{eff}(0)-W}{1+(f/f_p)^2} \qquad (5)$$

and $W_{eff}(0)$ can be obtained from equation (4), making f = 0. A simple computer program was written, and the effect of the dispersion on ε_{eff} and on the impedance of the line was calculated for different values of f.

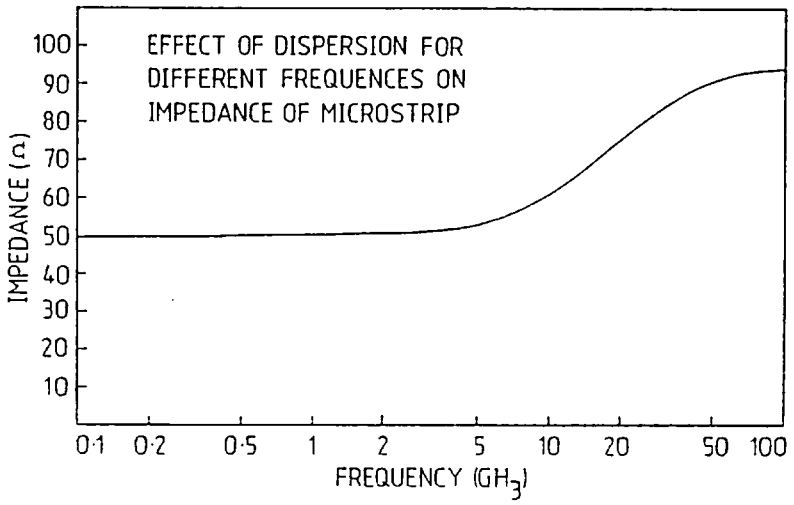

FIG 4.2 Effect of dispersion on the microstrip impedance

Figure 4.2 shows a plot on a semi-log scale of the variation of the impedance with the frequency of the signal travelling in the microstrip. The impedance of the microstrip is nearly 50Ω for frequencies ranging from 0Hz(d.c.) to up to a few GHz, but at 20GHz it is already 75Ω. For a 10ps risetime (corresponding to an upper frequency of ∿40GHz), the impedance experienced by different Fourier components will vary from 50Ω to ∿90Ω. Therefore dispersion will play an important role in limiting the fastest possible overall speed of the switch, and the length of the microstrip transmission line should be kept short, in order to minimize the loss of speed and sharpness of the leading edge of the voltage pulse switched.*

*(The dispersion relations (3),(4) and (5) should hold for substrates which are thin in comparison with $\lambda(=c_n/f)$ [6]. For a frequency ∿40GHz and $c_n=1.4 \times 10^{10}cms^{-1}$, λ=3.5mm, and therefore the thickness of the substrate (1.64mm) is not significantly smaller than λ. Also, these semi-impirical relations have not been tested experimentally for frequencies much higher than 10GHz. As a consequence, no numerical estimate for the risetime should be derived, but only qualitative conclusions should be drawn from the values calculated).

According to [5], the accuracy of expressions (1) and (2) is better than 1% provided dispersion can be neglected. Nevertheless, and independent experimental test was carried out to verify that the impedance of the microstrip constructed on the printed circuit board was in fact 50Ω. A time domain reflectometer (Tektronix 1S2 sampling unit) with a 100ps time resolution was employed to test a ∿15cm long stripline of 3.0mm width, which was fabricated on PCB. Fine adjustments of impedance were made, slightly altering the width of the conductive line with an additional thin strip of silver paint in contact with the copper. The results showed that a 3.0mm wide microstrip exhibited an impedance of 50Ω to within the experimental error of the measurement (< 5 %), and was therefore the width of the microstrips constructed throughout the work.

4.3 Preparation of the Semiconductor Switches

The fabrication of solid-state switching devices included the preparation of the microstrip transmission line and of the semiconductor chip (by cutting the crystal, polishing one or both faces, cleaning the slab, evaporating the electrodes and subjecting it to thermal treatment), and finally mounting it in the microstrip arrangement. Each one of these processes is described separately.

4.3.1 Cutting

The semiconductors that were used throughout the work were bought commercially (nearly intrinsic Si from Topsil Ltd, and semi-insulating GaAs and GaP from MCP Electronics Ltd). The crystals measured ∿ 3-6cm^2 and could therefore be cut into several slabs

adequate for fabricating the opto-electronic switches. Although the semiconductors were very brittle and could be cleaved, this process required a knowledge of the crystallographic directions of the materials. Furthermore, it was of interest to obtain slabs of nearly rectangular shape and of selected length and width. Therefore the crystals were waxed on to a thick block of glass, and cut with a diamond saw. The width of the blade was 0.5mm, and as a consequence some material was wasted. After cutting the semiconductor, the glass block was heated on a hot-plate which melted the wax, the several slabs were carefully removed with the use of twezers, and were finally immersed into a solvent, such as acetone, or more usually ethanol. In most cases the chips measured $\sim$ 4-7mm x 4mm, although smaller sizes were sometimes used.

4.3.2 Polishing

The procedure adopted for polishing varied from material to materials and the quality of the polish depended on the application for which the semiconductor was intended.

The crystals of GaAs were polished before being cut, and in some cases the semiconductor purchased already had a polished face. In general, however, the crystal was waxed to a flat disk of glass, and ground with successively finer grades of Alumina grounding compound (Linde A, C and B). The process was rather long, and it was done on a pitch of wax. The coarsest scratches on the polished face which resulted were thinner than 0.05μm, and the thickness of the semiconductor was reduced from 0.5mm and 0.25mm.

In the majority of the cases, the Si switches were activated by light pulses of 1.06μm, and since at this wavelength the penetration depth is quite long (c.f. figure 3.1), it is bulk rather than surface

conductivity the most important mechanism for transport of current. Therefore, it is doubtful that the top surface of the slab had to be polished for proper operation and in fact no significant detrimental effect was observed in early experiments, when the slab had rough surfaces. However, in order to minimize the differences from slab-to-slab and to allow the fabrication of better contacts, the Si crystals were also polished, following a similar procedure to that for GaAs. The resulting quality was not as good as for GaAs, due to the use of a paper pitch, leaving the crystals with an "orange-peel" structure.

The GaP crystals were much softer than GaAs or Si, and could be polished in $\lesssim$ 1hr. When water was used as a vehicle for the Linde powder, a strong smell was produced, which could be due to a hazardous compound. The replacement of water by parafin eliminated this problem, and when both surfaces of the GaP crystal were polished, the semiconductor was transparent with an orange colour.

4.3.3 Cleaning

After the slabs had been cut and polished, all the oil (from the diamond saw), wax and other contaminants where removed by a careful cleaning procedure. In some cases this process was reduced to a simple immersion of the semiconductor chip in ether, and then into either ethanol or methanol. The steps involved in the complete cleaning procedure are as follows: 1) Warm chip in Inhibisol for ~1 min; 2)Bring to boiling point in absolute alcohol; 3) Place chip in a perforated vessel of polythene, and immense it in a silver etch (0.5ℓ of HF,0.5ℓ of HNO_3, 100mg of $AgNO_3$) for ~ 30s; 4) Wash chip thoroughly in distilled water; 5) Bring to boiling point in absolute alcohol; 6) Store chip in alcohol. Sometimes the semiconductor was immersed in ether and placed

in an ultrasonic cleaner for a few minutes, prior to the steps described above. This complete procedure [7] which was originally developed for Si, was also sometimes used for GaAs.

4.3.4 Evaporation

The electrodes were usually prepared on the semiconductor by evaporation. A chamber was evacuated to $\sim 10^{-5} - 10^{-6}$ torr, and the chip was placed $\sim$ 30cm above the metal vapour source. In order to leave a gap between the electrodes, a mask was used to prevent the deposition of metal on part of the chip. It usually consisted of a copper wire, the diameter of which defined the gap length. The width of the metallic electrodes was also determined by masking, and was nearly always 3.0mm, so that the microstrip width did not change at the slab.

Various metals were evaporated, depending on the semiconductor used. Usually Al electrodes were employed, sometimes preceeded by a thin layer of In which was depositied to improve the adhesion, particularly for Si. When GaAs or GaP switches were prepared, a single metal was evaporated (Al, Au or Ag). The technique used for the deposition is standard, consisting in heating a sample of the metal to be evaporated either on a tungsten wire (Al), platinum coated molybdenum wire (Ag), tungsten spiral (Au), or on a molybdenum boat (In). The thick layer of metal (except for In) was deposited quickly ($\lesssim$ 15s), over the substrate at room temperature. The evaporation procedure adopted was simple, and the metal usually used (Al) was chosen for its availability and low price.

In some cases the electrodes were prepared by depositing a layer of conductive paint directly on the semiconductor. The quality of the contacts formed in this way was poorer, but the switches could be

readily fabricated. The voltage hold-off across the gap was lower (probably due to irregularities on the edge of the electrode), and the contacts were non-ohmic. Related effects are discussed in further detail in section 4.6.1.

4.3.5 Heat treatment

Following evaporation, the crystals were usually submitted to a heat treatment at 300C for 90s. This procedure was used for all Si chips which were coated with both In and Al. Although the heat treatment can improve the adhesion between the metals and the semiconductor due to diffusion, the temperature used was not high enough to allow the creation of an alloy between the Al and the Si, which happens at 577C [8, 9]. Also, because of the technological difficulties involved, the Si crystals were not doped at the electrodes, and therefore the contacts were not ohmic.

Some of the GaAs slabs provided with Al electrodes were also submitted to heat treatment of $\sim$ 300C, and although this temperature is relatively low, it is known that outdiffusion of Ga and indiffusion of Al take place [10, 11], and more reproducible (yet still Schottky) contacts are produced [12].

4.3.6 Mounting

Once the semiconductor chip was prepared, it was mounted on the microstrip which had previously been prepared on a double sided printed circuit board, typically measuring $\sim$ 2-3cm x 2cm. The fabrication of the microstrip on the board involved 4 steps. (1) The PCB was cleaned, and had a 3.0mm wide protective strip of plastic transfer applied along one face. The strip was interrupted at the centre for

$\sim$ 7mm, so as to allow the chip to be placed later. (2) The bottom face of the board was totally covered by a layer of varnish and left to dry. (3) The PCB was immersed in an etching solution (250mg Fe_2Cl_3, 50ml of HCl and 2.5l of H_2O) for $\sim$ 20 minutes. (4) After the etching had been completed, the printed circuit was thoroughly washed, and the protection for the copper was removed with ether and acetone. The width of the microstrip formed by this process was usually accurate to within $\pm$ 5%, and its impedance was very nearly 50Ω.

A small piece of optical wax was melted between the two copper strips with a hot-air blower or by heating the board on a hot plate. The semiconductor chip was placed on the melted wax with tweezers and left to cool for a few minutes. Very thin layers of wax ($\sim$ 1-10μm) were found to firmly secure the chip to the PCB, and when necessary the slab could be easily removed.

The electric connection between the metallic electrodes on the semiconductor and the copper strips of the board was made by a conductive paint (JMC 1402) containing 70% of silver. This compound dried in $\sim$ 1hr.

In order to launch the voltage pulses switched into 50Ω coaxial cables, connectors (such as BNC) were originally soldered to the copper strips of the PCB. Since time-domain reflectometer (TDR) traces showed that the mismatch was appreciable, the connectors were removed and the 50Ω coaxial cables were directly soldered to the PCB. The impedance was then very well matched, provided the exposed length of coaxial cable was $\lesssim$ 2mm. A comparison carried out with the time-domain reflectometer showed that if the semiconductor chip was fully saturated by the light pulse, the overall mismatch introduced by the switch was smaller than the one observed at a commercial through BNC (F-F) connector.

In a few applications when mode-locked CW lasers were used to activate the switching devices, a much smaller configuration was employed. The microstrip was fabricated directly on the semiconductor, and the width of the line was reduced to a fraction of a mm, to account for the different thickness of the substrate and different dielectric constant, and maintain the 50Ω impedance. In these cases a commercial microstrip wavequide launcher connected the device directly to the sampling oscilloscope.

4.4 Evaluation of Risetime and Recovery time

It is of primary interest to characterize the performance of semiconductor switches in terms of speed and recovery time, because this information can assist in the basic understanding of physical processes involved in the switching and also in the construction of better devices. In this section, the evaluation of the rise and fall times of the solid-state switches is described.

4.4.1 Direct measurements

The most convenient instrument with which to directly observe the time evolution of an electrical signal is the oscilloscope. Therefore, "direct measurements" of the switching characteristics are carried out by connecting the output of the device to a fast oscilloscope, and monitoring the voltage switched as a function of time. One of such measurements is shown in figure 4.3a, which is an oscillogram of the signal switched by a nearly intrinsic Si device when illuminated by picosecond light pulses. The time scale is 50ns/div, and it is clear that the fast risetime is followed by a long recovery, because of the slow decay of the electrical signal ($\sim$ 1.5μs FWHM). In this case it is

apparent that oscilloscope measurements allow the direct determination of the recombination time of carriers in the semiconductor, involving a simple experimental set up.

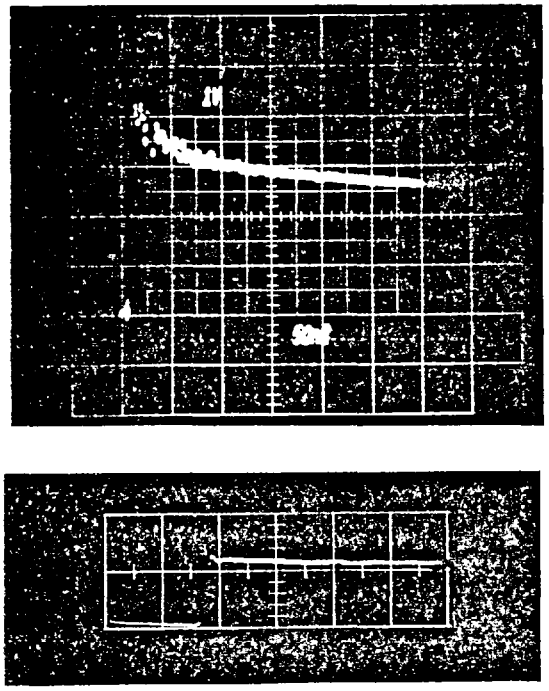

FIG 4.3 Response of a Si switch on 50ns/div(A) and on 2ns/div (B) time scale

Figure 4.3b shows the voltage switched by a Si device on a 2ns/div time scale, recorded on a Tektronix 519 oscilloscope (response time ∿0.3ns). It is apparent that it is not possible to determine the rise-time of the signal from the oscillogram, since the response of the switches is faster than the risetime of the single-shot oscilloscopes available. In fact, even the measurement of the recovery time of fast semiconductor can be oscilloscope limited, as illustrated in figure 4.4. A single pulse from a frequency doubled Nd:Phosphate glass laser was selected from the mode-locked train of pulses, and directed to a semi-insulating GaP switch, and the output signal was recorded on a storage oscilloscope (Tektronix 7834). The FWHM of the pulse is 0.70ns, and both the rise and the fall times of the signal displayed are significantly degraded by the limited frequency bandwidth of

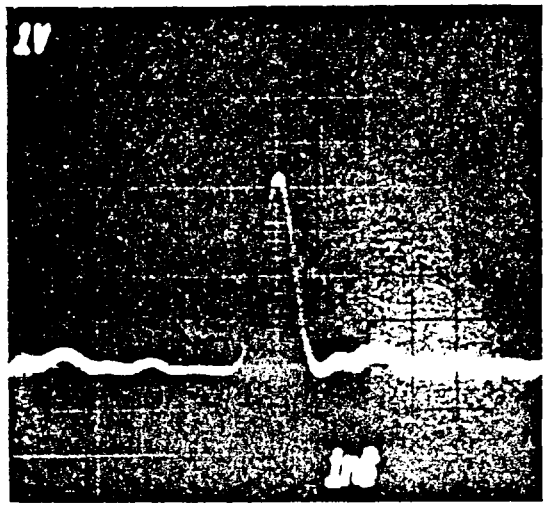

FIG 4.4 Response of a GaP switch to a single picosecond pulse on a 1ns/div time scale

the measuring instrument.

Although the energy of the light pulses used to activate semi-insluating GaAs or GaP switches was in several experiments high enough to saturate the device, the amplitude of the voltage pulses observed on the storage oscilloscope was always less than half of the d.c. applied, due to the slow response of the measuring equipment.

In order to be able to evaluate the switching efficiency and to estimate the recovery time of ultrafast semiconductor switches from oscilloscope measurements, a computer program was used to simulate the performance of the detector system. Initially, it was attempted to describe the oscilloscopes with a simple equivalent circuit, taking into account the limited risetime, fall time and 50Ω impedance for signals in a wide range of frequencies. However, it was found that a large number of components had to be introduced to approximately reproduce the shape of the voltage pulses observed on the oscillograms, and the model became so complicated that it lost its physical meaning. A different approach was then used, in which the response F(t) of the instrument to a step function applied at t = 0 was described mathmatically, taking into account the shape of the trace displayed, and its risetime. The response $V_s(t)$ of the oscilloscope to an arbitrary signal H(t) was then calculated numerically, by evaluating a convolution integral

$$V_s(t) = \int_o^t F(t-x)\, H'(x)dx - F(t)H(0), \qquad (6)$$

where H' is the time derivative of H, and F(t) H(0) provide the intial conditions [14].

Since the discharge line arrangement was widely used throughout the work, it is important to find an analytical expression relating the current delivered by the switch into a 50Ω transmission line to the

recombination time and the impedance of the semiconductor, following the illumination of the gap. Assuming that one of the carriers has a much more important contribution to the current than the other, that the recombination can be described by a single exponential decay in the number of free carriers, and that the risetime of the device can be neglected compared with the recombination time,

$$n(t) = N_o e^{-t/\tau}$$

Since the conductivity is proportional to the number of free carriers, i.e.,

$$\sigma = e\mu n,$$

it follows that the total conductance of the switch decays exponentially in time,

$$G(t) = G_o e^{-t/\tau}.$$

Therefore, since $Z(t) = G^{-1}(t)$, according to this model the impedance of the switch increases exponentially [13], i.e.,

$$Z(t) = Z_o e^{t/\tau}$$

where Z_o is the impedance of the device immediately after the impulse activation. Using Ohm's law for the circuit, for a 50Ω oscilloscope it is found that,

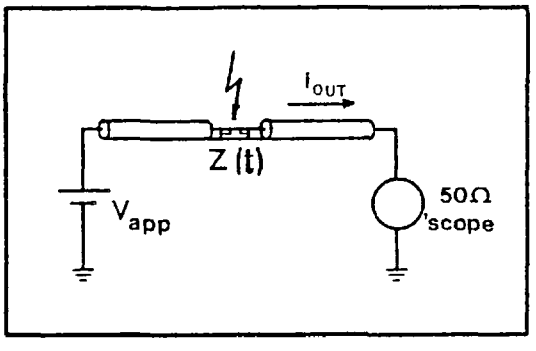

$$i_{out}(t) = \frac{V_{app}}{100+Z_o e^{t/\tau}}, \quad (7)$$

where it is assumed that the length of the cable connecting the switch to the power supply is relatively long ($2\ell >> c_n\tau$). It can be seen that the current switched decreases following the illumination, and for $t >> \tau$ it becomes negligible. The peak voltage that can be detected across the 50Ω load in this

configuration is $V_{app}/2$, and the voltage H(t) applied to the oscilloscope is given by:

$$H(t) = \frac{V_{app}}{100+Z_o e^{t/\tau}} \times 50.$$

Provided the impedance of the switch is always much larger than the 50Ω characteristic impedance of the circuit (i.e. for low light levels), H(t) decreases exponentially. However, if the switch is saturated by the activating pulse, the voltage applied to the oscilloscope is not an exponential, particularly for $t \lesssim \tau$. This is illustrated on figure 4.5, where the current switched by a device with $Z_o = 1\Omega$ is shown for five different values of τ, during the first two nanoseconds following the activation (still assuming negligible risetime). In this calculation it was assumed that a d.c. bias of 2KV was applied to the device, and it is seen that the peak voltage applied to the 50Ω oscilloscope is nearly 1KV for the various values of τ.

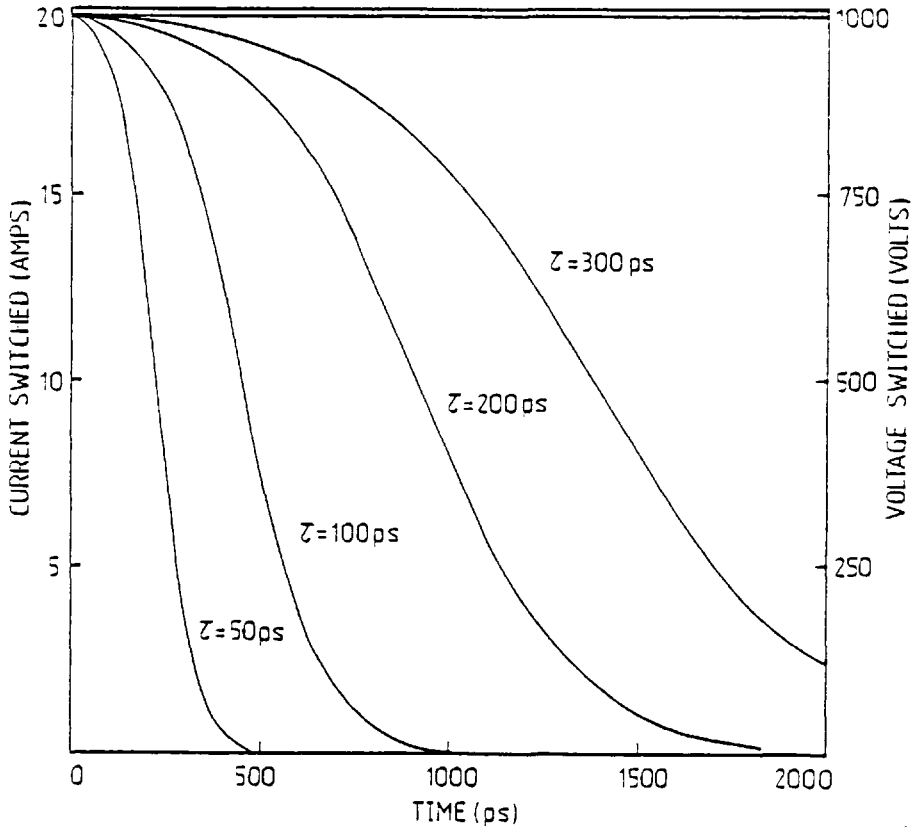

FIG 4.5 Voltage and current switched by a device with initial impedance $Z_o = 1\Omega$, for different values of τ.

In order to obtain the output traces corresponding to such input signals, it was assumed that the response of the oscilloscope to a unity step function could be well approximated by the function

$$F(t) = 1 - \frac{1}{1+Ae^{Bt}} \qquad (8)$$

which takes a value 1 for $t \to \infty$ and a very small value for $t = 0$, if A is sufficiently small. Constants A and B were determined empirically, so as to reproduce the shape and the $\sim$ 0.7ns risetime of the oscillograms observed when Si switches were employed to provide the step function for the oscilloscope, and the values chosen were A = 0.01 and B = 1/150ps. By replacing these values in (8), and using (7) and (6) it follows that

$$V(t) = \int_o^t \left[1 - \frac{1}{1+0.01e^{(t-x)/150}}\right]\left[\frac{-(Z_o/\tau)V_{app}\cdot e^{x/\tau}}{(100+Z_o e^{x/\tau})^2} \cdot 50\right] dx - \left[1 - \frac{1}{1+0.01e^{t/150}}\right]\left[\frac{V_{app}\cdot 50}{100+Z_o}\right]$$

Figure 4.6 shows the result of the above expression for the input signals of figure 4.5, and the curves simulate oscillograms that would be obtained for semiconductors of five different recombination times, assuming $Z_o = 1\Omega$. As can be seen, the curve obtained for the longest recovery time switch has a risetime of 0.70ns, a profile very similar to the oscilloscope traces observed experimentally, and a maximum amplitude which is nearly half of the 2KV d.c. voltage bias, as should be the case for the discharge line configuration. More important, however, is the effect of the limited risetime of the instrument on the peak voltage observed for ultrashort duration voltage pulses. For semiconductors with a recombination time of 50ps for instance, the peak voltage displayed would have been only $\sim$ 300V, which is much inferior to the 980V amplitude actually switched (at t = 0).

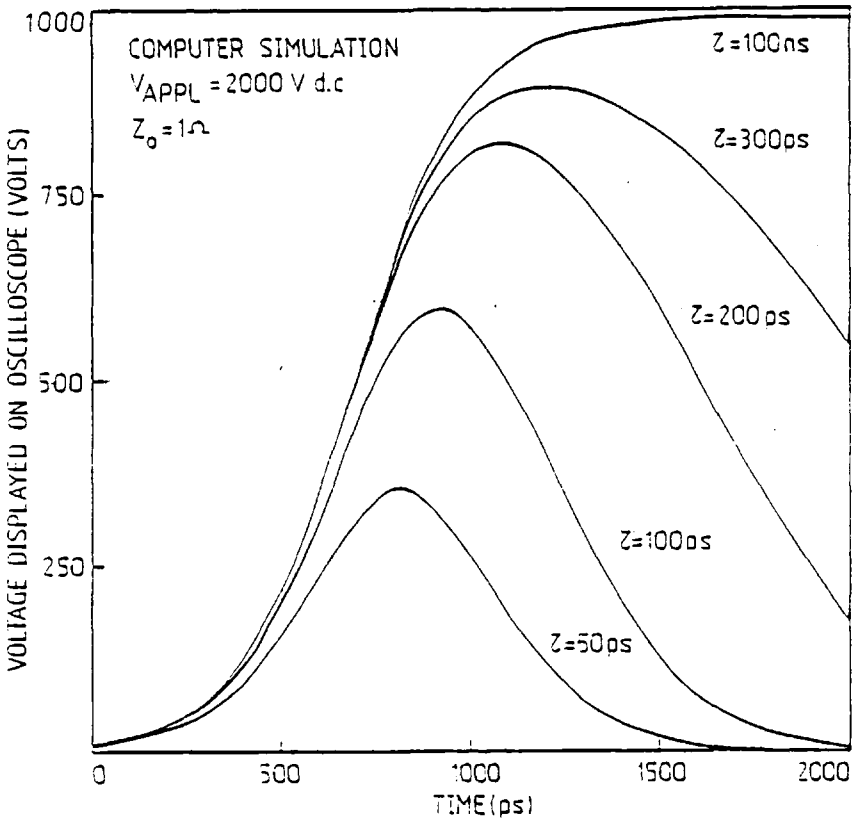

FIG 4.6 Computer simulation of the voltage displayed on the oscilloscope (Tektronix 7A19 amplifier) for the current pulses shown in FIG 4.5

These figures indicate that the switching efficiency of semi-insulating GaAs and GaP devices can not be directly determined from the peak voltage displayed on the oscillograms. However, provided the recombination time of the semiconductor is known, curves similar to the ones shown in figure 4.6 can be used to determine the value of the impedance of the device immediately following the activation. A computer program was written to generate such a set of curves, as seen in figure 4.7, where the initial impedance Z_o is related to the apparent switching efficiency (measured on a 700ps risetime oscilloscope), for four different values of τ. As an example, consider the conditions prevailing in the application of semi-insulating GaAs devices described in section 7.3. The switches were mounted on a discharge line arrangement and biased to 700V d.c., so that the peak voltage switched measured

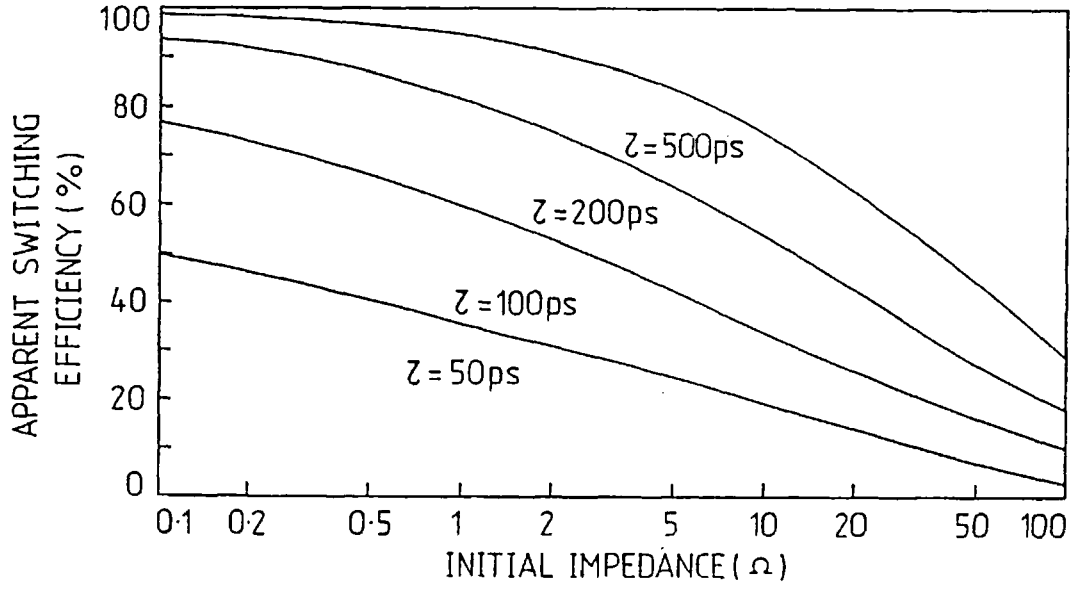

FIG 4.7 Switching efficiency measured on the oscilloscope for different values of the impedance following the activation. The switch is saturated (to within 10%) for $Z_o < 5\Omega$.

could have been 350V. The amplitude of the pulses observed on the oscillograms was ∿ 200V (i.e. an apparent switching efficiency of 60%) which, assuming a recombination time of ∿ 100ps, corresponds to an impedance $Z_o = 1\Omega$, as determined from figure 4.7. The knowledge of this value is important for the interpretation of the results discussed in section 7.3.5.

Finally, it is clear that the switching efficiencies shown in figure 4.7 differ significantly from unity even when the switches are fully saturated ($Z_o < 1\Omega$). Therefore, single-shot oscilloscopes can not be regarded in these cases as a direct method of measurement of the voltage pulses switched by the solid-state devices.

4.4.2 Indirect Techniques

From the preceeding discussion it is clear that while single shot oscilloscopes can provide direct measurements of the time evolution of slowly varying electrical signals, for ultrashort voltage pulses the oscillogram shows a convolution of the signal with the response function

of the instrument. The time resolution of commercially available fast single-shot oscilloscopes ($\sim 100^{s}$ps) [15] is $\sim$ 1-2 orders of magnitude slower than the risetimes of the voltage pulses obtained with semiconductor switches.

Since direct techniques of measurement were not adequate to resolve picosecond risetimes, indirect methods were used, in which the voltage signal switched was correlated with the response of another ultrafast element. The time resolution of such techniques greatly exceeded that of the single-shot oscilloscope, and the switching speed of the solid-state devices could be determined to a greater accuracy.

4.4.2.1 Electro-Optical Correlation

As mentioned in section 3.5, the leading edge of the high voltage pulse obtained with a Si device was examined by Le Fur and Auston [16] with an ultrafast risetime Pockel's cell. The voltage pulse was applied to a $LiTaO_3$ crystal which was placed between crossed polarizers, and the risetime of the electro-optical shutter was the correlation between the response time of the Pockel's cell and that of the semiconductor switch. The time resolution of this measuring technique was $\sim$ 20ps, but it involved the fabrication of a Pockel's cell in a microstrip configuration and a relatively complicated experimental procedure.

4.4.2.2 Electrical Correlation - Theoretical Aspects

A much simpler method to determine the switching speed of the solid-state devices was demonstrated by Auston [17, 18]. A picosecond light pulse is split into two components of equal intensity, one of which is delayed in relation to the other by an adjustable time lag. The two beams are focussed, and activate two different semiconductor

switches which are driven in series, so that the output of the first probes the transmission of the other for different delays. In Auston's original experiment two sub-pulses illuminated each Si switch, the second one (of 1.06μm wavelength) shorting the devices to ground and ensuring good time resolution. However, if fast recovery time semiconductors are used, or if alternative means are provided to terminate rapidly the switching action, a single light pulse can activate each device. The signal obtained, for identical switches subjected to the same illumination levels is the autocorrelation function of the form

$$V(\tau) = \int_{-\infty}^{\infty} f\,(t+\tau)\; f\,(t)dt,$$

and for single-shot lasers, the autocorrelation trace is obtained point by point, by varying the delay τ. By using different switches or different light levels, the curve obtained is the cross correlation

$$V(\tau) = \int_{-\infty}^{\infty} f_1(t+\tau)\; f_2(t)dt$$

The interpretation of the experimental results requires care, because of the intrinsic ambiguity of correlation techniques, and therefore it is worthwhile to consider theoretical aspects of the method. A simple model can be used to approximately describe the experimental results obtained.

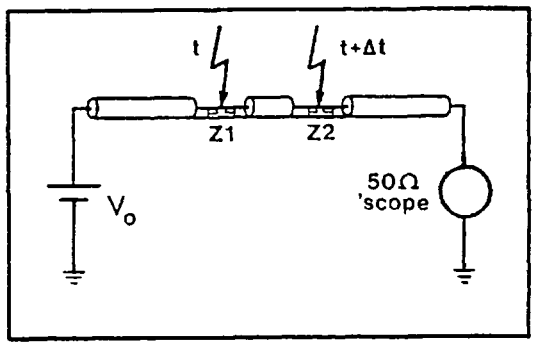

Assuming (a) that the recombination of electrical carriers is exponential and (b) that the rise-time of the devices is negligible compared to the recovery time of both switches, it follows that

$$I_1(t) = \frac{V_{app}}{100+Z_1(0)e^{t/\tau_1}}, \qquad (7)$$

where V_{app} is the d.c. voltage bias drop across the device on the left, $Z_1(0)$ is the initial impedance of the switch following the impulse illumination, τ_1 is the recombination time of the carriers, and $I_1(t)$ is the current flowing through the device (1) into the 50Ω transmission line connected to the other switch (2). Provided the response of the oscilloscope is slow ($\gtrsim$ 1ns), for each delay ΔT, the signal detected will be proportional to

$$V_{OUT}(\Delta T) = \int_{-\infty}^{\infty} \frac{1}{100+Z_1(0)e^{t/\tau_1}} \times \frac{1}{100+Z_2(0)e^{(t+\Delta t)/\tau_2}} dt \cdot \quad (9)$$

It is difficult to solve analytically expression (9), except when the denominators can be reduced to a single exponential term. Therefore, a computer program was written to evaluate numerically the integral, for a range of parameters $Z_1(0)$, $Z_2(0)$, τ_1 and τ_2. Altering the initial impedance corresponds, in the experiment, to changing the energy of the light pulse which illuminates each device, and by varying τ_1 and τ_2 one can simulate the response of different semiconductors.

The (normalized) calculated correlation signal of two identical semiconductor switches with a recombination time of 100ps is shown in figure 4.8a, for four different illumination levels. The curves are symmetrical in relation to the origin, and each wing approaches a single sided exponential for high initial impedances (low illumination levels). In this case the 1/e point of both wings gives the recombination time of carriers in the semiconductor. It is also clear that for low initial impedances (high illumination levels) the wings are no longer well approximated by exponentials, and the 1/e measurements do not correspond to the recombination time.

Figure 4.8b shows the result of the integral of expression (9) for two switches with identical impedance following the activation

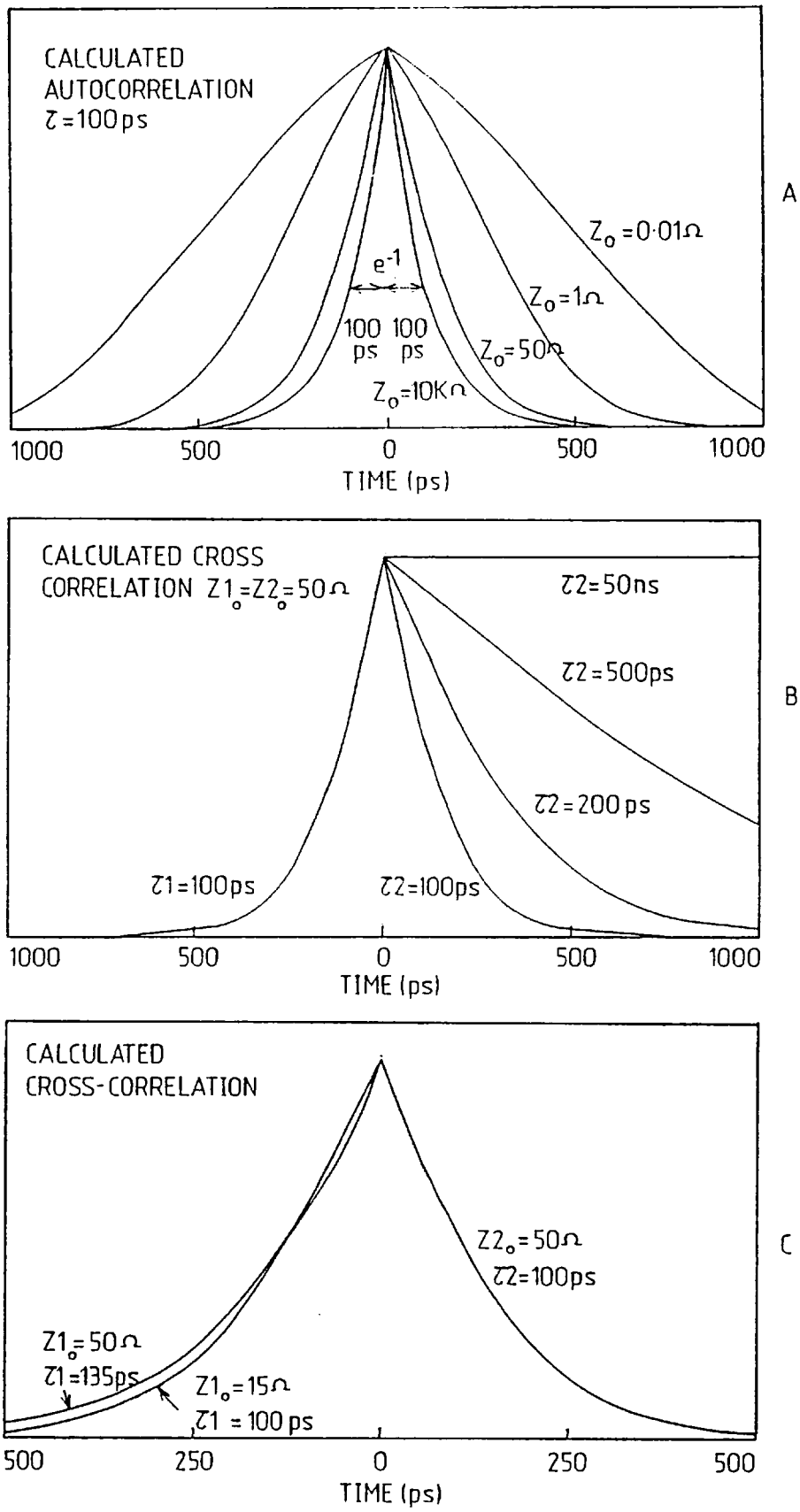

FIG 4.8 Computer simulation of autocorrelation (A) and cross-correlation (B and C) of semiconductor switches.

(Z_o = 50Ω), one with τ = 100ps and the other with four different values for the recombination time. The results shows that one of the wings of the correlation curve remains constant while the other changes dramatically, which indicates that each wing contains the information about one semiconductor switch. For very long recovery time semiconductors, the correlation curve shows a wing which is nearly horizontal.

Finally, it is worth demonstrating the ambiguity which arises from such a method of measurement. In figure 4.8c two correlation curves are shown, obtained by maintaining the parameters of one device constant ($Z_2(0)$ = 50Ω, τ_2 = 100ps), and evaluating the integral for the pairs of values ($Z_1(0)$ = 50Ω, τ_1 = 135ps) and ($Z_1(0)$ = 15Ω, τ_1 = 100ps). The curves have identical FWHM and very similar shape, so in an experimental situation it would be very difficult to distinguish between them and determine the exact recombination time of the carriers in the device (1), unless its initial impedance was known.

When hypothesis (b) does not hold, i.e. if the risetimes of the switches are comparable to the recombination time of carriers and can not be considered zero, each wing of the curve consists of two components, arising from the correlation of the response of one device with both the rise and fall functions of the other. As a consequence, the width of the curve in the actual experiment exceeds that of either of the components and therefore gives an upper limit for both the rise-time and the recombination time of the carriers in the semiconductor.

4.4.2.3 Electrical Correlation - Experimental Results

The correlation experiments carried out can be divided in three groups, performed to determine: (1) the recombination time of carriers in GaP; (2) the recovery time of GaAs devices; and (3) the risetime

of Si switches. A separate description of these measurements follows.

(1) GaP. The attempts to determine the recovery time of GaP switches with single shot oscilloscopes were limited by the poor time resolution of the instrument, as seen in figure 4.4. Therefore the correlation scheme shown in figure 4.9 was used. A single pulse of the second-harmonic from a Nd:Phosphate glass mode-locked laser was directed to a Michelson interferometer, which provided two subpulses separated by an adjustable time delay. One of the subpulses had either double or the same intensity as the other, depending on whether it passed a second time through the 50% beam splitter of the interferometer. Both subpulses were focussed, and directed to the GaP switches. The voltage switched by the first device was monitored on a 50Ω storage oscilloscope for every laser shot, and the amplitude of this signal was used to normalize the voltage that probed the response of the second device. Furthermore, the existence of a 50Ω impedance load connecting the switches to ground ensured that the d.c. voltage drop across the second switch was minimal, which greatly improved the signal-to-noise ratio of the measurement. Also, the initial impedance of the devices was estimated from the amplitude of the voltage pulse switched, which is important to unambiguously determine the recombination time of the carriers in the semiconductor, as seen from the theoretical discussion. It should be pointed out that although the interpretation of the results is simpler for low light levels, signal-to-noise considerations require that the impedance of the semiconductors should fall to a relatively low value following the activation, so that a voltage pulse of amplitude significantly higher than the background noise is detected for every

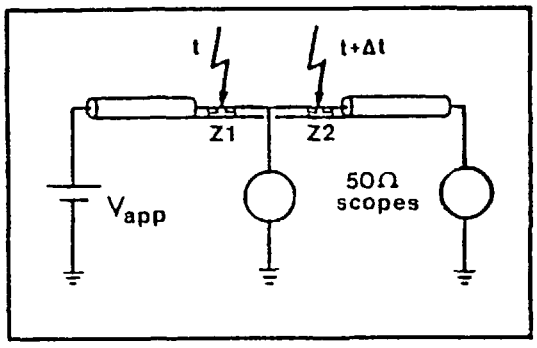

FIG 4.9

delay.

Figure 4-10a shows a correlation curve obtained from such a measurement. The widths at half maximum on either side of the peak are 136ps and 240ps and at 1/e, 200ps and 322ps, respectively. In order to relate these values to the actual recombination time of carriers, the model described in section 4.5.1 can be used. The average amplitude of the voltage pulses probing the second device was $\sim$ 25-30V for a 300V d.c bias, which corresponds to a $\sim$ 15-20% switching efficiency (for the discharge line arrangement), measured on a Tektronics 7834 oscilloscope. For a semiconductor with τ = 200ps, such switching efficiency corresponds to an impedance $Z_o \sim 100\Omega$, immediately after the illumination of the switches (c.f. figure 4.7). As can be seen from figure 4.8a, taking into account this limited value of the impedance, the recombination time of carriers in the semiconductor is found slightly above the 1/e point of the correlation curve, and is 177ps. Using the same procedure, the recombination time of carriers in the second device is determined to be 298ps. This pair of devices is clearly not identical and most probably differed in the number of recombination centres in the GaP crystals. By carrying out similar measurements with several different switches, recombination times as short as $\sim$ 60ps and as long as $\sim$ 500ps have been observed.

The trace fitted to the experimental data in figure 4.10a is to be compared with the calculated correlation curve shown in figure 4.10b, obtained when the following parameters are used: $Z_1(0) = 100\Omega$, τ_1 = 177 ps, $Z_2(0) = 200\Omega$, τ_2 = 298ps. Since the impedances were independently determined from the voltages switched by the device (1), the only values actually adjusted for the computer fitting were the recombination times (and a normalizing constant). The agreement between the two curves is relatively good, but the value of τ derived seems to be slightly over-

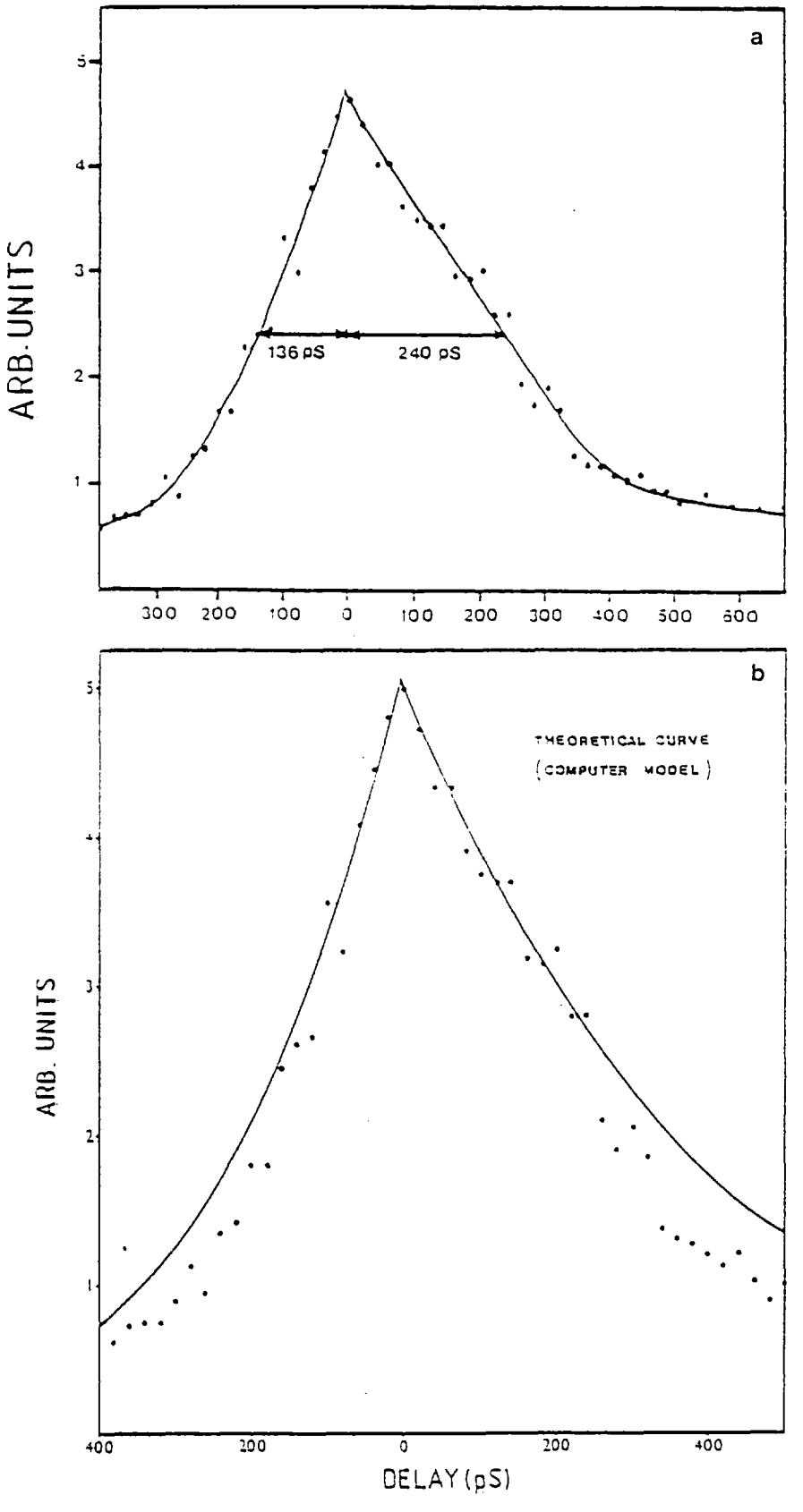

FIG 4.10 Cross-correlation between two GaP switches (A) experimental curve; (B) computer simulation

estimated (the best fit found was for τ_1= 140 ps and τ_2 = 240ps).

The results obtained by the correlation method are consistent with those obtained with a CW mode-locked Ar^+ laser, with which ∿ 100ps optical pulses were used to activate 25-100μm gap size switches. The output voltage pulses monitored with a sampling oscilloscope showed durations as short as ∿ 150ps FWHM, which corresponds to recombination times ∿ 110ps for the particular crystals employed.

(2) GaAs. Evaluating the duration of the voltage pulses obtained with semi-insulating GaAs switches was important for several applications which are described later, and therefore was the subject of a separate experiment. Measurements performed with devices of 25μm and 40μm gap sizes using sampling oscilloscopes (25ps time resolution) had shown that durations of ∿ 100-200 ps FWHM could be obtained, but the signals monitored had an amplitude < 1V. Longer gap size devices were constructed, and the correlation technique was used to study their recovery time under conditions which were more closely related to the ones existent in the active mode-locking experiments discussed in chapter 7.

A flashlamp pumped Rh6G dye laser provided a mode-locked train of light pulses, six of which were used to activate two GaAs switches connected in series. Voltage bias ranging from ∿ 200V to 400V d.c. were applied, and otherwise the set-up was similar to the one described for the GaP studies.

Figure 4.11 shows a correlation trace obtained under these experimental conditions. The two wings are different, and subtracting a constant background observed even when the second device was not illuminated, the widths at 1/e of the peak are determined to be 23.5ps and 97ps respectively. Such a result was reproduced a few times for

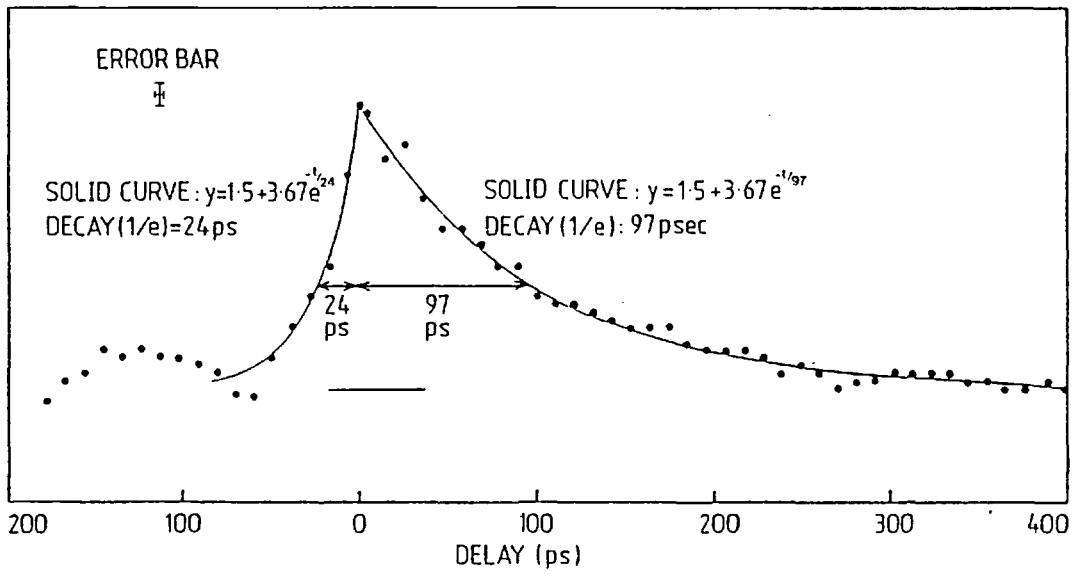

FIG 4.11 Cross-correlation between two GaAs switches

this pair of devices, and the secondary peak seen on the left was also systematically observed. The solid lines shown on the plot are the exponentials:

$$y = 1.5 + 3.67\ e^{-t/97} \quad \text{for } t(ps) \geq 0, \text{ and}$$

$$y = 1.5 + 3.67\ e^{+t/24} \quad \text{for } t(ps) \leq 0.$$

There is good agreement between the experimental values and the exponential wing on the right, which suggests that the recombination time of carriers in the second device is 97ps. Poorer agreement exists between the data and the exponential curve on the left where the 1/e width is 24ps, particularly for the points of low amplitude. Although it is reasonable to expect that the lifetime of photoexcited carriers in the first device is $\lesssim$ 30ps, the ambiguity of this kind of measurement makes it difficult to determine accurately the exact value.

It has been pointed out [19] that when the electric field applied to semi-insulating GaAs devices is sufficiently high to induce inter-valley scattering, much shorter duration voltage pulses are obtained. This could explain the extremely fast recovery time observed, although this feature needs further study. It should be also mentioned that the width measured 24ps at 1/e or 17ps at half maximum is also an upper

limit for the risetime of the second switch, which confirms that the risetime can be neglected when compared with recombination times $\gtrsim$ 100ps, as has been previously assumed.

(3) Si. The recombination time of carriers in nearly intrinsic Si can be determined directly from oscillograms, as shown in figure 4.3a, but the measurement of the risetime requires picosecond time resolution, and therefore a correlation scheme was employed. Ideally, the response of the Si device should be probed for different delays by a voltage pulse of negligible duration, and in this case the correlation curve would have the shape of the transmission function of the switch. However, it is difficult to generate voltage pulses of negligible duration compared with the risetime of solid-state switching devices, so the time resolution of the measurement was limited by the duration of the probe voltage pulse.

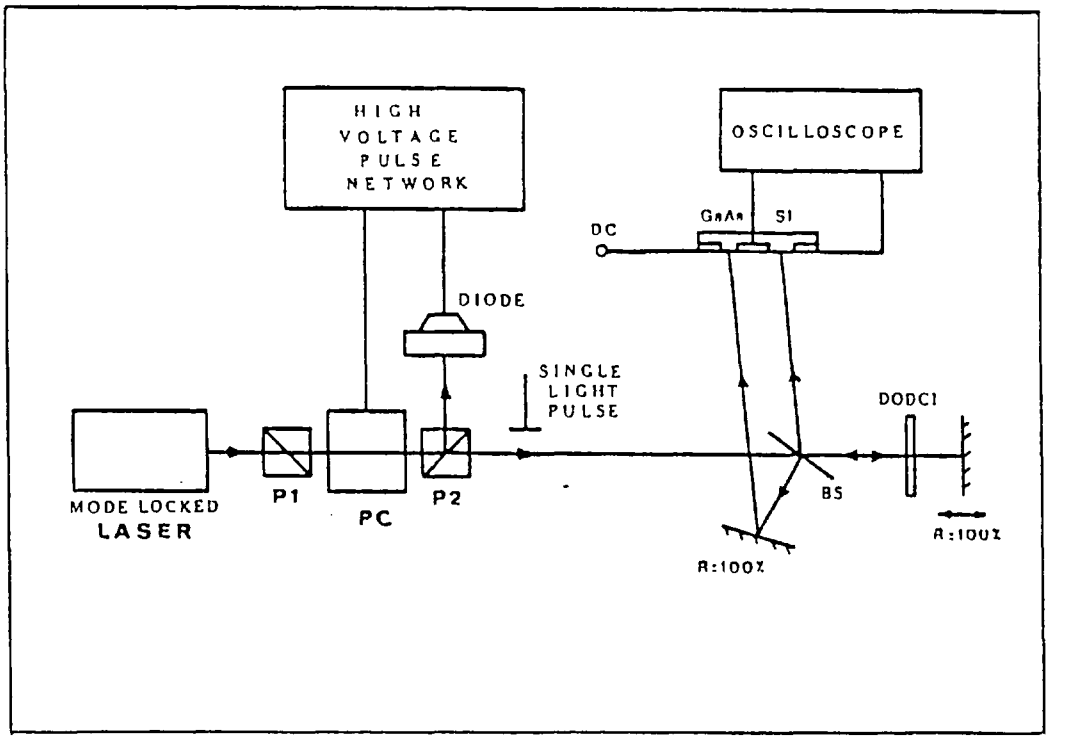

FIG 4.12 Experimental set-up of cross-correlation to measure the risetime of the Si switch

Since the measurements carried out with GaAs revealed that pulses

of durations as short as $\lesssim$ 30ps could be obtained, a cross-correlation experiment was set-up, where a semi-insulating GaAs device provided the voltage pulses that probed the transmission functions of a Si switch, as seen in figure 4.12. A single light pulse was used to activate the devices, and a cell of saturable absorber was introduced to reduce the effect of weak light pulses leaking through the selector and illuminating the Si device. Several combinations of switches were tested, and a typical result of the measurements is shown in figure 4.13a, where the time resolution is limited by the recombination time of carriers in GaAs, rather than by the actual risetime of the Si switch. Sometimes, however, correlation curves similar to the one shown in figure 4.13b were obtained. For this particular measurement, more than 200 laser shots were fired, and each point corresponds to the average of at least 4 experimental results. The risetime obtained is in this case $\sim$ 33ps, although risetimes as fast as 24ps were also observed. These values are only an upper limit for the actual risetime, and are probably still determined by the duration of the probing voltage pulses. Better time resolution is required, and could be obtained by switching the first device off with a second light pulse, or more conveniently, by discharging a short length charged line or by using a semiconductor of even faster recovery time than semi-insulating GaAs, such as amorphous Si.

4.5 Photoconduction Mechanisms

Solid-state switches closely resemble the devices used in photoconduction measurements, which have been performed even before the invention of the laser. Therefore it is only natural that semiconductor switches should be used to examine photoconductivity induced by pico-

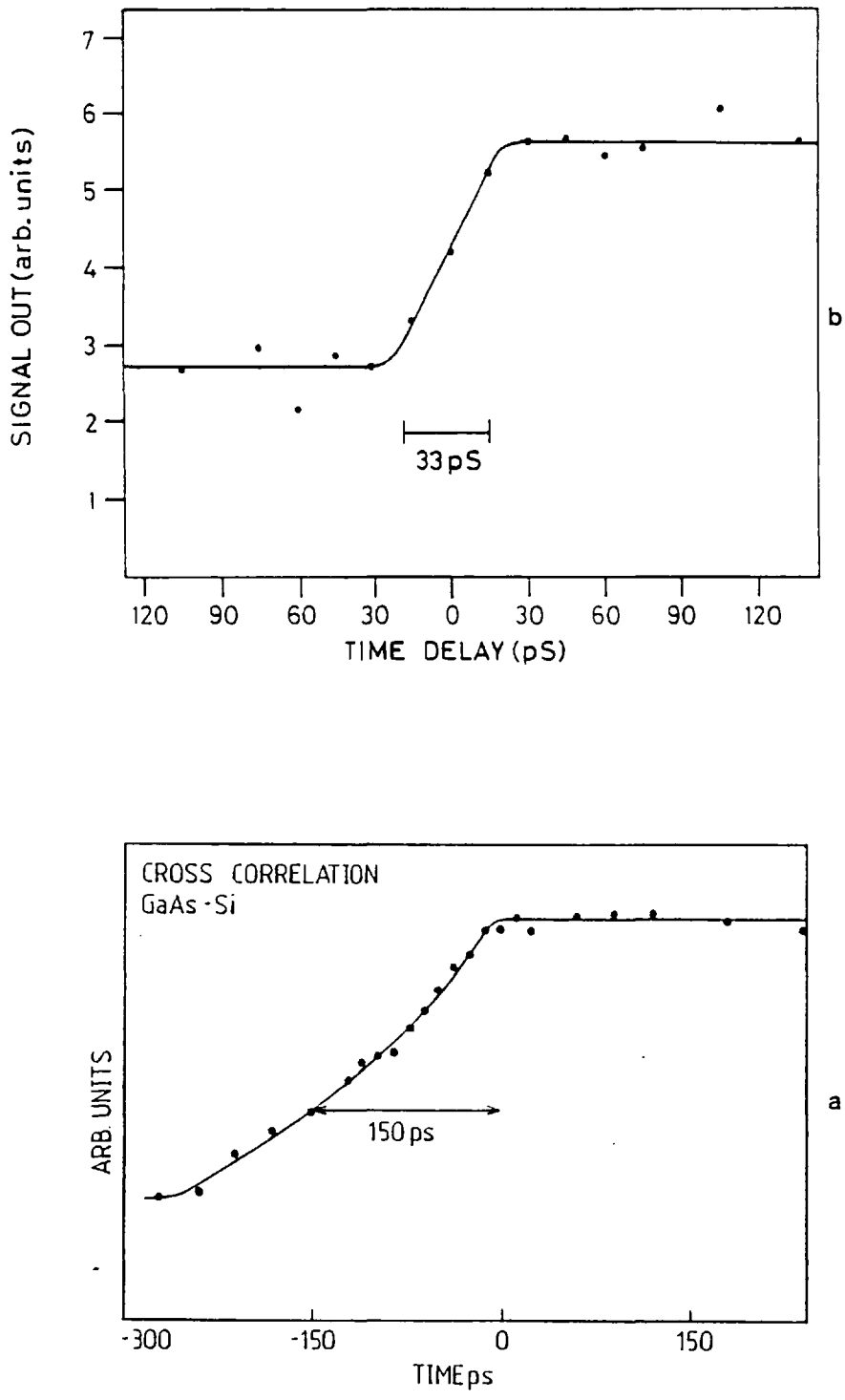

FIG 4.13 Measurement of the risetime of a Si switch by electrical cross-correlation where two different GaAs devices provide the probing pulses. Fastest risetime observed: 24ps

second light pulses. The demonstration of such technique was carried out for semi-insulating GaP crystals, and the experiments helped to improve the understanding of the photoconductive mechanisms involved in the switching.

The light pulse intensity that activated a 2mm gap switch with Al electrodes was varied and the conductance of the switch was plotted, for a constant d.c. bias. Both the fundamental at 1.05μm and the second harmonic of 0.53μm wavelength of a mode-locked Nd:Phosphate glass laser were used. The energy of the 0.53μm photons (2.35eV) is nearly coincident with the minimum energy necessary to promote electrons from the valence to the conduction band in GaP. Therefore, it was anticipated that a very strong single-photon dependence would be observed. When the fundamental radiation at 1.05μm was used, then a two-photon conductivity component was expected.

For both wavelengths the input train amplitude was monitored using a linear response photodiode and displayed on a storage oscilloscope. Another storage oscilloscope displayed the voltage switched by the GaP switch under test, which had a d.c. bias of 2.8KV. When necessary, calibrated electrical attenuators were introduced. The intensity of the light pulses illuminating the switch was varied with a set of calibrated neutral density filters. When the second harmonic was used, an optical filter was introduced to prevent any fundamental radiation from reaching the switch.

Figure 4.14 shows the behaviour of the GaP switch illuminated by 0.53μm light pulses on a log-log scale. It is seen that the conductivity increases linearly with the light intensity for almost five decades. The slope obtained with a least squares fit was 1.1, i.e,

$$n \alpha I^{1.1},$$

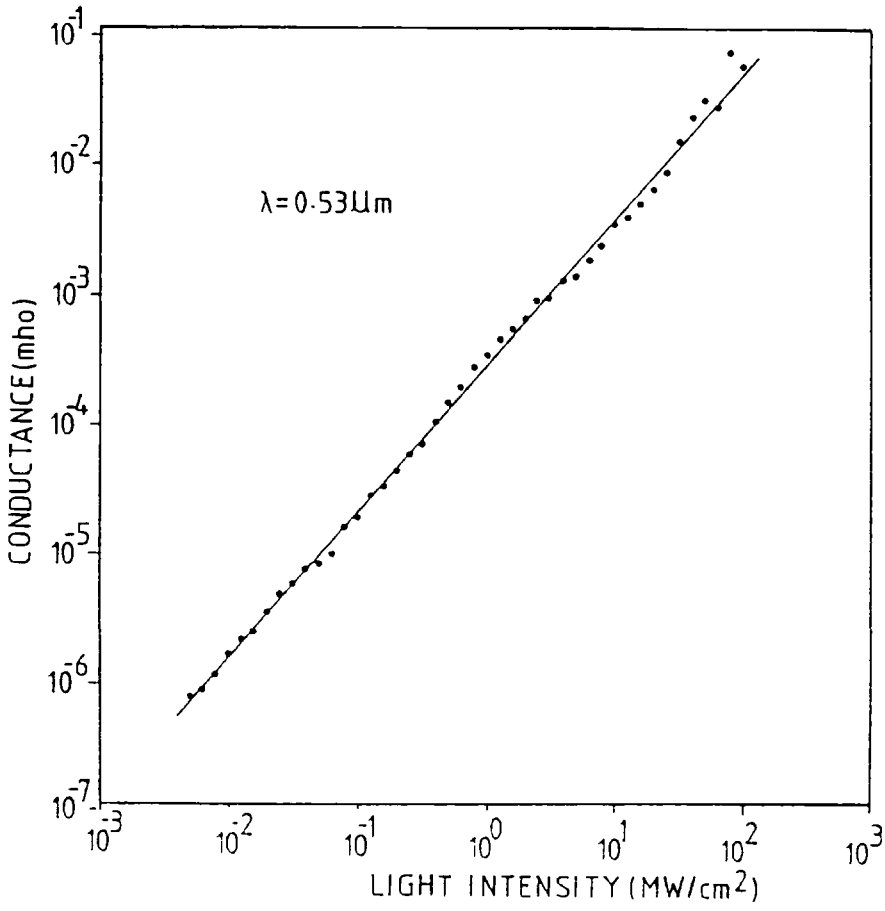

FIG 4.14 Conductance of a GaP switch for different intensities of 0.53μm picosecond radiation

which implies that the photoconductivity is predominantly a single-photon process for 0.53μm radiation.

These results can be used to derive the mobility of carriers in the semiconductor, according to the expression (2) derived in chapter 3,

$$(\mu_n + \mu_p) = \frac{(n_r+1)^2}{4n_r} \quad \frac{h\nu}{e} \quad \frac{G}{\varepsilon} \ell^2,$$

where $(n_r+1)^2/4n_r$ accounts for the fraction of the light absorbed by the GaP crystal, $h\nu/e$ is the energy of the photons in volts, and ε is the energy of the light pulse incident on the gap of length ℓ. For $\varepsilon = 20\mu J$, $G = 5 \times 10^{-2}$ mho, $\ell = 2$mm and $n_r = 3.37$ one finds

$$(\mu_n + \mu_p) = 330 cm^2/V.s,$$

which is in reasonably good agreement with the value $(\mu_n + \mu_p) = 240 cm^2/V.s$ quoted in the literature for GaP [20, 21]. The higher value found could be attributed to the difficulty in estimating the energy (20 ±10μJ) of the green light pulses incident on the semiconductor. This result is an independent confirmation of the validity of equation (2) of chapter 3, within the experimental error of the measurement.

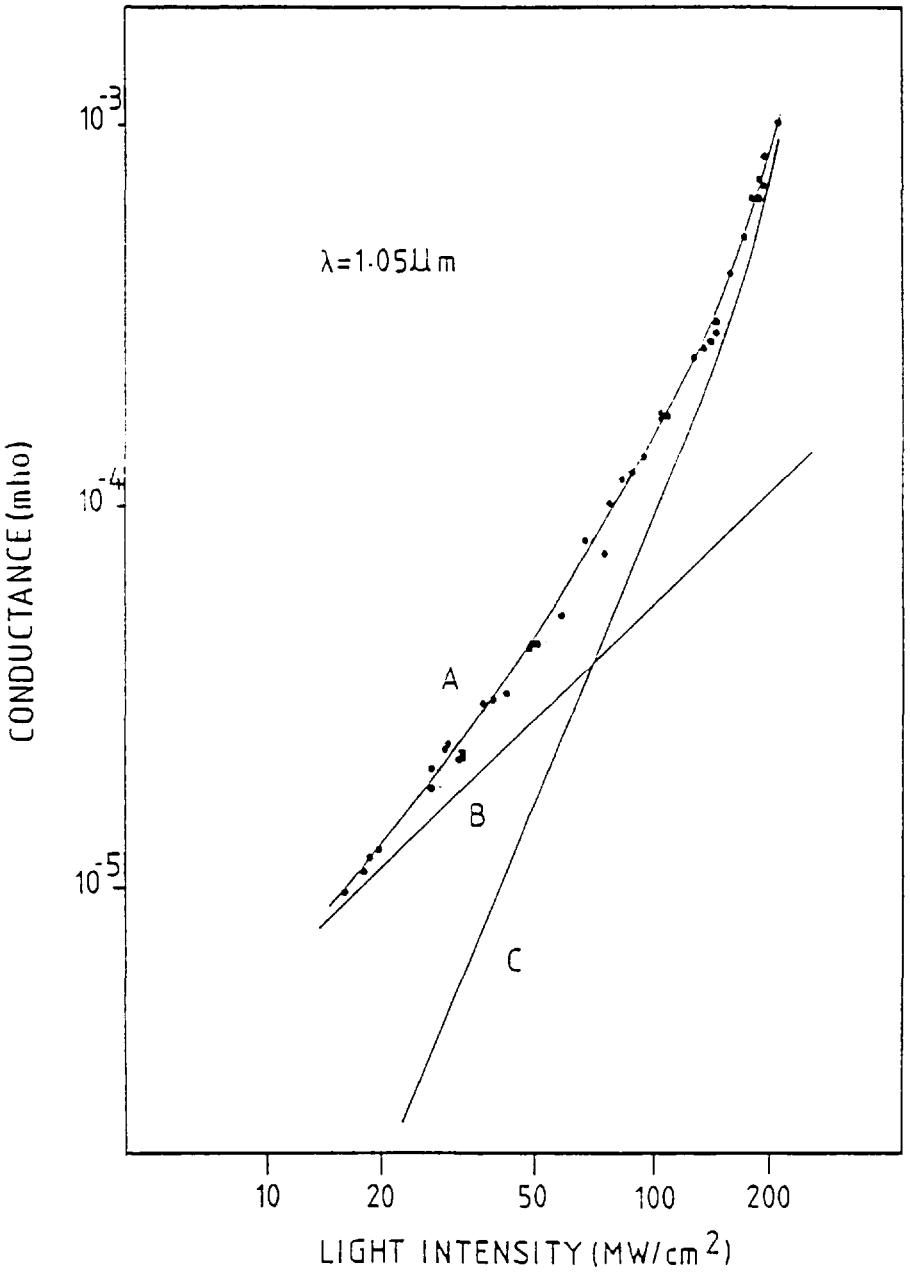

FIG 4.15a Conductance of GaP switch for different light intensities of 1.05μm picosecond radiation

Figure 4.15a shows how the conductivity changes as a function of the 1.05μm light intensity again on a log-log graph. It is seen that for light intensities below ∿15MW/cm^2 the curve can be very accurately approximated by a straight line (B) with slope 0.99. As the light intensity increases, the derivative also goes up, and at ∿ 200MW/cm^2 the slope of the curve is 2.7.

This result indicates that for low light intensities the multiphoton processes are not efficient, and the photoconductivity is mainly due to impurity centres being excited by single photons of the 1.05μm radiation

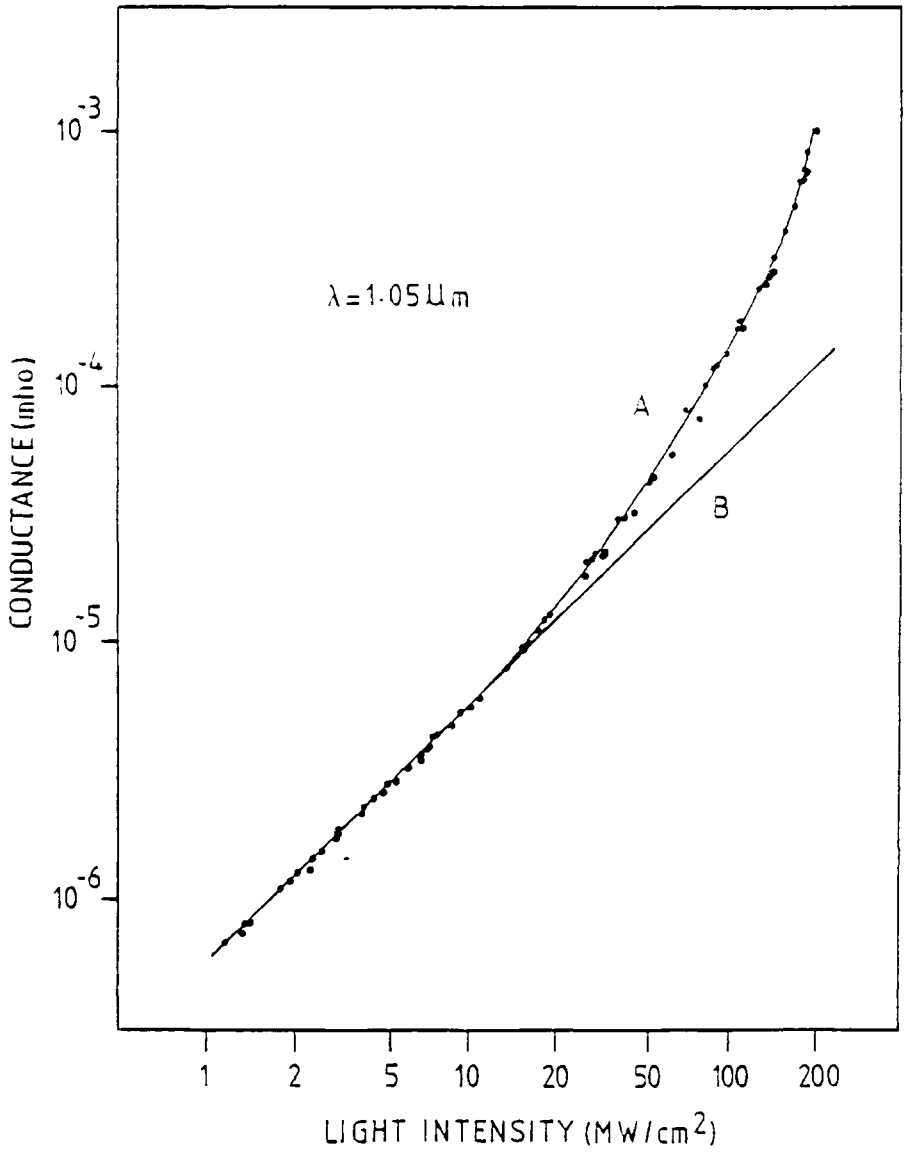

FIG 4.15b Portion of fig 4.15a on an expanded scale

For higher intensities of the light pulse, the efficiency of the multi-photon process increases and consequently the contribution from impurity centres becomes less important.

Figure 4.15b shows the result from the subtraction of the experimental curve (A) and the straight line (B) with slope 0.99 extrapolated from low light intensities. It is seen that the resulting curve (C) can be approximated to a straight line with slope 2.5 for intensities below 130MW/cm^2. The fact that the slope exceeds the value of 2 is somewhat unexpected, and suggests that for high light levels more than two photons are used in the creation of each electron-hole pair.

4.6 Transport Properties

From the preceeding section it is clear that information about the photoconductivity mechanisms is gained by examining the voltage switched as a function of the illumination level, when the voltage bias applied to the device was maintained constant. However, by altering the voltage applied (and consequently the electric field) across the switch, and measuring the signal output for a constant illumination level, one can study the transport properties of carriers in the semiconductor. Such characteristics are important not only from a physical point of view, but also for technological applications where there is a need for ultra-fast electronic components, whose speed depend on transport processes.

To illustrate the potential application of semiconductor switches in such studies, both Si and GaP devices have been used, and in order to describe the experiments it is worthwhile considering some properties of the electrodes of the devices.

The techniques used in the fabrication of the metal-semiconductor

junctions were described in section 4.3. It is often desirable to obtain ohmic contacts where the voltage drop across the function is negligible compared to that across the actual semiconductor gap, so that the contacts do not affect the I/V characteristic of the slab. Ohmic contacts allow the injection of carriers from the electrodes, i.e. as a carrier is collected at one side of the switch, another similar carrier is injected at the other end, so that the number of carriers available following the illumination depends only on the recombination mechanisms in the semiconductor. However, it is also possible to fabricate Schottky contacts, which when reversed biased can prevent injection from taking place. In this case the carriers will drift to the electrodes following the illumination and, since they are not replenished at the other end, the switching action finishes. It is possible in this way to generate voltage pulses of durations determined by the transit time of the carriers, rather then by the recombination time of the semiconductor [22].

As an illustration of such effect, the drift velocity of electrons in a Si crystal was measured from the oscillogram on a 50ps/div shown in figure 4.6. A CW synchronously mode-locked Oxazine 1 dye laser (round-trip time $\sim$ 14ns) was focussed, and activated a 25μm gap nearly intrinsic silicon device biased to 78V. The voltage pulse rise-time is $\sim$ 50ps, and because the injection of carriers is small, its duration at FWHM is $\sim$ 200ps, which is many orders of magnitude inferior to the recombination time $\sim$ 10μs. The pulse has a

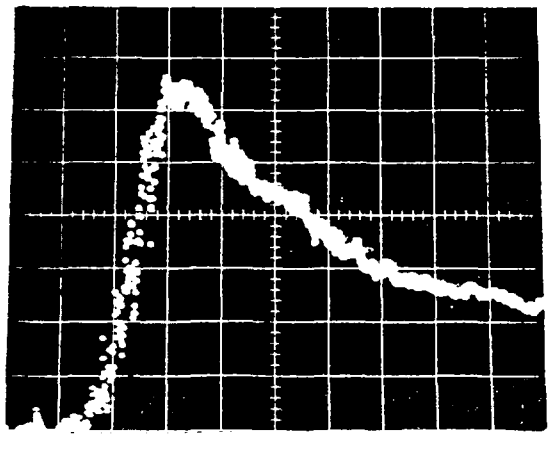

FIG 4.16 Oscillogram of pulses switched by a 25μm gap Si device. Time scale: 50ps/div.

width (at 1/e of the peak) of 311ps, and this corresponds to an average drift velocity of 8.0 x10^6cm/s, which is in good agreement with the values 6 x 10^6cm/s and 1 x 10^7cm/s quoted in the literature for Si under similar electric fields [23, 24]. It was observed that under different light focussing conditions much longer pulses were obtained, and the d.c. level increased appreciably. This can be explained by the fact that when light illuminates the junction, electron-hole pairs significantly reduce space-charge effects which otherwise prevent the injection of carriers. As a consequence, provided the light pulse illuminates the electrodes, carrier replenishment will take place, and a relatively ohmic behaviour will be insured. This was the case in the actual experimental conditions existent when recording the oscillograms of figure 4.3, and in the applications described in chapters 5, 6 and 7.

A very peculiar and dramatic effect was observed for several semi-insulating GaP switches which had silver painted electrodes. The amplitude of the voltage switched under relatively high electric fields ($\gtrsim$ 1500V/cm) showed significant instability, which happened on a fast time scale. This effect was observed when the switches were illuminated by trains of intense mode-locked pulses (at 0.53μm and 1.06μm wavelength), and also when CW laser light was used (at 0.514μm and at 0.488μm). Some oscillograms illustrating this effect are shown in figure 4.17. When the slabs were activated by the picosecond pulses (A, B, C) a photodiode simultaneously monitored the mode-locked train, always showing a smooth profile. When the CW Ar^+ laser was used (D-I) a chopper was introduced to prevent heating of the samples, and under these conditions the signal detected on the oscilloscope should have the shape of a square voltage pulse with slightly rounded edges. The expected behaviour of a semi-insulating GaP switch activated by a mode-locked train of pulses of 0.53μm wavelength is shown in the oscillogram A. Instabilities are shown in

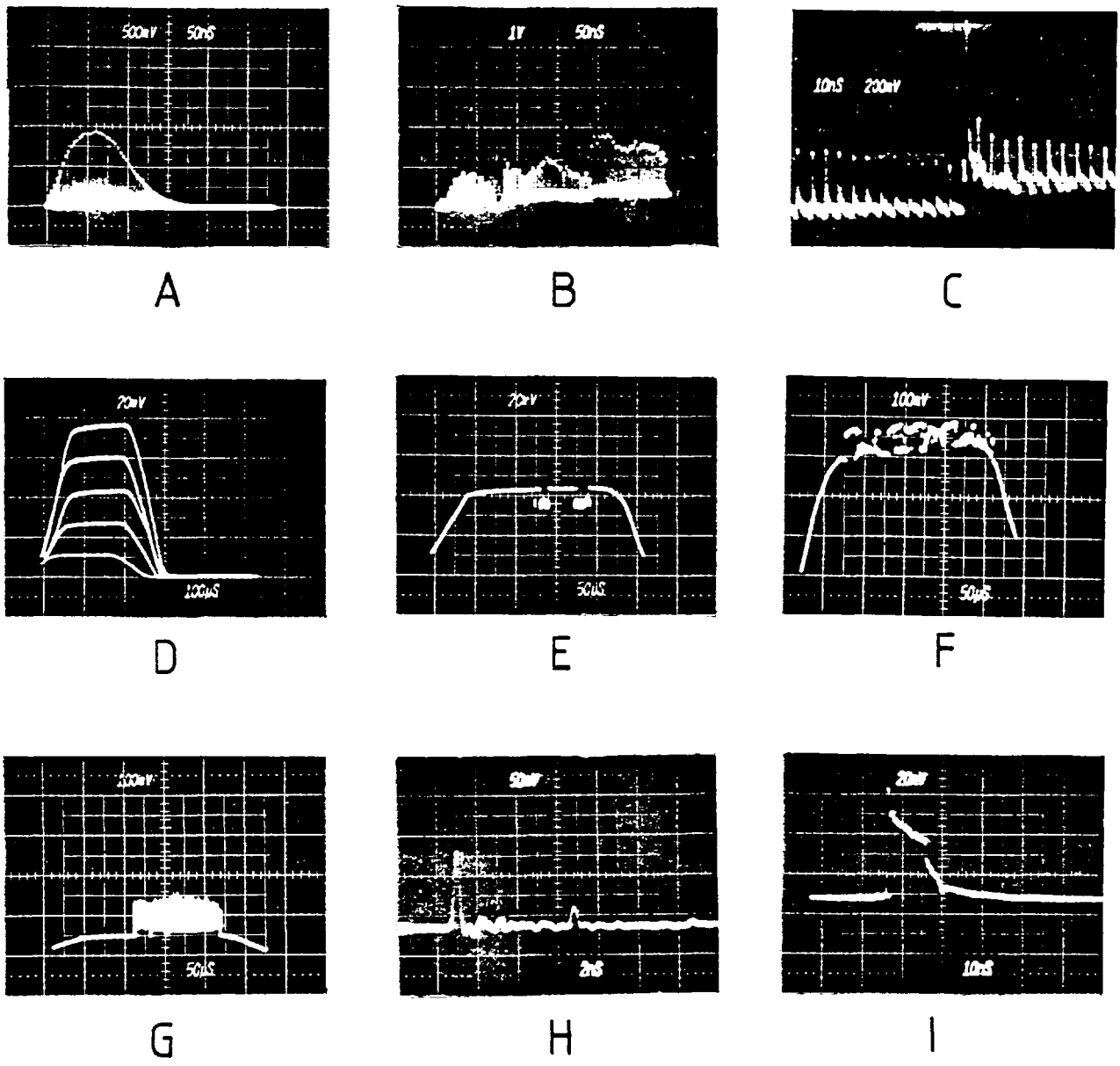

FIG 4.17 Oscillograms showing switching instability of GaP devices with silver painted electrodes, activated by (A-C) mode-locked laser (D-I)CW Ar^+ laser (chopped).

(B) and (C), and it was determined that their incidence did not necessarily coincide with the roundtrip of the laser. Figure (D) consists of the superposition of five different exposures on a 100μs/div obtained when a Au electroded switch was activated by a chopped Ar^+ laser beam, subjected to a d.c. bias of 200V, 400V, 600V, 800V and 1000V, respectively. No instability is observed in this case, which is in contrast with the oscillogram on a 50μs/div of figures (E) and (F), showing a signal of irregular shape obtained with a 1.4mm gap silver painted

electrodes device biased to 620V. The same device, subjected to 900V, and under different alignment conditions produced the signal seen on the oscillogram of figure (G). When examined on a faster time scale, very fast risetime pulses were seen, sometimes of ultrashort duration, as shown in figures (H) and (I). This effect was observed for several semi-insulating GaP switches, using different power supplies, oscilloscopes and laser sources, at various wavelengths. The instabilities seemed to depend on the fact that the electrodes were prepared by deposition of silver paint directly on the semiconductor, on a relatively strong electric field, and on the alignment conditions, which suggests that the process is related to the space-charge effects at the semiconductor-metal junction. The erratic nature, and the fast risetime exhibited by the voltage spikes could tentatively be attributed to electric breakdown happening between the GaP crystal and the metal on small regions of high electric field existing at the edges of the electrodes. The sparks would give rise to a fast increase in the current switched, and the devices should then show an ageing effect, which was observed in pactice. Similar instabilities were not seen on semi-insulating GaAs, nearly intrinsic Si, or when the electrodes were prepared on the GaP crystals by evaporation (of Al, In, Au or Ag).

In order to further characterize transport properties in semi-insulating GaP, studies were carried out to determine whether this semiconductor exhibited negative differential resistivity which has been observed for GaAs devices [1, 25]. Switches with electrodes prepared by evaporation, and of gap sizes ranging from 25μm to 2mm were irradiated by a chopped CW Ar^+ laser beam, and the voltage switched was measured on a 50Ω oscilloscope (as seen in figure 4.17b). As the electric field across the gap was increased to values as high as 10KV/cm, the output voltage always increased monotonically. Figure 4.18 shows

the current switched by a gold electroded 2mm gap GaP device as a function of the applied electric field, for two different average light powers. No saturation is observed, and the voltage switched increases almost linearly with the voltage applied. Similar results were found when picosecond pulses activated the devices, suggesting that GaP switches do not exhibit differential negative resistivity [26, 27, 28] for electric fields as high as 10 KV/cm.

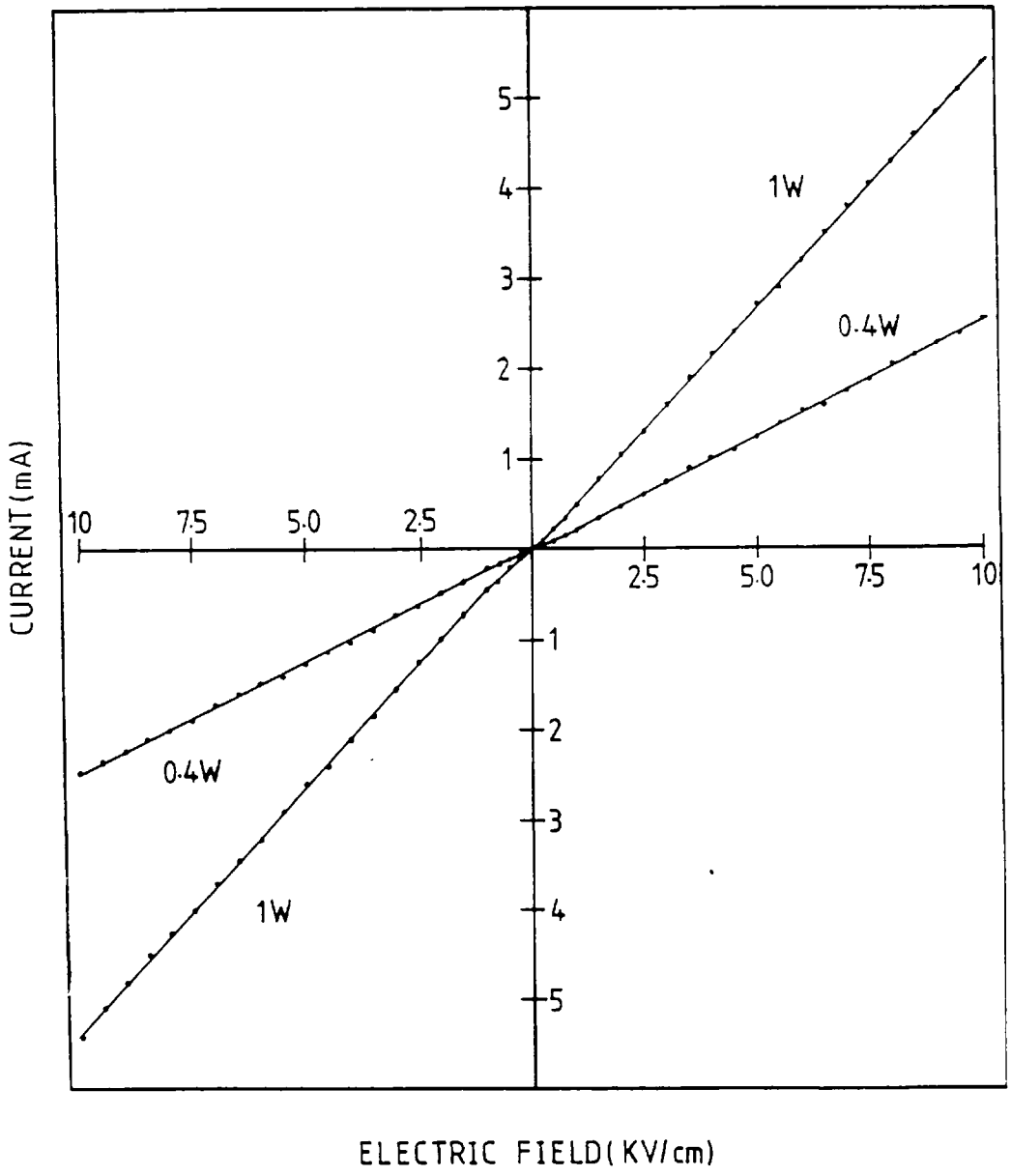

FIG 4.18 Current switched by GaP device as a function of applied electric field for 0.4W and 1.0W average light powers.

4.7 Conclusion

In this chapter the construction of the semiconductor switches was described and it was shown that useful information about the semiconductor properties can be obtained from these studies. The technique developed to fabricate solid-state devices was relatively simple and versatile, and both low and high voltages were switched with picosecond risetimes, obtained by using impedance matched microstrip transmission line structures of short lengths.

Fast oscilloscopes were employed to determine the response of the switches, but since direct measurements are only obtained when the signal is significantly slower than the risetime of the measuring instrument, a computer model was developed to allow the interpretation of the oscillograms, and is further used in the evaluation of the switching efficiency of the devices described in chapter 7.

Because of the potential applications of Si devices to switch high voltages with picosecond risetimes, and of semi-insulating III-V semiconductors to generate ultrashort duration high voltage pulses, the recombination time of semi-insulating GaAs and GaP and an upper limit for the risetime of a Si switch were determined by means of an electrical correlation technique. The time resolution obtained was much better than that of single-shot oscilloscopes, and at least as good as that of sampling systems. The results showed typical recombination times $\sim 10^2$ ps for both III-V semiconductors, and the risetime of Si switches was found to be as low as $\lesssim$ 24ps. These values obtained under single shot laser excitation are consistent with those measured from sampling oscilloscope traces used in conjunction with CW mode-locked laser sources.

Solid-state switches were also found to be useful tools in the

investigation of single and multiphoton conductivity processes, as well as in the observation of transport phenomena and of metal-semiconductor junctions effects. From all these experiments, it is clear that pico-second solid-state swtiches are valuable in the study of fundamental properties of semiconductor crystals and also useful sources of ultra-fast risetime and ultrashort duration voltage pulses, which find immediate applications as described on the following chapters of this thesis.

References - Chapter 4

[1] Chi H. Lee; Appl. Phys. Lett., 30, 84 (1977)

[2] M.W. Hosking; Wireless World, p.131 (March, 1973)

[3] M. Caulton, J.J. Hughes, H. Sobol; RCA Review, p.377 (Sept, 1966)

[4] A.H. Kwon; Microwave Journal, p.61 (Jan, 1976)

[5] I.J. Bahl, D.K. Trivedi; Microwaves, p. 174 (May, 1977)

[6] W.J. Getsinger; IEEE Trans. Microwave Theory Tech. MTT21, 34 (1973)

[7] ICI industrial cleaning procedure for Si - manual sheet

[8] E.H. Rhoderick; Metal-Semiconductor Contacts, Clarendon Press, Oxford (1980)

[9] M. Hansen; Constitution of Binary Alloys, McGraw-Hill, NY (1958)

[10] S.D. Mukherjee, D.V. Morgan, M.H. Hoves, J.G. Smith, P. Brook; J. Vac. Sci. Tehnol., 16, 138 (1979)

[11] K. Sleger, A. Christou; Solid State Elect., 21, 677 (1978)

[12] O. Wada, S. Yanagisawa, H. Takanashi; Japan J. Appl. Phys., 12, 1814 (1573)

[13] D.H. Auston; private communication

[14] B.P. Lathi; Communication Systems, John Wiley & Sons, NY (1968)p.80

[15] See for example, Tektronix Products Catalogue (1981)

[16] P. LeFur, D.H. Auston; Appl. Phys. Lett., 28, 21 (1976)

[17] D.H. Auston; Appl. Phys. Lett., 26, 101 (1975)

[18] D.H. Auston, A.M. Johnson, P.R. Smith, J.C. Bean; Appl. Phys. Lett., 37, 371 (1980)

[19] A.Antonetti, M.M. Malley, G. Mourou, A. Orszag; Opt. Commun., 23, 435 (1977)

[20] Chi H. Lee, P.S. Mak, A.P. DeFonzo; IEEE J.Quantum Elect. QE16, 277 (1980)

[21] MCP Electronics Ltd; Compound Semiconductors and High Purity Products Catalogue

[22] J. Degani, R.F. Leheni, R.E. Nahory, M.A. Polack, J.P. Heritage, J.C. DeWinter; Appl. Phys. Lett., 38, 27 (1981)

[23] C.B. Norris, J.F. Gibbons; IEEE Trans Elect. Dev., ED14, 38 (1967)

[24] C. Canali, G. Majni, R. Minder, G. Ottaviani; IEEE Trans. Elect. Dev., ED22, 1045 (1975)

[25] S. Laval, C. Bru, R. Castagné, C. Arnodo; 1980 Int. Cong. on GaAs and Related Compounds, Vienna, Austria.

[26] B.K. Ridley, T.B. Watkins; Proc. Phys. Soc., 78, 293 (1961)

[27] E.M. Conwell; Physics Today, June, 35 (1970)

[28] J.W. Allen, M. Shyam, Y.S. Chen, G.L. Pearson; Appl. Phys. Lett., 7 78 (1965).

CHAPTER 5

STREAK CAMERA SYNCHRONIZATION

5.1 Introduction

With the development of mode-locking it became necessary to extend the capabilities of ultrafast measuring techniques in order to fully characterize the picosecond light pulses available, and to study luminous phenomena with the new time resolution required [1, 2]. As mentioned in chapter 2, the use of the electron-optical streak camera became widespread. Because of its capability to directly register the intensity of the light event as a function of time with picosecond resolution, it provides unambiguous information about laser pulse shape and background. When it is used in conjunction with an intensifier system, extremely high sensitivity to low light levels can be obtained, and so streak cameras have been extensively employed in the study of non-laser events such as fluorescence and luminescence [3].

In spite of the fact that picosecond time resolution of streak cameras has been achieved several years ago [4], their operation still presents a limitation arising from the jitter. For reliable use of the instrument to be possible, the application of the voltage ramp to the deflection plates must be synchronized with the light event under observation. The lack of synchronization (jitter) makes the position of the streak on the screen change from shot-to-shot. In the extreme case, the photoelectrons miss the phosphor altogether, and the camera fails to record the event. Jitter can be a serious problem when fast writing speeds are used for good time resolution, and in particular for slow repetition rate systems, where it is important to obtain a result for every laser shot. If the streak camera is operated in the

recurrent mode (synchroscan [5]) jitter would prevent the perfect superposition of the streaks on the screen, therefore limiting the temporal resolution of the instrument [6].

In order to obtain the fast risetimes required for the voltage ramp, laser triggered spark-gaps, Krytrons and avalanche transistor stacks are generally used. Typical jitter times of systems incorporating these conventional elements are $\sim 10^{s}$-100^{s}ps, which is inconvenient and sometimes unacceptably large for many streak camera applications.

Semiconductor switching devices have been shown to switch several kilovolts with picosecond risetimes. Furthermore, picosecond synchronism exists between the switching action and the illumination of the gap by the light pulse. Therefore, solid-state switches should, in principle, be capable of providing the voltage ramp for the deflection plates of a streak camera. Unlike conventional switching elements, they can not be triggered by noise. Also, besides being compatible with streak camera systems today, the picosecond risetime could be also used for improved time resolution tubes which are likely to be developed and manufactured in the near future.

Therefore the possibility of reducing the jitter of streak cameras by employing semiconductor switches without sacrificing either time resolution or linearity of the sweep is attractive, and is the subject of the following sections of this chapter. Before that, a brief description of the construction and the performance of conventional systems is given for comparison.

5.2 Conventional Ramp Generators

The sweeping in conventional circuits is in general provided by a stack of avalanche transistors, by a laser triggered spark gap, by a hard valve, or by a Krytron. Each one of these has its advantages, but also some limitations.

When stacks of avalanche transistors are employed to generate the high voltage ramp for the streak camera, $\sim$ 20 transistors are mounted in series (so that the voltage is distributed between them), and as one element is activated, the whole chain triggers at approximately the same time. By carefully selecting the components used, the commercial Hamamatzu image converter [7] exhibits a total jitter of $\pm$ 50ps. However, the writing speed of $\sim 6.7 \times 10^9 cms^{-1}$ limits the time resolution of the instrument to a few picoseconds. Another streak camera system with similar time resolution was demonstrated [8], where a high sensitivity tunnel diode triggers a stack of 24 specially manufactured avalanche transistors, yielding a jitter of < 30ps at a writing speed of $\sim 6 \times 10^9$ cms^{-1}. A solid-state deflection circuit was also developed at the Lawrence Livermore Laboratories, where the avalanche transistor chain was triggered when a picosecond light pulse illuminated one of the components, which had its metal protection removed. In this case, a jitter of $\sim$ 100ps was achieved [9]. Although these systems are adequate for several applications, they make use of specially manufactured transistors which are not commercially available, and furthermore do not provide enough sweep speed to ensure subpicosecond time resolution which is at present already sometimes required.

Hard valves operating in a linear conducting mode are used to provide the deflection ramp for the Hadland streak cameras. Contrary

to all other circuits described in this section, the planar triode employed (a modified version of the Eimac 8757) does not rely on an intrinsically random avalanche breakdown process. As a consequence, the jitter obtained is relatively low ($\sim \pm$ 50ps), but the fastest sweep speed is only $\sim 4 \times 10^{9}$ cms^{-1} [10].

Laser triggered spark gaps have also been frequently used in providing the deflection ramp for streak cameras. In order to reduce the jitter (which is typically $\sim$ 1ns) and to control more accurately the breakdown process, high levels of optical energy are necessary. Furthermore relatively low writing speeds are usually obtained [11], although a Russian streak tube (UMI93ShS) was operated at a sweep speed of 2.5×10^{10} cms^{-1} [12]. A very low jitter of $\pm$ 20ps over 300 laser shots was reported [13] at a speed of $\sim 10^{10}$ cms^{-1}, where the spark gap had a thin dielectric introduced between the electrodes. However, when a similar arrangement was tested to synchronize the Hadland Imacon streak camera [14], it was found that the results were inferior in terms of jitter and sweep speed to those obtained with the hybrid avalanche transistor-Krytron circuit (which is shown in figure 6.2) [15]. This arrangement has been used in several experiments (see for instance [1]) and is usually adopted in Photochron streak camera applications which require picosecond resolution. It consists of a Krytron (EGG KN22) triggered by a stack of six avalanche transistors (BXZ61). The sweep speed obtained can be as fast as $\sim 2 \times 10^{10}$ cms^{-1} measured on the phosphor screen, and at this speed subpicosecond resolution was demonstrated [4]. However, although jitter as low as $\sim \pm$ 50ps can be achieved for brief periods of time [16], reliable performance can not be maintained for longer time intervals. Further adjustments are often necessary, and as a whole the system typically presents a jitter $\sim 100^{s}$ps. Therefore, although the sweeping is sufficiently fast for

most applications, the short and long term jitter restrict the use of such a circuit when very good time resolution is necessary.

It is clear that a switching device capable of providing a linear high voltage ramp which is automatically synchronized to the laser pulse with picosecond precision could greatly improve the performance of conventional deflection circuits.

5.3 The Choice of Semiconductor

The semiconductor chosen to provide the deflection voltage ramp for the streak camera was silicon. This choice was made because at the time when this work was started high voltage switching capability had only been demonstrated for this semiconductor. However, as can be seen on figure 4.3b, the shape of the voltage pulse obtained with Si devices on a few nanoseconds time scale can closely approach a step function, and the leading edge of the voltage switched can be used as the sweeping ramp. Because of the very long recovery time of nearly intrinsic Si devices ($\gtrsim$ 1μs), it should be possible to introduce integrators to slow down the risetime of the ramp. The writing speeds can then be conveniently altered, which is an important feature when slow as well as fast sweeping is required. In this manner, streak records with durations ranging from $\sim$ 250ps to $\sim$ 50-100ns should be possible.

However, as mentioned in chapter 3, the resistivity of commercially available n.i. Si crystals is relatively low ($\rho \lesssim 10^5 \Omega$cm). Therefore, in the case of d.c. bias, heat dissipation leads to premature electrical breakdown and ultimate destruction of the switch. There are two ways of avoiding this problem and make the use of Si possible. One of

them is to cool the semiconductor device to cryogenic temperatures (e.g. 77K), and the other is to pulse the bias voltage for a short time.

Although it is always more convenient to work at room temperatures, liquid nitrogen technology is widespread and relatively cheap. Therefore it does not present any major problems. The strong (exponential) temperature dependence of the number of thermally excited carriers in the sample for intrinsic semiconductors, makes the resistivity of Si increase by many orders of magnitude when the crystal is cooled from 300K to 77K [17]. The effect of the temperature on the mobility of the free carriers is not so pronounced, although in general, less frequent collisions with the lattice give rise to higher mobilities. In the case of Si, $\mu \alpha T^{-2.5}$ [18]and therefore, the sensitivity of the device should increase as the temperature is lowered, since a higher current is switched for the same input light intensity. Another interesting process to be observed at low temperatures is avalanching, although the discussion of possible applications of this effect is postponed to chapter 8.

The use of Si switches at cryogenic temperatures has recently been demonstrated, and excellent results were obtained [19, 20]. However, when commercially available nearly intrinsic Si crystals were employed, electrical breakdown was observed for relatively low fields ($\sim$ 1000 V cm^{-1}). This was attributed to the high kinetic energies gained by the carriers along the increased mean free path, accelerated by the electric field [19]. The semiconductor crystals were then doped with gold impurities, which effectively acted as scattering centres for the carriers. Unfortunately, special doping of semiconductors requires high technology, and therefore the specially prepared crystals that were employed in [20] are not as readily available as nearly intrinsic Si.

The way adopted to prevent electrical breakdown across the gap, as suggested by Le Fur and Auston [21], was to pulse the bias voltage on to the switch. It was determined experimentally that it takes $\sim$ 8-10ns for surface breakdown to occur across a $\sim$ 1mm gap Si device ($\rho = 1.7 \times 10^4 \Omega cm$) at room temperature. Therefore if the bias pulse duration is limited to $\lesssim$ 10ns, and if the picosecond light pulse necessary for the switching illuminates the gap during that period, than a picosecond risetime voltage ramp will be switched. If for any reason the light pulse does not activate the device, the duration of the applied bias is sufficiently short to avoid a spark that would damage the semiconductor surface. Furthermore, heating effects caused by current leakage on a 10ns time scale are negligible.

In this case, care has to be taken to make sure that the light pulse illuminates the switch during the application of the bias. Since the jitter of Krytrons and other conventional high voltage switching elements can be as low as $\sim$ 1ns, it should be possible to synchronize the voltage bias lasting for $\sim$ 10ns with the arrival of the light pulse at the switch.

It should be noted that pulsing the voltage for a few nanoseconds introduces two limitations to the operation of the streak camera: (1) Very slow sweeping is not possible because the voltage pulse delivered to the deflection plates returns to zero when the bias finishes. However, since for slow sweeps the jitter is usually not a serious problem, conventional systems can be used in such cases; (2) when the bias returns to zero, a second voltage ramp of opposite direction to the first ramp is applied to the deflection plates (flyback). Therefore, in order to obtain a unambiguous streak record on the phospor screen, it is important to ensure that a single light event is studied at a time, by selecting a single pulse with the pulse selector. It

has been shown, however, as mentioned in section 3.5, that if the voltage bias for the Si switch has a slow risetime (> 100ns), it can have durations of several microseconds without causing premature electrical breakdown [16]. In this case neither of the above mentioned limitations exists.

5.4 Synchronization

5.4.1 Conventional Approach

An initial attempt was made to bias the Si device with a ∿ 5ns square voltage pulse generated by a Krytron in a charged line configuration as shown in the schematic of figure 5.1. A flashlamp

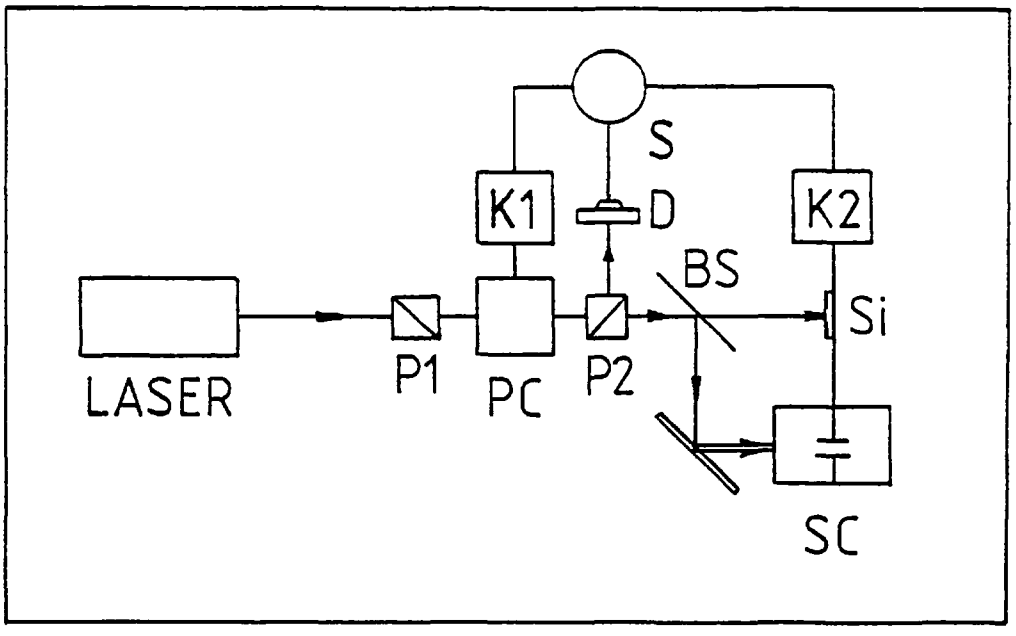

FIG 5.1

pumped dye laser [12] (similar to the one described in section 7.3.2.1) was used to activate the switch. It delivered pulses of ∿ 30μJ at 0.6μm wavelength. The mode-locked train was monitored with a S20 biplanar vacuum photodiode(D) used in conjunction with a Tektronix 519 oscilloscope . The gate signal from the oscilloscope simultaneously

activated two stacks of six avalanche transistors, each stack triggering one Krytron (KN22) [15]. The high voltage signal from the first Krytron (K_1) biased a Pockel's cell in a Blumlein arrangement for single pulse selection. The second Krytron (K_2) provided a square high voltage bias pulse with small ripple (< 5%) for the Si switch.

When this experimental set-up was tested, it was found that the subnanosecond jitter of Krytrons was difficult to achieve in practice. All the unreliability encountered in circuits incorporating a single high voltage fast switching element was much worse in this case, where two Krytrons had to trigger synchronized to within $\sim$ 1ns. The dead time of the valves was not the same, and changed with the voltage applied. Because the circuits had to be interconnected, they were much more susceptible to electrical noise pick-up. As a consequence the avalanche transistor stacks would sometimes trigger as the laser was fired, before the gate signal from the oscilloscope was delivered. Noise from one valve would also trigger the other, but several nanoseconds later. As a whole, the system was unreliable, and in practice it was very difficult to properly synchronize the bias for the switch to the single pulse selector.

The solution found for this problem was to eliminate the need for the second Krytron. For single pulse selection, the square voltage pulse applied to the Pockel's cell should have a duration equal to the roundtrip time of the laser, which is typically between 4 and 8 nanoseconds. During this time, a $\sim$ 1mm gap Si switch should hold-off the $\sim$ 5KV bias pulse, since electrical breakdown does not have enough time to develop. Therefore, the coincidence of the hold-off time for Si and the roundtrip time of typical single shot mode-locked lasers allows great simplification in the electronic circuitry. By modifying

the Blumlein configuration, a fraction of the voltage provided for the single pulse selector was also used for biasing the switch. Consequently, a single Krytron was needed, and the voltage was applied to the switching device automatically synchronized to the selection of the light pulse.

5.4.2 The Modified Arrangement

Before examing the new configuration, it is worth describing the traditional Blumlein pulse forming network, which is schematically shown in figure 5.2a. The Krytron (or other conventional high voltage fast switching element) is represented by (K). The cable impedance is usually 50Ω. The impedance Z has a value chosen to be twice that of the cable, and in practice consists of a 100Ω resistor. The Pockel's cell is connected in parallel with Z, and does not significantly alter the resistive character of the impedance. When the Krytron is activated, a voltage pulse of amplitude V_o is developed across the impedance Z and therefore also across the Pockel's cell. It lasts for $2L/c_n$, where L is the length of each arm, and c_n is the speed of the electromagnetic wave inside the coaxial cable. The pulse shaping mechanism of a Blumlein network is described in detail in [22]. Briefly, as the Krytron switches, a negative voltage front travels along

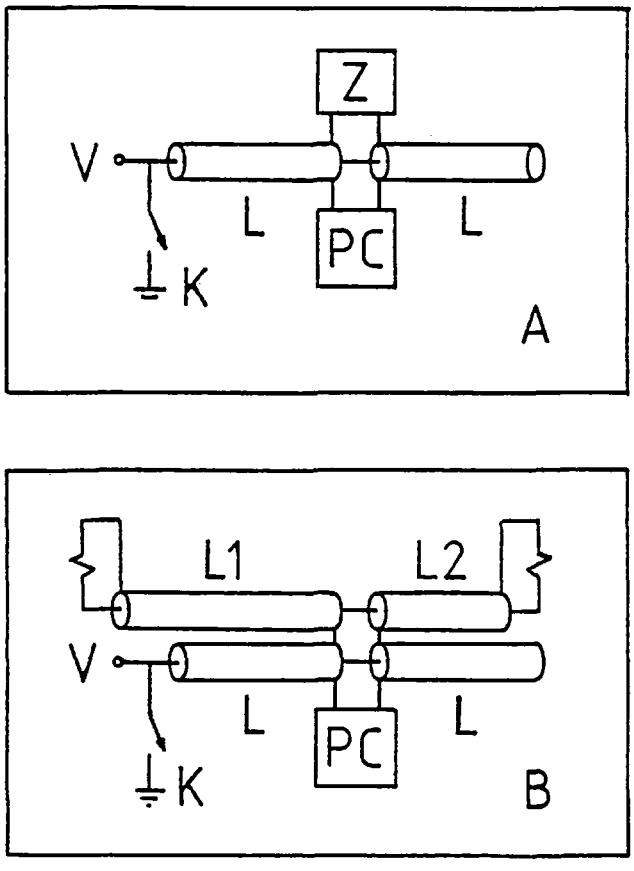

FIG 5.2

the left branch of the line until it reaches the discontinuity at the Pockel's cell. Because of the impedance mismatch, half of the voltage front is reflected and half is transmitted into the other 50 Ω branch, leaving a difference of potential V across the cell. As the fronts reach the end of the coaxial lines they are once more reflected with a net π phase difference, and cancel each other as they arrive simultaneously at the centre of the arrangement.

Figure 5.2b shows a schematic representation of the modified arrangement, where the 100 Ω resistor is replaced by two 50Ω coaxial cables connected effectively in series (because a pulse switched by the Krytron experiences their combined impedance). Therefore, when the valve is triggered, a voltage pulse with the same amplitude and duration as in the conventional configuration develops across the Pockel's cell. As a consequence, this arrangement is equally capable of providing the high voltage bias for the single pulse selector.

It can also be seen that two replicas of the voltage pulse applied to the Pockel's cell travel down the coaxial lines of arbitrary lengths L1 and L2. They have opposite signs, and due to the equal impedance of the cables, they have half of the amplitude of the pulse developed across the Pockel's cell. If the two lines are terminated in 50Ω loads, no reflections will appear at the ends.

The length of the lines L1 and L2 can be easily determined. Therefore, the voltage pulses with amplitude $V_o/2$ develop across the loads RL1 and RL2 with a known delay in relation to the opening time of the light pulse selector. The uncertainty of the cable lengths measurements lead to errors that correspond in time to $\lesssim$ 100ps. When one of the loads (e.g. RL2) is replaced by the Si switch, a careful measurement of light path and length of cable ensures that the picosecond

light pulse that activates the switch will arrive during the application of the pulsed bias. Synchronization is thereby conveniently achieved.

The replacement of a 50Ω termination load by a high resistance semiconductor slab gives rise to some reflection. This can lead, in the less favourable case, to a second weak light pulse being selected by the Pockel's cell, a few nanoseconds after the main switching process. This second pulse was never observed with the streak camera, in practice. Therefore, no further attempts to properly impedance match the arrangement were made.

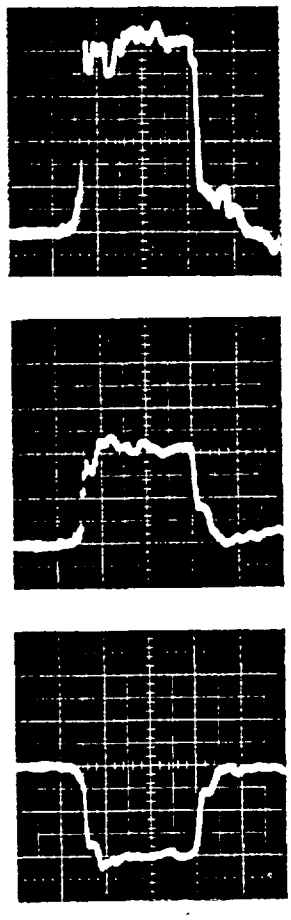

FIG 5.3 - Voltage pulse developed across the Pockel's cell (top) and across the two resistors (centre and bottom)

The use of this set-up should not be limited to this particular experiment. Further changes can be made, according to the amplitude of the voltage required at the load; for instance, a square voltage pulse with the full amplitude V_o will be transmitted along a coaxial line of 100Ω impedance, if it replaces the two 50Ω cables L1 and L2. In this case, a series of electro-optic components, such as semiconductor switches or Pockel's cells [23], could be activated in synchronism by a single Blumlein pulser.

The voltage bias for the switch and for the Pockel's cell can be monitored if the other 50Ω load (e.g. RL1) is replaced by a 50Ω high voltage probe-oscilloscope combination. Figure 3a shows a voltage pulse lasting for 100ns with 6KV amplitude developed across a 100Ω resistor, as in the conventional arrangement of figure 5.2a. The oscillograms of figures

5.3b and 5.3c show the corresponding voltage pulses that travel down the coaxial lines L1 and L2, in the new scheme. They have half of the amplitude (3KV each) with opposite signes, as expected. The ripple observed is mainly due to noise pick-up by the high voltage probe and by the oscilloscope, but it is also partly because of imperfections in the Blumlein pulse-forming network.

5.5 The Experimental Set-up

When biasing the Si switch with a voltage pulse provided by the same Krytron circuitry used for the single pulse selector, the experimental set-up became much simpler. A schematic diagram is seen in figure 5.4.

A Nd:Phosphate glass laser [24] was used instead of the dye laser employed earlier. According to the expression (2) derived in

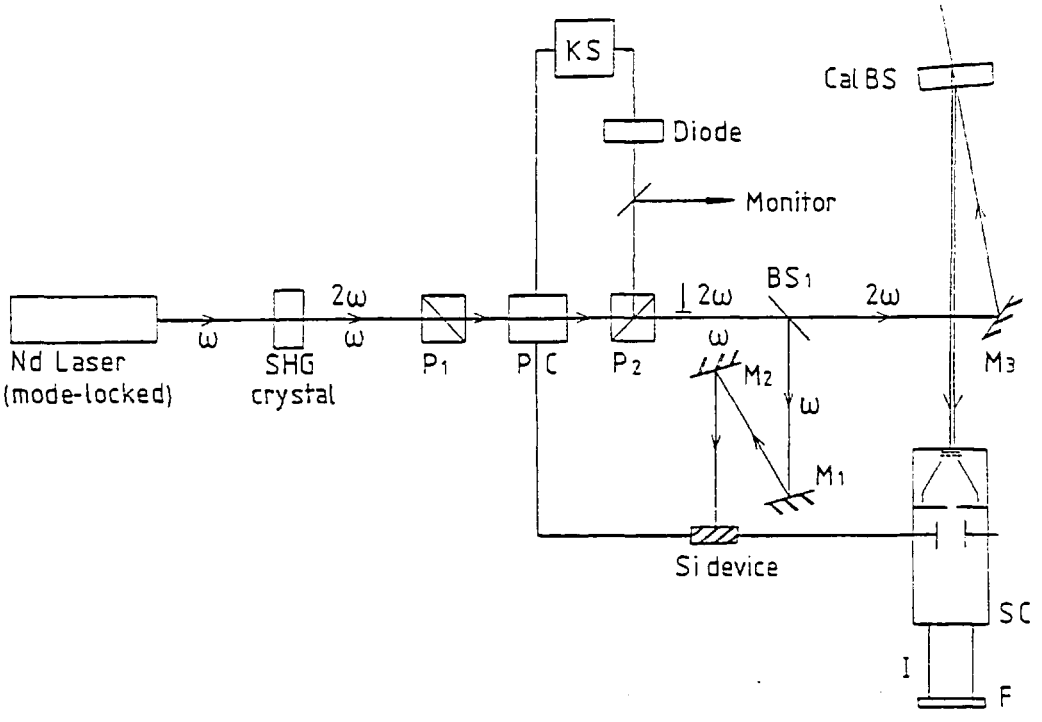

FIG 5.4 Experimental arrangement

section 3.4, the impedance of a 1mm gap Si device becomes negligible when it is irradiated by a few microjoules of optical energy. Losses occur at the pulse selector, due to absorption and scattering, and at the switch, due to misalignment and to the beam shape. Therefore, the actual energy required to fully saturate the switch for every laser shot is several microjoules. As a consequence the neodymium laser can supply the necessary energy more easily than the dye laser, since it is able to deliver ∿1mJ in a picosecond pulse, as compared to∿40μJ for the Rh6G laser system.

The Nd:Phosphate laser produced mode-locked trains of pulses with a roundtrip time of 7ns at 1.05μm wavelength. The laser rod was 16.7cm long, had 9.5 mm diameter, and was pumped by a single helical xenon flashlamp. Approximately 1.5KJ of electrical energy was dissipated in the flashlamp by two 47μF capacitors charged to ∿ 5.5KV. A water cooling system was provided to avoid excessive heating of the rod, but nevertheless the repetition rate was only ∿ 1 laser shot per minute. Air was pumped into the cavity head to displace the ozone formed by the discharge of the flashlamp.

The mode-locking dye used was a 10^{-4}M solution of Kodak 9860 dye diluted in diclorethane contained in a ∿ 250μm thick cell adjacent to the 100% reflecting, 2m radius of curvature back mirror. The cell had a red glass front window that prevented short wavelength radiation from reaching the dye, therefore avoiding photodissociation. The output coupler was a 50% transmission (at 1.06μm wavelength) plane mirror.

Each laser shot produced trains with ∿ 80-100 pulses, having a total energy of ∿ 100mJ. No transverse mode selector was used, and the individual pulses had durations between ∿6-10ps. Due to the divergence of the multimode laser beam and losses in the pulse selector

and light delay (mirrors M1 and M2), it is estimated that the energy of the picosecond light pulses used to activate the switch was approximately $\sim$ 20-30μJ.

Since the streak-camera used in the experiment was not sensitive to 1.05μm radiation, the mode-locked train of pulses was directed into an angle-tuned second harmonic generation ADP crystal with typical conversion efficiency of $\sim$ 10%.

A single picosecond light pulse containing both fundamental (ω) and second harmonic (2ω) components was selected from the mode-locked train by a Pockel's cell (PC) placed between two Glan-Thompson polarizers (P1 and P2). The light rejected by the polarizer P2 was partly used for monitoring the pulse selection with a photodiode and a storage oscilloscope, and partly used for the triggering of the pulse selector. A second photodiode provided a signal $\gtrsim$ 8V which activated a stack of 6 avalanche transistors. This in turn, provided a fast risetime 1KV electrical signal to trigger a Krytron (KN22B) in the Blumlein arrangement described in the previous section. Typically a 7ns long, 9KV square voltage pulse was applied to the Pockel's cell, and half of this voltage pulse was also used to bias the Si switch.

The length of cable connecting the Pockel's cell and the switch was measured so that the device was illuminated at the middle of the application of the bias voltage. In other words, the picosecond laser pulse arrived at the switch 3.5ns after the voltage pulse (with $\sim$7ns total duration) had started to develop across the Si crystal. Jitter of the Krytron circuit in the single pulse selector was then well accommodated, and in practice, the synchronization of the 7ns duration bias with the illumination of the switching device was found to be extremely reliable.

The fundamental radiation component of the laser pulse was reflected off the beam-splitter BS1 (R $\sim$ 100% at 1.05μm), delayed, and directed on to the Si slab. The delay provided by mirrors M1 and M2 was adjusted to ensure that the laser pulse arrived when the bias pulse had just been established across the switch.

The second harmonic component of the single pulse was strongly attenuated at the pulse selector. It was then transmitted by the beam-splitter, and passed through a calibrated optical delay line (cal BS), which provided two pulses of known time separation. These pulses were then finally directed on to the input slit of the streak camera. When necessary, further optical attenuation was added with the introduction of neutral density filters. A diffuser was also introduced, to ensure that the whole slit length was uniformly illuminated.

The streak camera system [25] incorporated a Photochron I image tube with a S11 photocathode, and the output phosphor was lens-coupled to a magnetically focussed image intensifier (EMI 9694). The resolution of the camera as operated was $\sim$ 3ps for the 0.53μm radiation, at a sweep speed of 2×10^{10} cms^{-1}. The streak tube deflection sensitivity was 300 Vcm^{-1}, and a voltage ramp of 1.5KV provided a 5cm streak length. In the streaking mode, it is estimated that the spatial resolution of the camera was $\sim$ 5 l.p.mm^{-1}, and the static spatial resolution was $\sim$ 10 l.p.mm^{-1}. A 1.17 demagnification was measured, and the width of the slit was usually 80μm (focussed to $\sim$ 20μm on the photocathode). The blue light gain of the image intensifier was 10^6.

The semiconductor switch was constructed according to the procedure described in detail in chapter 4. The nearly intrinsic Si slab measured 6mm by 4mm by 0.5mm thickness and had a resistivity of $1.7 \times 10^4 \Omega$cm. The dark impedance of the switch was $\sim$ 1MΩ, across the

1mm long gap.

5.6 Results

Typically a 4.5KV, ∿ 3.5ns duration voltage pulse was applied to the deflection plates of the streak camera, the deflection voltage ramp consisting of the leading edge of the pulse. The capacitance of the plates, which was a few picofarads, and the stray inductance of cables and connectors limited the risetime of the voltage ramp, so that the maximum writing speed recorded was 2.3×10^{10} cms^{-1}. A streak tube with better bandwidth deflection circuit should allow faster speeds to be obtained. However, even at the usual writing speed obtained of 2×10^{10} cms^{-1}, the 3ps time resolution of the camera was limited by the spread in energy of the photoelectrons emitted by the photocathode, rather than by the time taken to sweep a single resolution element on the phosphor screen. Therefore no attempt was made to increase the writing speed to even higher values.

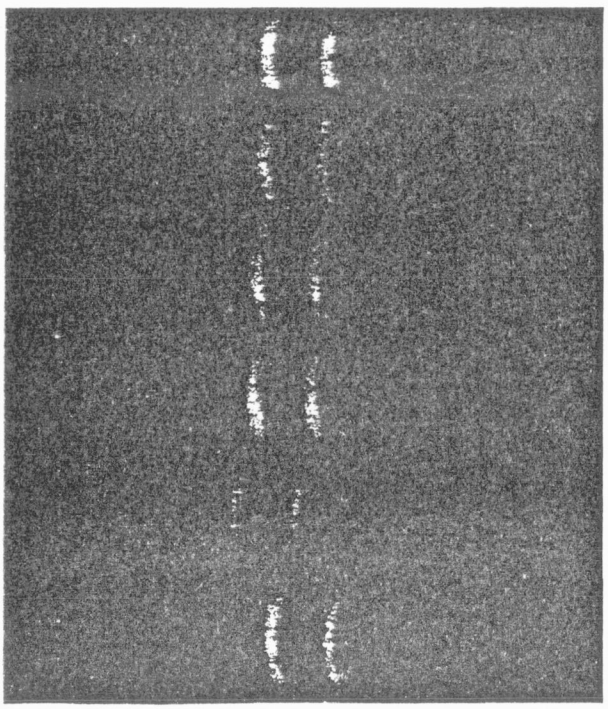

FIG 5.5 Six consecutive streak records showing jitter of ±11ps. Each pair of pulses has a separation of 50ps

Figure 5.5 shows a series of six consecutive streaks recorded on Polaroid film (type 410). In each streak the pair of pulses is separated by 50ps (front and back reflections off the calibrated optical delay line). The jitter - standard deviation from the average position on the screen - is ± 11ps. For a period of ∿ one month during which ∿ 5×10^3

shots were fired, the overall system jitter was consistently below ± 15ps. For several consecutive shots, however, much lower values were obtained (e.g. the four top streaks in figure 5.5 show ±6ps jitter). Both short and long term jitter was consistently low. It was found, for instance, that streaks were obtained at the centre of the phosphor screen at writing-speeds of 2×10^{10} cms^{-1} from the very first laser shot of the day, after having had all the equipment switched off for a night, or even for a week-end. This kind of performance can not be easily matched by conventional systems incorporating a Krytron to generate the deflection voltage. As mentioned in section 5.2, even when the short term jitter of Krytrons is low, it is very difficult to maintain the same operating characteristics in the longer term, e.g. from day-to-day.

Although a voltage ramp of 1.5KV should be adequate for a full sweep, the streak voltage amplitude was increased to ensure linearity. Usually ∿ 4.5KV were applied to the deflection plates, but voltages up to 6KV were sometimes employed. The linearity of the streak was checked by adding a second calibrated beam splitter to the optical delay line. Figure 5.6 shows a series of five consecutive shots recorded on Polaroid film, where both pairs of pulses in each streak have separations of 50ps. In order to determine more accurately the degree of linearity of the sweep, Ilford HP5 film was used, allowing

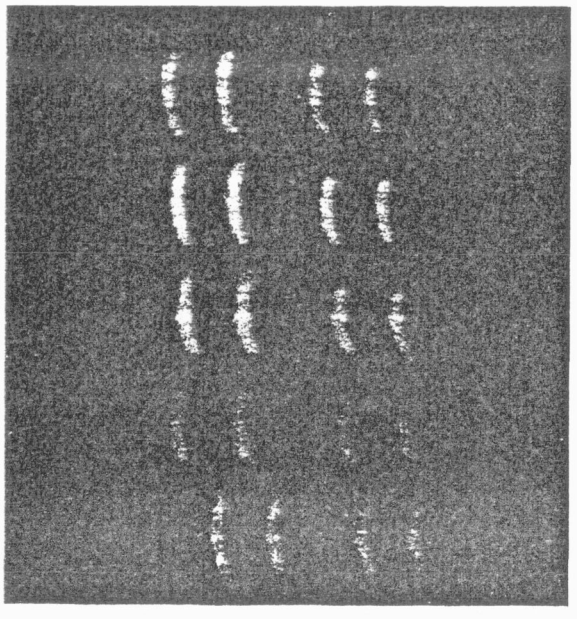

FIG 5.6 Five consecutive streaks of pulse trains used for calibration of the streak camera

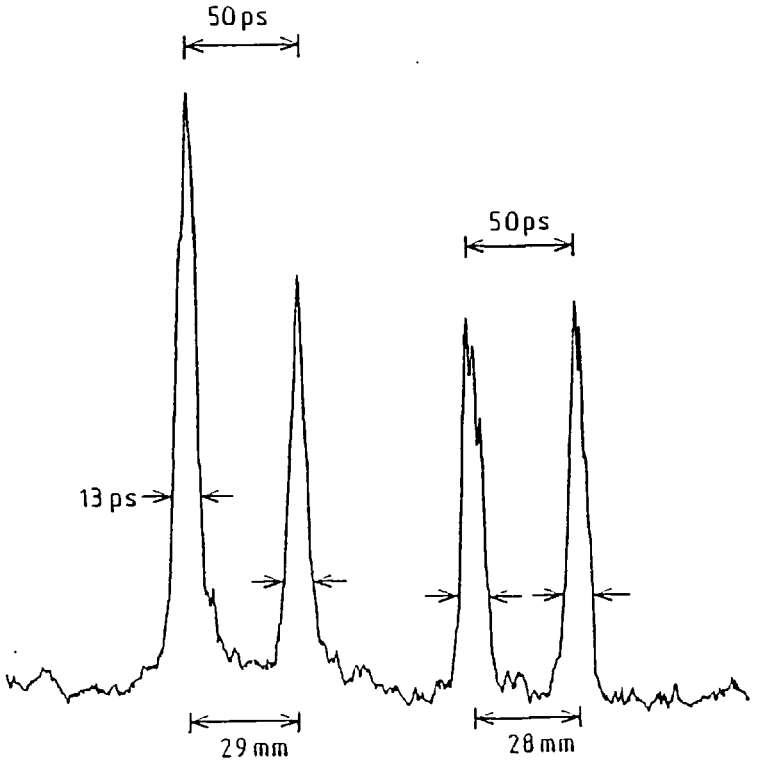

FIG 5.7 Microdensitometer trace of streak record showing linearity of the sweep

microdensitometry to be carried out. Figure 5.7 shows a microdensitometer trace of streak records, again obtained at a writing speed of $2 \times 10^{10} cms^{-1}$. The sweep is linear to within $\pm$ 2% over the complete range of the streak (250ps).

The writing speed of the streak camera was varied by altering the amplitude of the bias voltage pulse to the semiconductor switch. Writing speeds as low as $1 \times 10^{10} cms^{-1}$ were used, and the records obtained showed that the jitter remained consistently better than $\pm$ 15ps.

5.7 Discussion

The results presented above show that the use of semiconductor switches can considerably improve the synchronization of single-shot streak cameras, as compared to conventional systems. However, it is

useful to examine the causes of the remaining jitter, so that even better performances can be obtained.

For the Krytron activated streak cameras, jitter is due to the lack of synchronization between the beginning of the voltage ramp and the ultrashort light pulses. Streak camera systems incorporating Si switching devices do not present this problem to a great extent, due to the inherent synchronization insured by the photoconduction mechanism involved in the generation of the ramp. The main reason for the remaining jitter is the fluctuation in the amplitude of the voltages switched, from shot-to-shot. The maximum value of this voltage varies for two reasons: different bias at the moment of the switching, and different switching efficiencies. These two problems are independent, the first related to the bias voltage pulse, and the latter depending on the laser pulse activating the device.

Before examining the experimental limitations giving rise to jitter, it is interesting to consider what happens as the amplitude of the voltage switched changes from shot-to-shot. A few important simplifying assumptions are made: (1) The bias applied to the switch does not change significantly during the time taken for a full sweep, since the voltage bias varies slowly compared to the RC time of the deflector; (2) the risetime of the voltage ramp is determined by the characteristic RC time of the deflection circuit (which is the same for different laser shots), and not by the risetime of the switch; (3) the voltage is assumed to increase linearly in time, which implies that the impedance seen by the switch must be always the same, so that the deflection plates (which act as a capacitor) charge up at a constant current; (4) The beginning of the voltage ramp is assumed to be always synchronous to the arrival of the activating light pulse.

If these important simplifications are made, for a particular laser shot the voltage ramp can be represented by a straight line with maximum value

$$V = \alpha \bar{V},$$

where $\bar{V}$ is the average of V over a large number of shots, and α is a dimensionless factor (of value ~ 1), which accounts for the fluctuation of the voltage switched, from shot-to-shot. Let

$$\Delta V = \bar{V} - V$$

be the measure of the deviation of V from the average value $\bar{V}$. In reference to the figure 5.8, let T_{TOT} risetime of the ramp, T_{MIN} and T_{MAX} define the time interval displayed on the phosphor screen for the particular laser shot, and $\bar{T}_{MIN}$ and $\bar{T}_{MAX}$ define the average, for several laser shots, of the time interval over which a luminous event is studied. (The time origin is given, for each shot, by the arrival of the light pulse at the switch). By simple geometric arguments, the following relations can be derived:

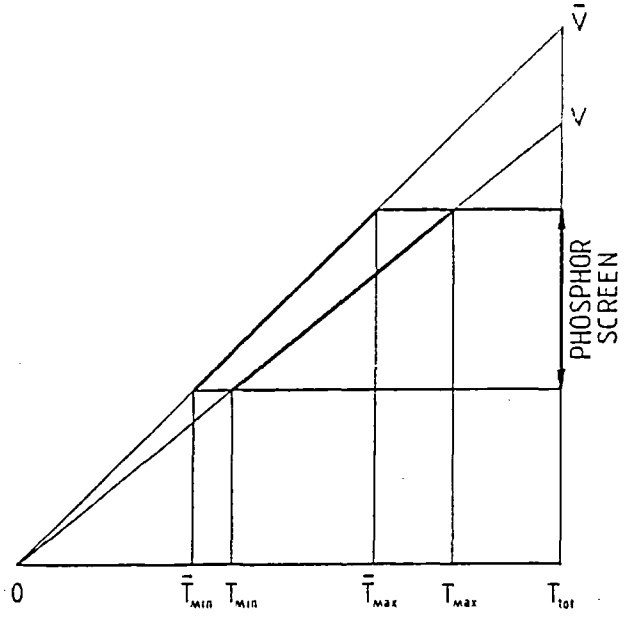

FIG 5.8

$$T_{MIN} = \bar{T}_{MIN}/\alpha \qquad (1)$$

$$T_{MAX} = \bar{T}_{MAX}/\alpha \qquad (2)$$

$$T_{MAX} - T_{MIN} = (\bar{T}_{MAX} - \bar{T}_{MIN})/\alpha \qquad (3)$$

Equation (1) shows that the origin of the time interval displayed on the screen changes, and equation (3) means that the full screen size corresponds to different time intervals, from shot-to-shot. Therefore if the maximum voltage switched is altered, not only the position of

the streaks is shifted, but also different writing speeds are obtained. Longer sweeps correspond to lower amplitude bias and faster writing speeds to higher voltages switched. As a consequence, an independent time calibration (such as the calibrated delay line) is required for evaluating the performance of a streak camera system incorporating a semiconductor switch.

It is clear that the concept of jitter in this case is not as meaningful as when only the origin of the time interval displayed shifts from shot-to-shot, since it does not fully describe the compression or expansion of the time interval studied. More significant here is the measure of α, i.e., how little the amplitude of the voltage switched differs from the average, for each laser shot. However, it is possible to derive an expression relating the fluctuation of the value of α (measured by σ_α) to the jitter of the streaks, which is defined as the standard deviation from their average position on the screen.

Let $\bar{X}$ be the average position on the output phosphor of streaks of an event recorded for several laser shots, $\bar{T}$ be the average time to which $\bar{X}$ corresponds (for the average writing speed), and let ΔX define for a particular shot, the distance between the position of the streak X from the average $\bar{X}$. It is clear that because the amplitude of the voltage switched varies from shot-to-shot, streaks of the same time event appear each time spatially displaced on the screen. Therefore, for the particular laser shot where the streak was recorded at X (and not at $\bar{X}$), the event will be interpreted as having happened at a time T (not $\bar{T}$). By simple geometrical arguments, the following relation can be derived (c.f. figure 5.9).

$$\bar{T}V = T\bar{V}$$

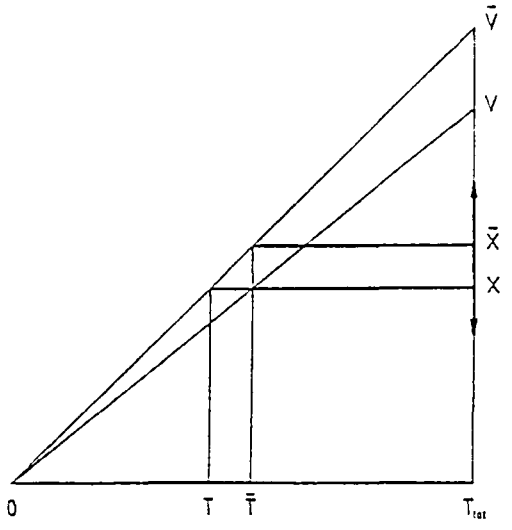

FIG 5.9

Therefore,

$$T = \alpha\bar{T} \qquad (4)$$

and so, if the amplitude of the voltage ramp switched for a particular laser shot is say, 5% lower than the average for several shots, the streak will also be displaced in time by 5%. Because of the linear contraction, larger differences should be observed for streaks of events happening later. Therefore, the jitter at one end of the screen should be larger than at the other, although the voltage percentual change from the average is constant along the screen.

The jitter is defined, for a large number of events, by the formula

$$\sigma_T = \sqrt{\frac{1}{N-1}\sum_{N}(T - \bar{T})^2}\ .$$

From equation (4), it follows that

$$\sigma_T = \bar{T}\sqrt{\frac{1}{N-1}\sum_{N}(\alpha - 1)^2} = \bar{T}\,\sigma_\alpha \qquad (5)$$

It is useful to consider a numerical example to illustrate the implication of expression (5). Assuming that the maximum voltage switched is $\sim$ 4.5KV, the voltage window is 1.5KV, and that only the central part of the ramp is used, for a 250ps full screen size sweep the following table can be constructed:

$\bar{T}$ \ σ_α	± 2%	± 4%	±10%
250 ps	± 5ps	±10ps	±25ps
375 ps	± 8ps	±15ps	±38ps
500 ps	±10ps	±20ps	±50ps

Given the percentual variation of α, the jitter (σ_T) depends on the particular instant $\bar{T}$ at which it is measured. For a $\pm$ 10% variation in the amplitude of the voltage switched, for instance, the jitter will be $\pm$ 25ps on one side of the screen, $\pm$ 38ps at the center, and $\pm$ 50ps at the other side of the output phosphor. (The experimental results were usually measured at the centre). When the maximum voltage switched is higher, for the same 1.5V voltage window and using the central part of the ramp, the time interval displayed starts later and ends earlier, and in this case the variation of jitter along the length of the screen is smaller.

At this point it is useful to compare experimental results to values predicted theoretically from this simple model described. However, the measurement of α is difficult in practice due to parasitic electrical noise and to the degree of precision required. In fact, all accurate measurements of ultrafast high voltage pulses were complicated by the use of non-ideal probes and oscilloscopes with limited bandwidth. Nevertheless, a semi-quantitative comparison can be carried out. The results obtained with the streak camera showed a jitter of $\pm$ 15ps measured at the centre of the screen, when only the central third of the ramp was used, corresponding to the time interval 250ps - 500ps. According to equation (5), since $\bar{T}$ = 375ps and $\sigma_T = \pm$ 15ps, one obtains $\sigma_\alpha = \pm$ 4%. In other words, the variation of α due to the combined effect of bias fluctuation and non-perfect saturation of the semiconductor switch by the light pulse should be $\sim$ 8%, from shot-to-shot. This value is in reasonable agreement with the variation of α estimated from oscilloscope measurements.

Jitter due to changes in the bias occur if the voltage pulse delivered by the Krytron is not reproducible in amplitude, or if its

profile is not flat (i.e. presents some ripple) and the switching action takes place, from shot-to-shot, at different places within the bias pulse. It was found experimentally that the shape and amplitude of the bias pulse was quite reproducible, but the oscillograms showed a profile with a ripple amounting to 5-10% of the total amplitude. Part of the ripple observed could be attributed to noise pick-up by the high voltage probe and the oscilloscope used for monitoring (Tektronix 7834). However, it is likely that the voltage switched will vary by a few percent from shot-to-shot, because at the instant when the device is illuminated, it is subjected to different bias amplitudes. Smoothing the profile of the bias pulse should lead to lower jitter of the streak camera system. The use of a stabilized voltage supply for the Krytron, which biases both the single pulse selector and the semiconductor switch, should also help to reduce the jitter.

The switching efficiency depends on the total energy of the activating picosecond pulse, and on its shape. The duration of the light pulses ($\sim$6-10ps) was always much shorter than the time taken for a full sweep ($\sim 100^{s}$ps), and therefore it was neglected in the simple theoretical model presented. For the same reason, the most important consideration for efficient switching to take place is the energy, rather than the shape of the pulse. The optical energy used to activate the device was $\sim$ 20-30μJ, which is nearly the minimum required to reduce the impedance of the Si slab to a negligible value, as seen in section 3.4. Therefore the shot-to-shot fluctuation of the pulse energy might have led to variations of a few ohms in the "on-state" impedance of the switch, and consequently change the amplitude of the voltage ramp by a few percent.

By focussing the light on to the gap, more energy was available for the activation of the switch. However, the effect of low level

light pulses leaking through the single pulse selector was integrated by the Si crystal prior to the main activation, resulting in the creation of (long lived) electron-hole pairs. Therefore, the impedance of the device was already quite low by the time the main pulse illuminated the gap, and voltage leaked through the switch when it should still be on its "off-state". The use of a higher rejection ratio single pulse selector should prevent leakage of light, and allow tighter focussing on the gap, so that better switching efficience and lower jitter should be achieved.

Finally, for systems where the amplitude of the ramp is the same for every laser shot, changes in the shape and duration of the activating light pulse might no longer be negligible.

5.8 Synchronization of a Streak Camera Incorporating a GaAs Switch

The results obtained with the Si device suggest that the jitter of single-shot streak cameras can be reduced to such an extent that successive records may be superposed on the phosphor screen without significant loss of temporal resolution. Integration of streak records is desirable because of the better signal-to-noise ratio obtained, allowing increased timing accuracy of the measurements, besides being of great value where low intensity light signals are studied (e.g. where photodissociation of samples is to be avoided).

There are two ways of accumulating streaks on the phosphor screen: either by superposing records of consecutive pulses from a single mode-locked laser train, or else by superposing the streaks of pulses resulting from several consecutive laser shots. In the first case, (which is the synchroscan mode of operation), a voltage ramp has to

be provided to the deflection plates every few nanoseconds, and the "memory" of the phosphor retains the image of the streaks. In the other case, the repetition rate of the ramp can be as low as that of the laser, and the records should be either stored on a multichannel analiser or on a single photographic plate.

As seen in chapter 2, synchroscan requires recurrent sweeping in synchronism with the light pulses, and since this is achieved in conventional systems by using the linear part of a sine wave voltage for the deflection, it is generally used in conjunction with CW lasers [26, 27]. On the other hand, jitter-free single-shot picosecond streak cameras would allow the superposition of streak records to be obtained with single-shot lasers, which are versatile sources of intense ultrashort light pulses at several wavelengths.

In order to be able to eliminate the jitter of streak cameras with semiconductor devices, the amplitude of the deflection ramp switched has to be constant for each sweep, demanding reproducible switching efficiency and bias amplitude. It is obvious that the simplest way to obtain a reproducible bias for the solid-state switches is to use d.c. voltage. However, when Si is employed under these conditions, the crystal has to be cooled to cryogenic temperatures. Also, the superposition of streak records of consecutive pulses from a single mode-locked laser train would be complicated by the relatively long recovery time of the switches. On the other hand, semi-insulating III-V semiconductors such as GaAs or GaP can hold off high voltages (d.c.) at room temperature, and switch kilovolt pulses with picosecond risetimes. They should enable the superposition of streaks from different laser shots on the phosphor screen, and also of streaks of several pulses from the same mode-locked train, due to

the fast recombination times of carriers in these semiconductors. The only remaining problem to ensure very low jitter in a streak camera system incorporating a GaAs switch would then be to make sure that the solid-state device is fully saturated by every activating light pulse.

If the streak camera is operated synchronously with several picosecond pulses from a single laser shot (synchroscan), care should be taken to ensure that the duration of the light pusles studied is the same, since it can vary considerably within the mode-locked laser train, as discussed in chapter 2. Such a system could be used, for instance, in conjunction with flashlamp pumped dye lasers, where typical mode-locked trains contain hundreds of picosecond pulses within a smooth envelope [28].

A preliminary attempt was carried out to superpose streaks on the phosphor screen, using a single-shot streak camera synchronized by a semiconductor switch. The number of pulses used was limited to two, in order to observe any loss of temporal resolution due to jitter, when accumulating the records. The pulses were selected from the same mode-locked train and several shots were fired in succession, so that the jitter from shot-to-shot could also be estimated.

A diagram of the experimental set-up is shown in figure 5.10. A second harmonic generation crystal was again introduced because the S11-photocathode of the streak camera employed was not sensitive to 1.05μm wavelength. Fundamental and second harmonic light trains were separated by the first polarizer (P1) of the single pulse selector. The calibrated delay line consisted of a single 5mm thick quartz plate, providing two reflected components separated by 50ps, which were directed into the slit of the streak camera.

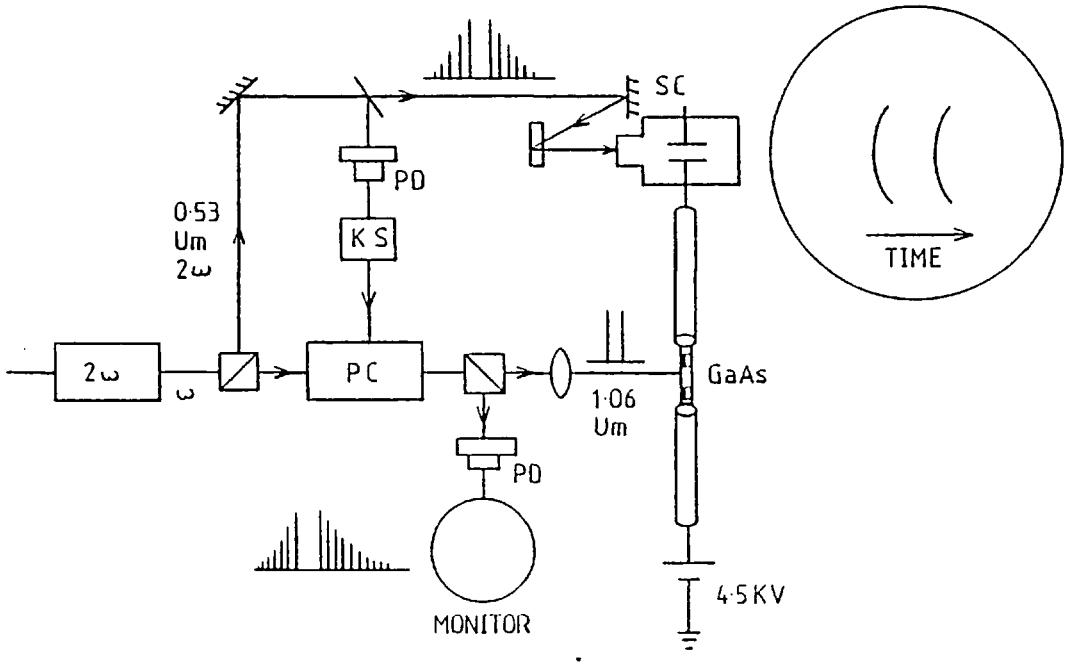

FIG 5.10 Experimental Arrangement

Although the whole second harmonic radiation train of pulses illuminated the calibrated delay line, only two of the fundamental wavelength light pulses activated the GaAs switch, so that only two voltage ramps were provided for the deflection. The two light pulses activating the semiconductor device were transmitted by the pulse selector formed by polarizers P1 and P2, and the Pockel's cell PC. The voltage bias for the Pockel's cell lasted for 14ns, (the roundtrip of the laser being 7ns), and was generated by a Krytron switch in a conventional arrangement. The pulses selected were monitored with a ITL vacuum photodiode, and displayed on a storage oscilloscope (Tektronix 7834).

The GaAs device was biased with a d.c. voltage of 4KV, provided by a stabilized power supply (Brandemburg Alpha Series). It had Al electrodes leaving a long gap measuring $\sim$ 4mm, and otherwise its

construction was identical to the one described in chapter 4. Since the bias was not pulsed, a 50Ω termination resistive load was connected in parallel with the deflection plates, in order to eliminate reflections and to allow the initial d.c. voltage drop to appear across the switch.

Although a focussing lens was used to increase the energy available in the activation of the switch, it is estimated that only ∿ 50-75μJ of optical energy illuminated the gap. Again, this value was comparable to the minimum necessary to cause full saturation of the device, and if the pulse selector slightly reduced the intensity of one of the light pulses, the two voltage ramps applied to the deflection plates differed in amplitude, and the streaks did not overlap exactly.

The maximum sweep voltage generated by the switch in this configuration was 2KV, which was enough for a full sweep. Although a systematic evaluation of the linearity of the sweep was not carried out, it is apparent from different streak records that the writing speed was constant to a few percent for each laser shot.

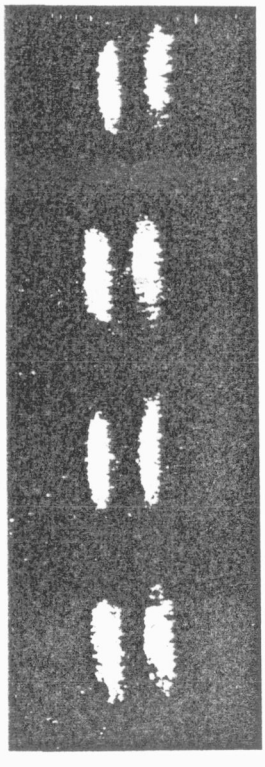

FIG 5.11

Preliminary results obtained are shown in figure 5.11. The four records seen were obtained from four consecutive laser shots, where the spacing between the pairs of streaks corresponds to a time separation of 50ps. Each streak recorded on the photograph resulted from the overlap of two pulses from the mode-locked train on the phosphor screen. It is apparent that the streaks can be made to superpose, although some loss of resolution is observed, from

comparisons made with records where a single pulse is displayed. From microdensitometer traces of streaks similar to the ones shown, it is estimated that the loss of resolution due to the overlap was as low as $\sim$ 5ps in some cases.

The shot-to-shot jitter in figure 5.11 is $\pm$ 7ps, although the bottom three streaks show a jitter inferior to 5ps, obtained at a writing speed of $1 \times 10^{10} cms^{-1}$. This result suggests the feasability of overlaping not only streaks of pulses from a single mode-locked train, but also overlaping streaks of pulses resulting from different laser shots.

The major cause for the remaining jitter in this preliminary experiment was the high energy levels required to saturate the 4mm long solid-state switching device. In order to ensure that the switch would hold off the d.c. voltage bias, the gap length was relatively long, and the amount of light energy available to activate the device was approximately equal to the minimum necessary to reduce its impedance to a negligible value. As seen in section 3.4, the "on-impedance" of the switch varies with the square of the separation between the electrodes. By employing higher resistivity semiconductor crystals (such as semi-insulating GaP) or by using thinner slabs, it should be possible to significantly reduce the gap lengths. Another possible method of improving the experiment is diagramatically shown in figure 5.12. Higher currents can be obtained by reducing the characteristic impedance of the switching circuit to 25Ω, provided the GaAs device

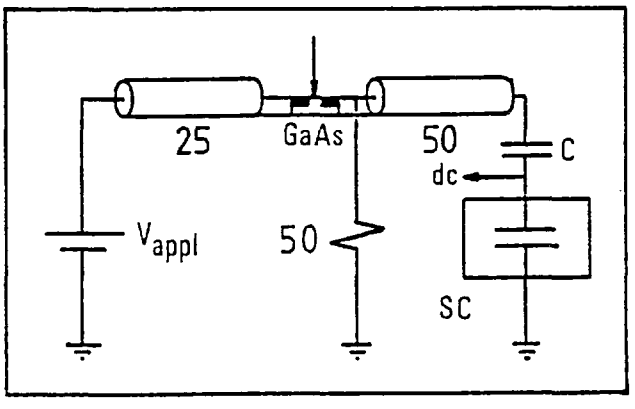

FIG 5.12

is fully saturated by the light pulse. The impedance matching is obtained by connecting a 50Ω resistor near to the switch in parallel with a 50Ω coaxial cable leading to the deflection plates of the streak camera. No termination is required at the sweep plates, because any reflections travelling back towards the semiconductor device are dumped at the 50Ω resistor. This kind of impedance matching should also allow the operation of the streak camera in a recurrent mode. Furthermore, using this principle faster writing speeds can be obtained, so that the d.c. bias (and consequently the gap length) can be reduced.

Although the preliminary results obtained with the d.c. biased GaAs switch, were encouraging, the publication of a paper [29] describing a $\pm$ 2ps jitter streak camera system proved that the Si switching devices could show such a low shot-to-shot jitter, that the margin for further improvement was very narrow. The Si switches were biased with voltage pulses, in a set-up resembling the one described in section 5.5. However, the use of d.c. biased switches at room temperature is certainly the most convenient way of synchronizing streak cameras, and an arrangement very similar to the one presented here incorporating a GaAs switch was recently demonstrated [30].

5.9 Conclusion

Semiconductor switching devices can be of great value to improve the synchronization of streak cameras. Using a Si switch, both shot-to-shot and long term jitter were reduced to $\lesssim \pm$ 15ps, at a writing speed of $\gtrsim 2 \times 10^{10}$ cms^{-1}. The linearity of the sweep was measured to be as good as $\pm$ 2%, and the fast writing speeds obtained indicate that semiconductor switching devices are compatible with the higher time resolution

streak tubes which are likely to be manufactured in the near future.

In order to ensure low jitter and constant writing speed from shot-to-shot, it was established that the gap of the switch must be illuminated by a picosecond pulse with enough energy to effectively reduce the impedance of the device to a negligible value for every laser shot. The remaining jitter observed in the system including the Si switch could be attributed to the changes in the bias and in the switching efficiency by a few percent, leading to a jitter of a few picoseconds. The effect of alterations in the shape of the light pulse activating the device was negligible, compared to the above mentioned problems.

The use of semiconductor switches demands an activating picosecond pulse of several microjoules optical energy. Although this light level is not as high as those used in laser triggered spark-gaps, it is nevertheless significantly higher than those necessary to activate sweeping systems with avalanche transistors or Krytrons. For this reason the use of semiconductor switches to synchronize streak cameras is restricted to relatively high power laser applications. Furthermore it is difficult to incorporate these devices in all-electronic deflection circuits because they can not be activated by electric signals, although this is in general turns out to be advantageous, since they are not liable to be triggered off the electrical noise present from the discharge of the laser. Otherwise, the comparison between the performance of the semiconductor switches and conventional ramp generation circuits shows that the solid-state devices can provide deflection ramps with a reliability and speed which are difficult to achieve by alternative means. The jitter due to the plasma breakdown process in Krytrons is usually so severe theat small variations in the sweeping speed, as discussed for the Si switches, are difficult to observe, and are of

minor importance.

The use of solid-state devices, on the other hand, provided a high voltage ramp synchronized with the picosecond light pulses to a high degree of precision. Preliminary experiments performed with a d.c. biased GaAs device indicated that streak records can be made to overlap on the phosphor screen without significant loss of time resolution. The streaks thus obtained should show an improved signal-to-noise ratio, and measurements could be performed with an even higher timing accuracy than that obtained with conventional streak camera systems.

References - Chapter 5

[1] D.J. Bradley; Ch.2 in Ultrashort Light Pulses, ed. by S.L. Shapiro, Topics in Appl.Phys. vol 18, Springer-Verlag, NY (1977)

[2] E.P. Ippen, C.V. Shank; Ch.3, ibid

[3] E.K. Zovoisky, S.D. Fanchenko; Appl. Opt. 4, 1155(1965)

[4] E.J. Bradley, W. Sibbett;Appl.Phys.Lett 27, 382 (1975)

[5] R. Haddland, K. Helbrough, A.E. Houston; Proc. 11th Intern. Con. High Speed Photography, ed by P.J. Rolls (Chapman and Hall, London 1974), p.107.

[6] M.C. Adams, D.J. Bradley, W. Sibbett; Picosecond Phenomena, ed. by C.V. Shank, E.P. Ippen, S.L. Shapiro (Springer-Verlag NY 1978) p.108.

[7] Hamamatzu Temporaldisperser C979 Technical Brochure

[8] B. Cunin, J.A. Miehé, B. Sipp, L.A. Lompré, G. Mainfray, G. Thébault; Proc. of the 12th Int. Cong. High Speed Phot. ed by M.C. Richardson SPIE vol 97; Toronto, Canada (1976) p.3

[9] S.W. Thomas, L.W. Coleman; Appl. Phys Lett 20, 83 (1972)

[10] Hadland Photonics; Imacon Streak Camera technical brochure.

[11] D.J. Bradley, B. Liddy, W.E. Sleat; Opt. Commun.2, 391 (1971)

[12] M.Ya.Schelev; Proceedings of the 13th Cong. of High Speed Photography and Photonics, ed by S. Hyodo, SPIE vol 189, Japan (1979) p.142.

[13] A.J. Lieber, H.D. Sutphin, C.B. Webb, A.H. Williams; in Proc. of the 12th Int. Cong. High Speed Phot., ed by M.C. Richardson; SPIE vol 97, Toronto, Canada (1976) p. 194

[14] W.E. Sleat; Private communication

[15] S.F. Bryant; PhD Thesis; University of London (1977)

[16] W. Sibbett; PhD Thesis; The Queen's Univ. of Belfast (1973)

[17] G. Mourou, W. Knox; Appl.Phys.Lett 35, 492 (1979)

[18] R. Bube; Photoconductivity of Solids, p272 (J. Wiley & Sons,NY,1960)

[19] M. Stavola, G. Mourou, W. Knox; Opt.Commun. 34, 404(1980)

[20] M. Stavola, M.G. Sceats, G. Mourou; Opt. Commun, 34 409 (1980)

[21] Le Fur, D.H. Auston; Appl.Phys.Lett. 28, 21 (1976)

[22] D.A. Preston; PhD Thesis- The Queen's Univ. of Belfast (1972)

[23] G. Mourou, J. Bunkenburg, W. Seka; Opt. Commun 34, 252 (1980)

[24] J.R. Taylor, W. Sibbett, A.J. Cormier; App. Phys.Lett 31, 184 (1977)

[25] D.J. Bradley, S.F. Bryant, J.R. Taylor, W.Sibbett; Rev.Sci.Instrum 49 215 (1978)

[26] M.C. Adams, W.Sibbett, D.J. Bradley; Opt. Commun 26, 273 (1978)

[27] M.B. Holbrook, W.E. Sleat, D.J. Bradley; Appl. Phys.Lett. 37 59 (1980)

[28] J.R. Taylor; PhD Thesis, The Queen's Univ. of Belfast (1974)

[29] G. Mourou, W.Knox; Appl. Phys. Lett 36 623 (1980)

[30] W. Knox, G. Mourou; Opt. Commun. 37, 203 (1981)

CHAPTER 6

VUV STREAK CAMERA STUDIES

6.1 Introduction

Several important studies at the UV and VUV regions of the spectrum require picosecond time resolution [1, 2, 3]. In the context of this thesis, the relevant examples include the generation of ultrashort light pulses of wavelengths in the range of ∿ 30-400nn by harmonic generation [4], nonlinear mixing [5],injection mode-locking [6] and direct mode-locking of UV rare-gas halide lasers (c.f. chapter 7).

Streak cameras have been extensively employed in picosecond visible light and UV pulse measurements and would be of great assistance in characterizing optical events in the VUV as well. Having in view the newly developed and expanding techniques for picosecond pulse generation of short wavelengths, it becomes even more important to evaluate the performance and limitations of VUV streak cameras. In this chapter, an attempt to determine the time resolution of a gold-photocathode streak camera is described, where the sweeping ramp was provided by a Si switch.

6.2 The VUV Ultrashort Pulses

In order to test the camera, high order harmonics of intense infrared mode-locked laser pulses were generated, ensuring that the short wavelength radiation had picosecond duration. Previous experiments carried out with X-Rays of ∿ 1KeV energy had shown that the gold-photocathode Photochron streak camera was capable of resolving events

separated in time by ∿ 22ps. This limit was attributed to the duration of the plasma source [7, 8], and highlighted the need of probing pulses of shorter pulsewidths.

The wavelength of the radiation used in the experiment was 177nm, which was near the cut-off of the photocathode and consequently adequate for testing the best possible resolution of the tube, since the energy spread of photoelectrons is in this case minimal, as seen in chapter 2. The picosecond 177nm radiation was obtained by initially frequency doubling an intense mode-locked 1.06μm wavelength light pulse, and subsequently by generating the third harmonic of the green light in a gas cell [9].

Second harmonic generation has been briefly described in chapter 2. An angle tuned KDP crystal was employed, and kept at a constant temperature of 30°C to prevent detuning and absorption of water. Due to the high pulse intensities, the conversion efficiency from 1.06μm to 0.53μm wavelength radiation was typically ∿ 25%.

The fundamental frequency was filtered out and the green light focussed into a gas cell placed at the entrance slit of a vacuum monochromator. Several rare gases were employed, although measurements carried out with a specially designed vacuum photodiode showed that the highest conversion efficiency was obtained for Xenon at a pressure of ∿ 280 torr, and therefore most measurements were carried out under these conditions. However, because the third harmonic generation from 0.53μm to 0.177μm in Xenon is a non-resonant process, the efficiency was very low (∿ 10^{-8} - 10^{-9} at power densities approaching 10^{15} W/cm^2). The use of a heat-pipe system with a metal vapour [10] should enable the amplitude of the VUV signal to be increased by several orders of magnitude provided appropriate phase-matching conditions are satisfied.

6.3 The Streak Camera

The streak image tube employed has been described in detail [7, 8, 11], and was a modified version of the Photochron II image converter. Although it was possible to operate it on a reflection mode by illuminating the photocathode from the same side as the photoelectrons are emitted, the transmission mode was prefered for its convenience.

The photocathode was prepared either on a quartz or a LiF substrate and consisted of 1μm thick evaporated layer of chromium interrupted at its centre by a 110μm wide, 2cm long slit obtained by masking. A 150Å thick layer of gold was then deposited, so that the incident VUV photons transmitted through the substrate would only reach the layer of gold through the thin "aperture slit" on the chromium. The photoelectrons were then generated from a 110μm wide source, which allowed good time resolution to be obtained.

The mesh of the streak camera was separated from the photocathode by $\sim$ 0.75mm, and an electric field of $\sim$ 13KV/cm quickly accelerated the photoelectrons as required for picosecond time resolution [12]. The tube was maintained at a 10^{-5} torr vacuum obtained with an oil diffusion pump, but when required, it could be let up to air for adjustments.

The streaks displayed on the phosphor screen were fibre-optically coupled to an image intensifier (Mullard 50/40) [13] providing a gain of $\sim 10^5$. The intensifier was pulsed in synchronism with the laser, in order to improve the signal-to-noise ratio of the records, and its output was also fibre-optically coupled to the photographic film.

The records were taken on Polaroid 410 film, and when the system was considered to be operating near the time resolution limit of the streak camera, Ilford HP5 film was used to allow microdensitometry. Alternatively, an optical multi-channel analiser (OSA) was used, and an intensity versus time readout was immediately available.

6.4 The Experimental Set-up

6.4.1 General

A schematic diagram of the experimental set-up is shown in figure 6.1. The laser system consisted of a passively mode-locked Nd:Silicate glass oscillator and three amplifying stages. The mode-locking dye (Eastman-Kodak 9860) was dissolved in dichoroethane and concentrations of $\sim 2 \times 10^{-5}$M were employed. The dye cell was 100μm thick and contacted the back mirror, which was 100% reflecting at 1.06μm and had a radius of curvature of 2m. The oscillator rod was pumped by the light from a single helical flashlamp in which ∿2KJ of electrical energy was dissipated. The output coupler was a flat, 50% reflector at 1.06μm and a TEM_{oo} mode selector was introduced in the cavity, so that the spatial properties of the beam were optimised, which was important in the harmonic generation processes. The roundtrip time of the oscillator was 8.5ns, and the total energy output at 1.06μm was ∿ 2mJ, in a train typically lasting for ∿ 800ns.

The first few pulses in the mode-locked train had a duration of ∿ 3-5ps, but later pulses were longer mainly due to self-phase modulation [14, 15]. In order to test the VUV streak camera it is preferable to employ nearly bandwidth limited light pulses of ensured ultrashort duration and with the highest possible intensity, which enables efficient high harmonic generation. A single pulse selector consisting of a Pockel's cell(PC) and two Glan-Thompson polarizers(P1 and P2) was then introduced between the oscillator and the first amplifier, and operated to select a pulse early in the mode-locked train. The ∿ 9KV square voltage pulse used to bias the Pockel's cell was delivered by a Krytron switch (KS) in a modified Blumlein configuration, as described in section 5.4.2, and lasted for the roundtrip time of the laser, 8.5ns.

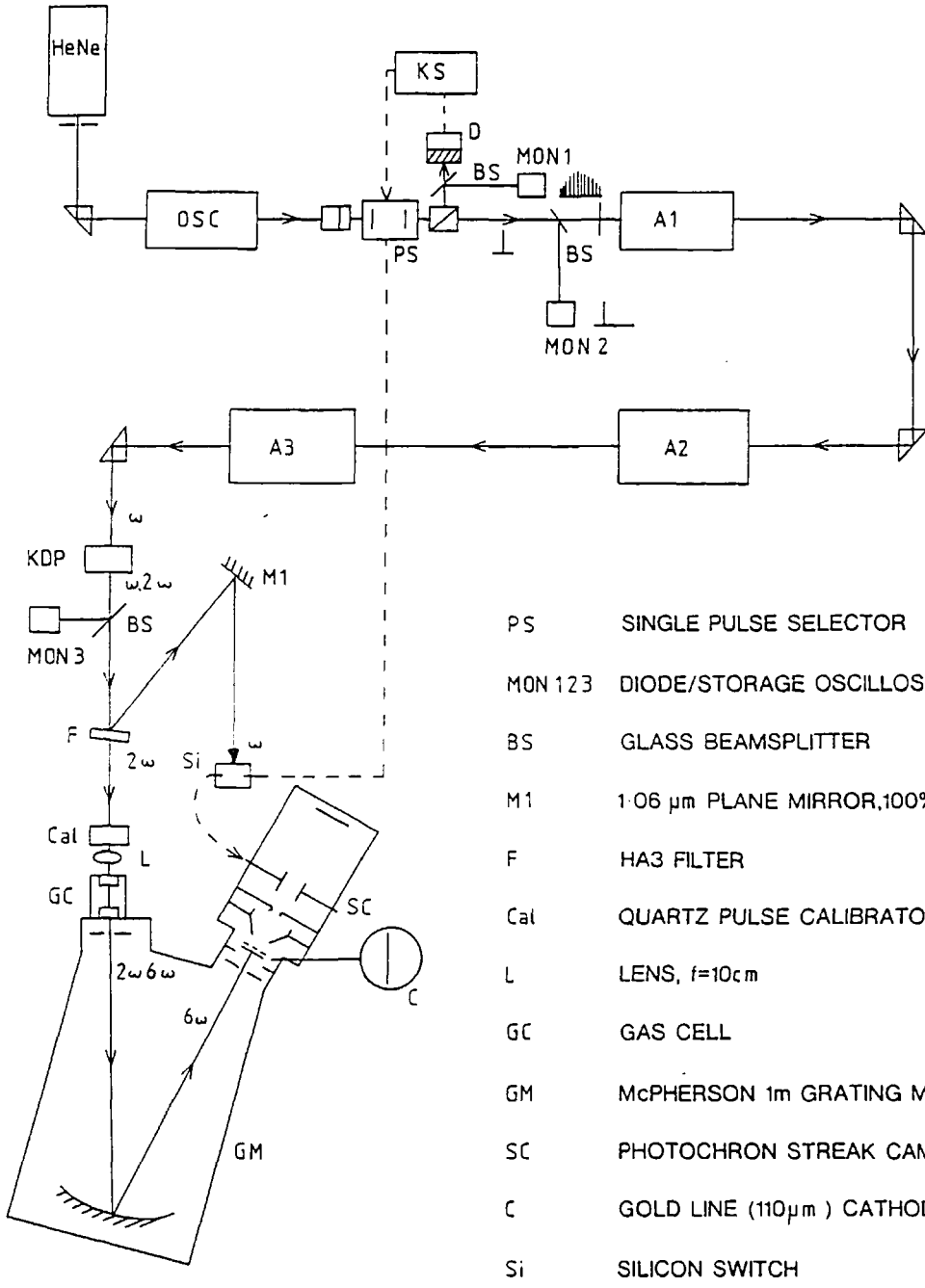

FIG 6.1 Experimental Set-up

The 1.06μm light amplifiers (A1, A2 and A3) were used in a single-pass mode of operation, as seen in figure 6.1. The Nd: Silicate glass rods had 6.4mm, 12.7mm, and 12.7mm of diameter. A1 was pumped by one, and A2 and A3 by two flashlamps, each lamp typically activated by ∿ 1KJ of electrical energy (38μF capacitor banks at ∿ 7KV charging voltage). A cooling system with flowing water was provided to improve heat dissipation, but the repetition rate of the laser was nevertheless limited to one shot every 7 minutes, for relatively reproducible performance.

The windows of the amplifiers and oscillator were Brewster - angled for minimal losses of horizontally polarized light, and since the radiation transmitted by the second polarizer (P2) was vertically polarized, a $\lambda/2$ waveplate was introduced before the first amplifying stage.

The gain of the amplifiers varied with alignment and with the amount of energy deposited on the flashlamps, but typical values were 13, 8 and 6 for A1, A2 and A3 respectively. At the KDP second harmonic generation crystal (Xtal), the energy of a single pulse was ∿ 40mJ. Approximately 10mJ of green light was directed to a HA3 fitter (T=75% at 0.53μm) which was used to eliminate the fundamental, and focussed by a 10cm focal length quartz lens (L) into the quartz windowed gas cell (GC). The cell was placed at the entrance slit of a 1m vacuum monochromator M (McPhersun 225) which selected the 177nm radiation to illuminate the photocathode of the streak camera. No additional lenses were employed to focus the output from the monochromator on the gold photocathode because of the difficulty in the alignment that became apparent when such procedure was preliminarily adopted.

6.4.2 The Pulse Selector

Originally, a fast S1 vacuum photodiode was used to activate the Krytron switch of the single pulse selector, represented by D in figure 6.1. However, this arrangement did not allow the selection of a pulse early enough in the train, due to the low light intensities available at the photodiode. Also, electrical noise problems prevented the use of fast electrical amplifiers to increase the amplitude of the signal delivered to the avalanche transistor chain. The photodiode was then replaced by a Si switching device with a 0.1mm gap between electrodes and biased with a d.c. voltage adjusted between 30V and 60V.

The switch was constructed as described in chapter 4, with Al electrodes evaporated on the top surface. The signal switched by the solid-state device activated a chain of avalanche transistors, which provided a ∿ 1KV triggering signal for the krytron [16]. Since the coupling of the voltage delivered to the base of the first transistor was made by a 10pF capacitor, a 50Ω resistive load was connected between the switch and ground, as shown in figure 6.2. As a consequence, the d.c. voltage applied did not charge the capacitor through the switch,

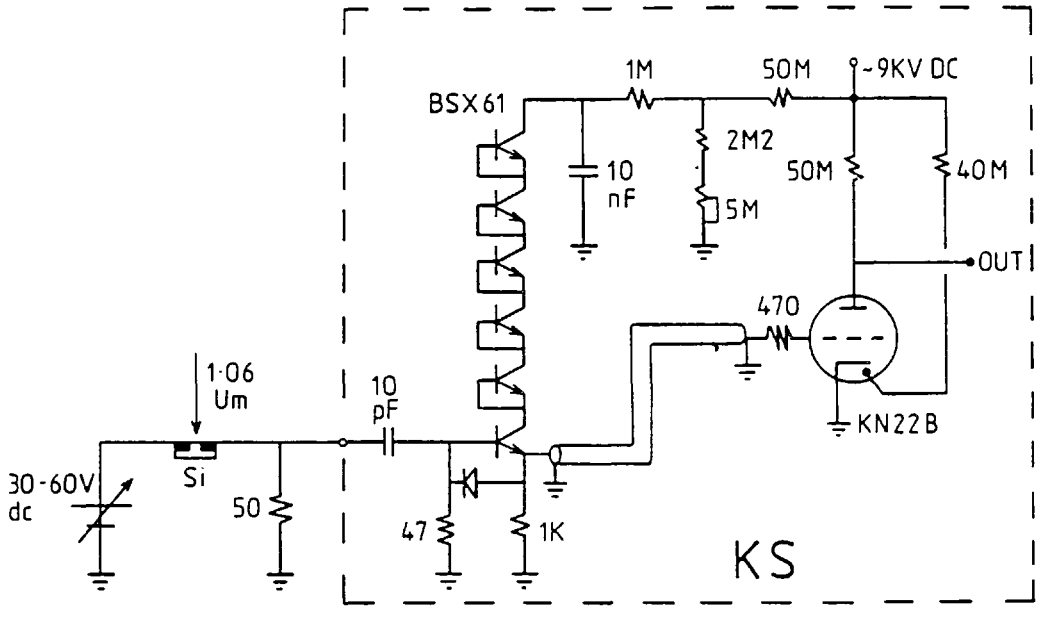

FIG 6.2 Krytron switch activated by small Si switching device

but instead appeared across the electrodes of the device, d.c. biasing it.

The intensity of the light pulses illuminating the small Si switch was adjusted with the introduction of a diverging lens and neutral density filters, so that when the gap was illuminated by a picosecond light pulse (rejected by P2), the voltage switched was only a small fraction of the voltage applied. In other words, the amount of light irradiating the switch was not enough to saturate it, and consequently the effect of consecutive pulses of the train was added, since the recombination time of Si is much greater than the separation between pulses. Therefore the output voltage from the device raised with a staircase shape, until the voltage transmitted was ∿ 8V, enough to trigger the avalanche transistor chain. Figure 6.3 illustrates this mode of operation (where the Si switch was illuminated by dye laser pulses).

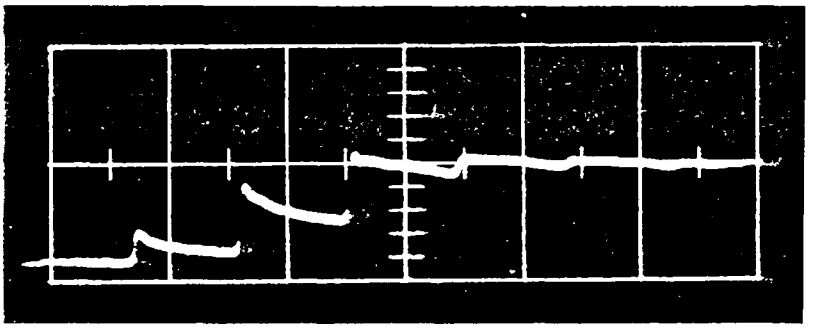

FIG 6.3 Output from a Si switch illuminated by several weak light pulses

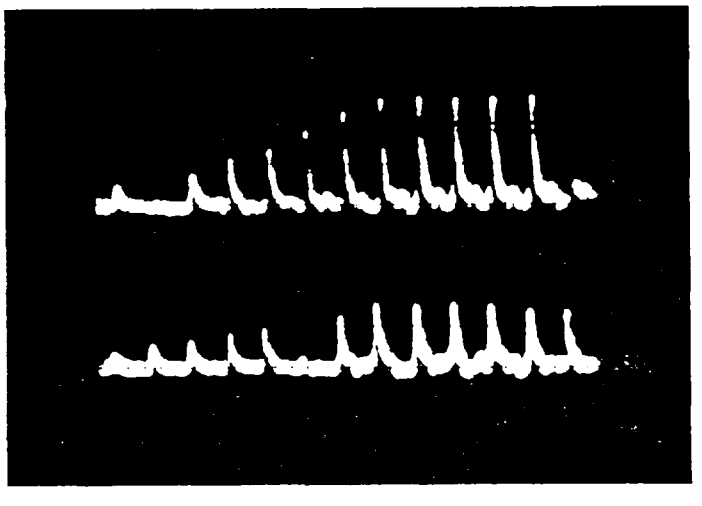

FIG 6.4 Two oscillograms showing selection of pulse early in the mode-locked train with the arrangement of fig 6.2

Figure 6.4 is an oscillogram of the trains rejected by P2 for two different laser shots and shows that the second and fifth pulse in the trains, respectively, have been selected. Under the same

conditions, the selection with the photodiode arrangement occured typically between the 9th and 13th pulses.

With this experimental configuration, earlier pulses in the train could be selected by increasing either the voltage applied, or alternatively, the amount of light falling on the switch, and thus it provided two convenient ways of choosing which picosecond pulse was to be amplified. The replacement of the photodiode previously used by the small Si switching device allowed the selection of pulses $\sim$ 40-80ns earlier in the mode-locked train than before, and therefore was of great value in the experiment to test the VUV streak camera.

6.4.3 The Main Si Switch

There were several requirements for the sweep circuitry, such as reliability, low jitter and insensitivity to electrical noise. Furthermore, a high voltage ramp with good linearity and fast risetime was necessary to determine the highest possible time resolution of the VUV streak camera. All these requirements were met by the system described in chapter 5, where the deflection voltage ramp was provided by a 1.0mm gap Si switch. A similar device was then employed in this experiment as well.

Fine adjustments in the alignment were made easier by providing the mount of the microstrip containing the Si slab with translation stages and the position of the 1.06μm light pulse falling on the semiconductor was checked with an infrared viewer. The radiation necessary to activate the switch was obtained from the 4% front reflection of the filter(F), which contained two components, of $\sim$ 1-2mJ at 1.06μm and $\sim$ 100μJ at 0.53μm wavelengths. The infrared component was delayed and directed to the Si switch by mirror M1 (R $\sim$ 100% at 1.06μm) as shown

in figure 6.1. The relatively high level of energy available to activate the switch was spread over a large area ($\sim$ 1cm^2), ensuring complete illumination of the gap. No lenses were used, and when necessary neutral density filters were introduced to reduce the effect of low intensity light reaching the device prior to the main switching pulse.

The voltage bias for the Si device was obtained from the Krytron used in the pulse selector, and the length of cable connecting the Pockel's cell to the solid-state switch was measured, so that the picosecond light pulse activated the device in synchronism with the 8.5ns long bias pulse. The behaviour of the switch was checked regularly with a high-voltage-probe-oscilloscope combination, and the voltage switched was measured on the oscilloscope to be typically equal to half of the voltage applied to the Pockel's cell, within 20%. In some instances the bias for the device was further attenuated, so as to reduce the writing speed, and values as low as $\sim$ 1 x 10^{10}cm/s were obtained.

As with the conventional photochron streak camera deflection circuit, a capacitor (500pF, 30KV d.c) coupled the voltage ramp to the sweep plates, and allowed a d.c. bias to be applied so that the sweep started off-screen. The bias used was in the range $\sim$ 1.2-2.6KV, depending on the amplitude of the voltage ramp, i.e. on the writing speed employed.

6.5 Operation and Results

In order to accurately calibrate the streak camera it is necessary to use at least a pair of light pulses of known separation. Since the 177nm radiation is absorbed in air, two pulses of 0.53μm wavelength were provided, one of them delayed, and each one focussed into the gas cell to produce two components of VUV separated by 50ps. Different configur-

ations were tested, and the one that gave best results, in spite of difraction problems, consisted of introducing a 3cm thick quartz block on the light path, so that only one half of the beam would propagate inside the quartz, while the other half would travel in air. The two green light sub-components thus obtained were separated in time by 50 ps, as shown in figure 6.5.

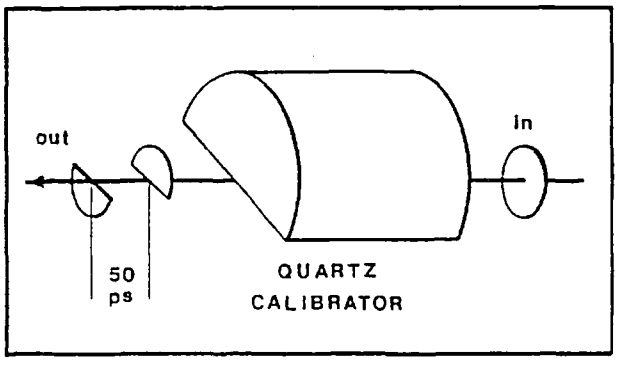

FIG 6.5

The procedure adopted to test the performance of the streak camera was as follows. The oscillator was initially adjusted so that it reliably generated mode-locked trains with a TEM_{oo} mode structure. Then the Krytron switch, small semiconductor device and Pockel's cell were set so that a single pulse very early in the train was efficiently selected. Then the chain of amplifiers was aligned and the beam directed to the SHG crystal. The switching efficiency of the main Si device was then checked on a storage oscilloscope. Withouth the quartz delay the green light was focussed into the gas cell, and the 6th harmonic light intensity monitored with a streak camera operating in the focus (static) mode with zero d.c. bias. The position of the lens and other parameters were varied until the intensity of the 177nm radiation recorded was considered to be high enough to be examined in the sweeping mode of operation. Finally when streaks were observed, the quartz calibrator was introduced.

Streak records of 177nm wavelength pulses obtained with the gold photocathode streak camera are reproduced in figure 6.6, which shows a trace from the multichannel processor (B & M - OSA/WP1) coupled to the image intensifier. It is apparent that the time resolution of the system for 177nm radiation can be at least as good as 13ps. However, the shortest

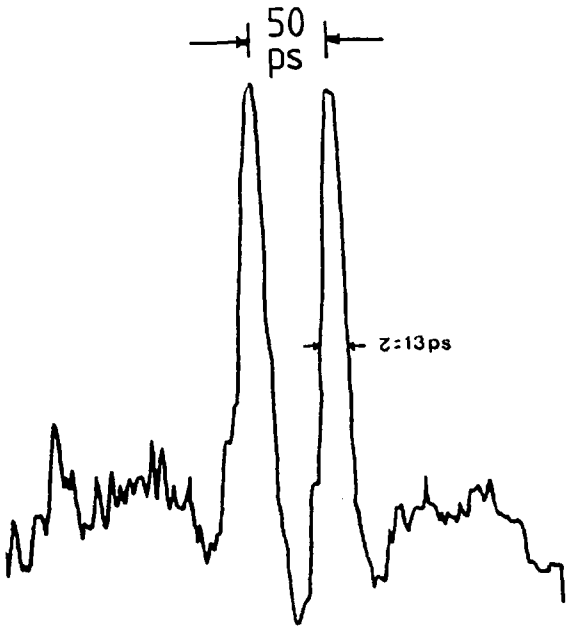

FIG 6.6 Streak record of 177nm wavelength picosecond pulse

pulse recorded was still somewhat longer than expected, since the duration of the light pulses examined was supposed to be $\lesssim$ 3ps, and the theoretical limit for the time resolution of the camera at fast writing speeds was $\sim$ 5ps [7]. The reasons for this discrepancy were examined in detail in [11], where it is pointed out that the longer durations observed could be partly due to the effect of the monochromator, since that as the picosecond pulse illuminates the dispersive element, the spectral narrowing is accompanied by a considerable broadening of the pulsewidth [17]. Furthermore, the width of the exposed line (110μm) on the photocathode also limits the shortest possible recorded duration.

It must be emphasised that the experimental problems encountered due to the unreliability of the equipment employed and the low repetition rate of the system made it extremely difficult to optimize the different parameters involved. For this reason, the semiconductor switch proved to be a significant improvement to the operating characteristics of the deflection circuitry. However, the poor conversion efficiency from 0.53μm to 177nm wavelength radiation also rendered difficult estimating the performance of the switch, since in many occasions the amount of light illuminating the photocathode was barely enough to be recorded. From the position of the streaks seen on the screen without the quartz calibrator, the jitter is roughly estimated to be $\sim$ ±50ps in this unoptimized situation.

An independent evaluation of the performance of the Si device was obtained when the 0.53μm wavelength light pulses were examined on a conventional Photochron streak camera. This study was important to ensure the picosecond durations of the pulses used in the harmonic generation in the Xe cell, but unfortunately limited time did not allow simultaneous measurements at 0.53μm and 177nm wavelengths to be carried out. The switching device used to provide the voltage ramp for the S11 photocathode streak camera was the same that had been used in the gold-photocathode system.

In spite of the poor repetition rate of the laser, and of the fact that the streak camera had to be set-up in the laboratory and proper delay lines and cables had to be provided, streaks showing pulse durations $\sim$ 3ps were readily obtained, and the whole measurement was concluded in a total of three working days. This once more illustrates the reliability and easy operation achieved with the semiconductor switches. Since the experimental conditions were kept the same as for when the gold-photocathode streak tube was being tested, and since the deflection circuit is similar for both cameras, the jitter obtained in this case gives a good estimate of the jitter expected in the other experiment. Figure 6.7 shows a series of three streak records obtained from consecutive laser shots. The pulse separation is 50ps and the jitter was in this case $\sim \pm$ 30ps at a writing speed of $\sim 10^{10} cms^{-1}$. This result suggests that the jitter in the VUV streak camera system was inferior to $\pm$ 50ps.

6.6 Conclusion

The use of a semiconductor switch to synchronize the XUV streak camera illustrates several potential advantages of such system. Since the best possible temporal resolution of the instrument was investigated,

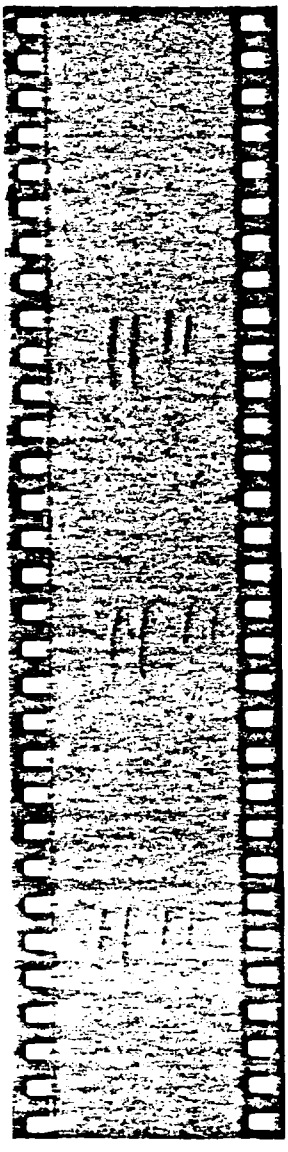

FIG 6.7
Three consecutive streak records of 0.53μm wavelength pulses

fast writing speeds were required. On the other hand, due to the low repetition rate of the laser the jitter had to be low in order to ensure that every light event would be recorded. The extremely low conversion efficiency of the harmonic generation process combined with several other experimental difficulties (such as alignment and long time between consecutive laser shots) prevented the optimization of the system, and consequently very low light levels were recorded. It is therefore apparent that being able to superpose several streak records on the same photographic plate without loss of temporal resolution would have been in this case a major improvement to the experiment. Although this was not possible, the results obtained with the Si switch in the deflection circuit of the camera indicate that fast writing speeds ($\sim 10^{10} cms^{-1}$) and low jitter ($\sim \pm$ 50ps) was achieved, and therefore the semiconductor device was a significant contribution to the experiment carried out.

References - Chapter 6

[1] D.J. Bradley; in Lasers in Physical Chemistry and Biology, ed by Jussot Dubieh; Elsevier Publishing Co., Amsterdam (1976) p.7.

[2] V.S. Letokhov; Physics Today, Nov. 1980, p. 34.

[3] S.C. Shapiro, A.J. Campillo, V.H. Kollman, W.B. Goad; Opt. Commun. 15, 308 (1975).

[4] J. Reintjes, C.Y. She, R.C. Eckardt; IEEE J. Quantum Elect., QE14 581 (1978)

[5] M. Bass, P.A. Franken, A.E. Mill, C.W. Petters, G. Weinreich; Phys. Rev. Lett 8. 18 (1962).

[6] G. Reksten, T. Varghese, D. Bradley; Appl. Phys. Lett 38, 513 (1981)

[7] D.J. Bradley, A.G. Roddie, W. Sibbett, M.H. Key, M.J. Lamb, C.L.S. Lewis, P. Sachsennmaier; Opt. Commun. 15, 231 (1975)

[8] D. Landheer, W. Sibbett, M.H. Key, M.H. Lamb, C.L.S. Lewis, J. Lunney; Proc. 12th Cong. High Speed Phot., SPIE vol 97, ed by M.C. Richardson, Toronto, Canada (1976) p. 207.

[9] D. Cotter; Opt. Commun, 31, 397 (1979).

[10] R.B. Miles, S.E. Harris- IEEE J. Quantum Elect. QE9, 470 (1973)

[11] A.J. Cormier; PhD Thesis, University of London (1981)

[12] D.J. Bradley, B. Liddy, W.E. Sleat; Opt. Commun 2, 391 (1971)

[13] D.J. Ruggieri; IEEE Trans. on Nucl. Sci, NS19, 1 (1972)

[14] T.R. Royt; Opt. Commun 35, 271 (1980)

[15] J.R. Taylor, W. Sibbett, A.J. Cormier; Appl. Phys. Lett 31, 184 (1977)

[16] S.F. Bryant; PhD Thesis, University of London (1978)

[17] N.H. Schiller, R.R. Alfano; Opt. Commun. 35, 451 (1980)

CHAPTER 7

ACTIVE MODE-LOCKING OF LASERS WITH SEMICONDUCTOR SWITCHES

7.1 Introduction

As discussed in chapter 2, passively mode-locked flashlamp pumped lasers are simple and relatively low cost sources of picosecond pulses. These systems include the neodymium, ruby, and the widely used dye lasers. The tunability and ultrashort pulse durations provided by the passively mode-locked dye lasers is somewhat restricted by the difficulty in obtaining suitable saturable absorbers which can be used over the complete spectral range of lasing dyes [1]. To overcome this difficulty, several alternative mode-locking techniques for flashlamp pumped dye lasers have been reported.

A coumarin dye laser was actively mode-locked with the use of an acousto-optic modulator inside the resonator [2], and individual pulse durations of several hundred picoseconds were obtained. Upon illumination of the saturable absorber of a dye laser by picosecond pulses generated in another dye laser (passively mode-locked), a second pulse train was produced at a slightly different wavelength [3], with an independent roundtrip time [4]; a Q-switching technique led to the generation of nanosecond pulses [5] with the use of a rapidly gated intracavity Pockel's cell; also in a Q-switching technique using a rotating interferometer, picosecond pulses were generated [6]; by modifying the physical parameters of a saturable absorber (DOCI), passive mode-locking of a Coumarin 102 dye laser was achieved [7]; and other mode-locking techniques have also been suggested [8]. The approach of different research groups

varies not only because each method has some kind of limitation but also because the equipment required is not always readily available. Ultrafast semiconductor switching devices have been used in a series of experiments in conjunction with Pockel's cells (c.f. section 3.6). The transmission of Pockel's cell crystals is compatible with a wide lasing wavelength range [9]. Therefore it should in principle be possible to use the picosecond voltage pulses switched by a semiconductor device to activate an intracavity Pockel's cell acting as loss modulation element. The pulses generated by the laser should then show a fast and deep modulation. Also, the range of lasing frequencies over which this active modulation technique can be applied should be very large, and it should be suitable for very different laser systems. Although longer pulses are usually generated when active mode-locking techniques are employed as compared to passive mode-locking [10], the compatibility of active mode-lockers with virtually all lasing dyes render such systems attractive.

In the following sections of this chapter, the use of semiconductor switches in such an active mode-locking technique is demonstrated. Since the solid-state switching devices require an independent source of picosecond light pulses, a second laser (passively mode-locked) was needed. While this is clearly a disadvantage of this method, most flashlamp pumped mode-locked lasers can be used and two synchronized trains of light pulses at different wavelengths are produced. Furthermore, the versatility of the active mode-locking technique is demonstrated by its use in conjunction with dye lasers operated with several different Coumarin dyes (c.f. section 7.2), and with an excimer laser (c.f. section 7.3).

7.2 Active Mode-locking of Dye Lasers

7.2.1 Experimental Set-Up

7.2.1.1 The Lasers

The schematic diagram of the experimental arrangement is shown in figure 7.1 where two similar dye lasers were employed. The passively mode-locked Rhodamine 6G dye laser (master) activated the semiconductor switch, from which short duration voltage pulses were generated, and applied to a Pockel's cell placed inside the cavity of the other laser (slave). The cavity heads of both lasers were identical [11, 12], measuring 18cm in length and having elliptical cross section. The gain medium consisted of a quartz cylindrical dye cell of 13mm external diameter (o.d.) and 6mm internal diameter (i.d.), through which the dye

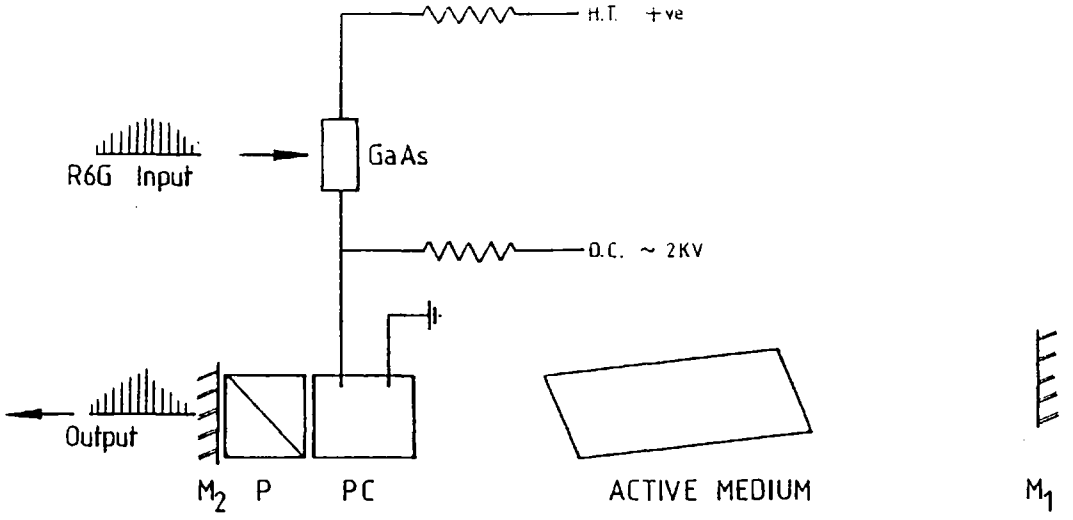

FIG 7.1 Experimental Set-Up

flowed. In the master laser a 1.5×10^{-4}M solution of Rhodamine 6G in ethanol was used. Most measurements were made when the slave laser operated with a 1.5×10^{-4} M ethanolic solution of Coumarin 6. The

dye cell was placed at one focus of the elliptical cavity head, and pumped by a single linear ablative flashlamp placed at the other focus. The flashlamp, which was made of quartz, measured 18mm o.d. and 10.5mm i.d., and was evacuated to $\sim 10^{-3}$ torr by a rotary pump. The electrical energy delivered by the 10μF capacitor banks was ∿ 1KJ for each laser at a charging voltage of ∿ 15KV. The windows of both laser heads were Brewster angled and transmitted predominantly horizontally polarized light.

The master laser had a 75cm long cavity defined by mirror M1 (R ≈ 100% at 0.6μm) and the output coupler M2 (R ≈ 50% at 0.6μm). It was passively mode-locked by a 5×10^{-5}M solution of DODCI in ethanol, contained in a 2mm thick dye cell in contact with the back mirror. The output of the Rhodamine 6G dye laser consisted of mode-locked pulse trains lasting for ∿ 3μs, at ∿ 610nm wavelength. Typically, the individual pulses contained ∿ 200μJ of optical energy and had ∿ 5ps duration [13] at the later part of the train.

The slave laser cavity was defined by the broadband total reflector M3 and the output coupler M4, which either had 90% or 40% reflectivity at the lasing wavelength. The active modulating elements were a 1cm long Glan Thompson polarizer (P) and a 25mm long KDP Pockel's cell (PC). These elements were placed in close contact with each other and less than 1mm away from the output coupler. The roundtrip time of the Pockel's cell-polarizer arrangement was ∿350ps.

Synchronizing the two lasers was not difficult, since they had similar triggering characteristics. A 30KV trigger pulse was delivered by a spark gap to activate both flashlamps simultaneously, and the jitter between the two systems was always smaller than the duration of the laser pulse.

7.2.1.2 The Switch

The requirements for the semiconductor switch were: fast recovery time, high voltage d.c. hold-off and high voltage switching capability when activated by the mode-locked dye laser. As discussed in chapters 3 and 4, III-V semiconductors can satisfy all these requirements. Semi-insulating crystals are commercially available, exhibit very high dark impedances and recovery times of $\sim$ 100ps. In particular GaAs and GaP had been shown to be capable of delivering high voltage trains of pulses, and therefore were suitable candidates for activating the Pockel's cell. Because of the high energy gap of GaP, multiphoton excitation was required to produce electron-hole pairs (neglecting impurity conduction). Therefore GaAs switches were used for most measurements, although GaP devices were also employed in the experiment, yielding similar high repetition rate ultrashort high voltage pulses.

The gap length of the switches was typically $\sim$ 4mm so that d.c. voltages of $\sim$ 3KV could be held off, and in some cases a layer of transparent insulator was deposited on the semi-insulating GaAs crystals to prevent surface and air breakdown. The GaAs slabs were 0.25mm and the GaP crystals 0.5mm thick.

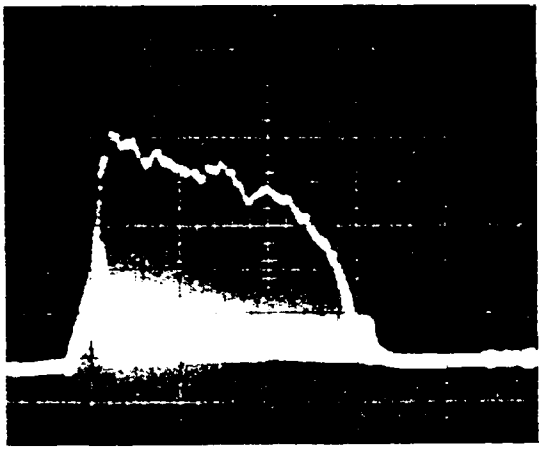

FIG 7.2 High voltage train of pulses switched by GaAs device.

No lens was used, and $\sim$ 50% of the laser output illuminated the device. Because of the relatively high optical energy available, kilovolt amplitude trains of pulses were obtained. Figure 7.2 shows such an output from a GaAs switch with peak amplitude of $\sim$ 1.5KV, and lasting for the duration of the master mode-locked train.

7.2.2 The Active Mode-locking Technique

The operation of the system can be described in the following manner: In the simplest configuration, a single power supply V1 is used. The polarizer has preferential transmission (vertical) orthogonal to that of the Brewster angled windows (horizontal). Therefore if no voltage is applied to the Pockel's cell, most light flux reaching the polarizer is rejected. Since little feedback is allowed, the slave laser does not reach threshold.

When the mode-locked master laser is fired at the same time, and activates the ultrafast switch, it generates a series of short duration high voltage pulses. If a voltage pulse is applied to the Pockel's cell, a short duration burst of light has its polarization rotated. Part of this burst of light is then transmitted by the polarizer to and from the output coupler. It returns to the Pockel's cell vertically polarized. If voltage is still present at the Pockel's cell, the burst of light will suffer another rotation of polarization. Some of this light will then be fed-back and amplified. The return of this short duration burst of light to the Pockel's cell after a roundtrip in the laser is made to coincide with the application of a subsequent voltage pulse. Therefore further amplification is allowed, and a train of ultrashort light pulses is obtained. Picosecond sychronization between the arrival of the light pulse and the application of the voltage pulse to the Pockel's cell is ensured by the semiconductor switch, provided the roundtrip of the two lasers is the same.

Maximum transmission of the modulating system is obtained when the polarization is rotated by 90° at the Pockel's cell, which is attained for the half-voltage $V_{\lambda/2}$. Typically this voltage was $\sim$ 4KV for a lasing wavelength of 0.53μm (Coumarin 6 dye). Since the amplitude

of the voltage pulses switched was significantly below this value, the experimental configuration was slightly modified. A second power supply (V2) was introduced to provide a d.c. bias for the Pockel' s cell, which was low enough so that the laser gain would still not exceed the cavity loss. The ultrashort voltage pulses switched by the semiconductor device were then added to this d.c. bias. Up to ∿ 2KV d.c. could be applied to the Pockel's cell without leading to free-lasing by the slave laser. The addition of the voltage pulses then led to the generation of a mode-locked train.

7.2.3 Operation and Results

Both dye lasers were aligned in a conventional way. Undesired feedback from the faces of the Pockel's cell and polarizer was avoided by slight misalignment of these elements.

When the d.c. voltage applied to the Pockel's cell exceeded ∿ 2KV the slave laser could reach threshold. The highest output energies were obtained for V2 ∿ 4KV, and a ∿ 3μs long unmodulated pulse was then generated, as seen in the oscillogram of figure 7.3a. The d.c. voltage V2 was reduced to 2KV, and ∿ 5KV d.c. were applied to the other terminal of the switch, so that the voltage drop across it was ∿ 3KV. When the master laser output illuminated the gap, a train of high voltage pulses was generated and applied to the Pockel's cell. A mode-locked light train showing complete modulation, and lasting for ∿ 3μs was then produced, as shown in figure

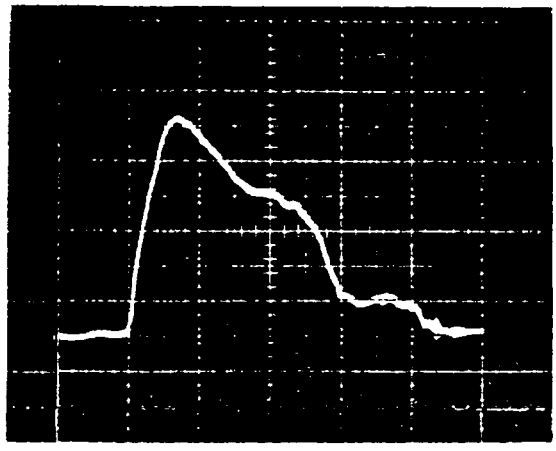

FIG 7.3 Oscillograms showing
a) Unmodulated output from Coumarin laser

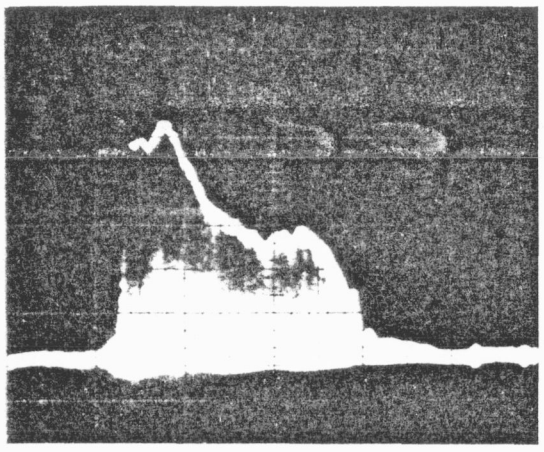

FIG 7.3bMode-locked train of pulses

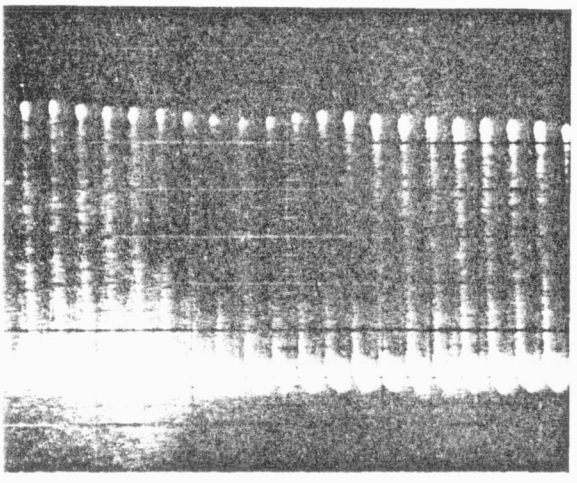

FIG 7.3c Same as (b) on 10ns/div time scale

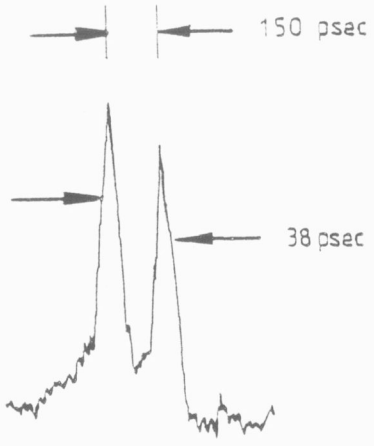

FIG 7.4 Microdensitometer trace of streak record showing 38ps pulses

7.3b. The profile of the envelope of the train was similar to that of the unmodulated output. When examined on a faster time-scale, the Coumarin mode-locked laser pulses were seen to have detector-limited durations. Such an oscillogram can be seen in figure 7.3c, where the horizontal time scale is 10ns/division. The total energy in the train of pulses was $\sim$ 5mJ.

In order to determine the output pulse durations and the effect of cavity mismatch, a Photochron I streak camera was used [14]. It was operated at a writing speed of $\sim 6 \times 10^{8}$ cm s^{-1}, and assuming a dynamic spatial resolution of $\sim$8 lp/mm this corresponds to a 20ps time resolution. The slave laser output pulses were directed to a optical delay line, which sub-divided each pulse in two components separated by 150ps.

Figure 7.4 shows a microdensitometer trace of a 38ps pulse recorded $\sim$ 0.4μs from the beginning of the actively mode-locked output train. Typically the pulsewidths

recorded were in the range 30-50ps, although some shorter pulses, approaching the 20ps time resolution of the camera were sometimes observed. On the other hand, much longer pulses were also sometimes generated, as shown in the microdensitometer trace of figure 7.5. Besides being longer, the streak shows structure, and also a slow rise and fall time. For this particular record the streaked pulse occured ∿ 500ns into the train.

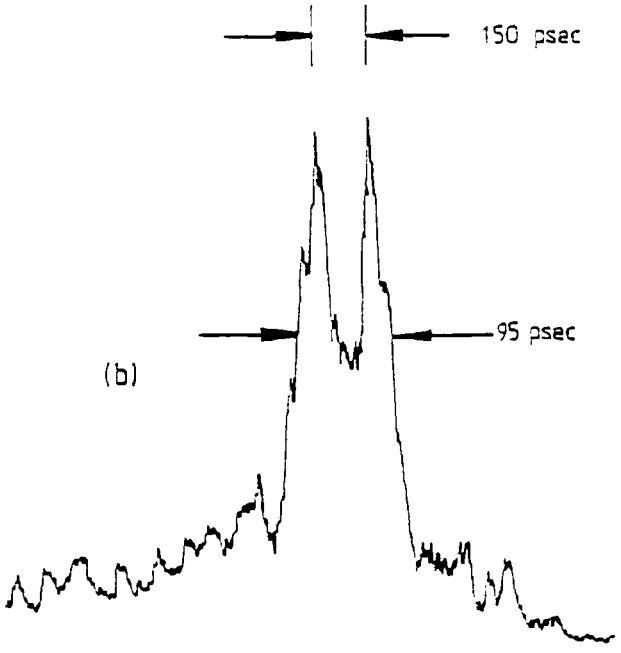

FIG 7.5 Microdensitometer trace of trace of streak record showing pulses with substructure

No significant difference was found between the spectral width of the Coumarin dye laser with and without active modulation, and the bandwidth limited product was several times smaller than that obtained here.

To demonstrate the versatility of this mode-locked system, the slave laser was operated with different dyes. A wide wavelength range (430nm to 535nm) was covered by the Coumarins 120, 2, 47, 102 and 30. Mode-locked trains were obtained with all these dyes, for which 100% modulation and photodiode-oscilloscope limited pulse durations were displayed. The introduction of a Fabry-Perot would allow tuning the dye laser to a particular frequency within its bandwidth.

7.2.4 Discussion

One important feature of this mode-locking arrangement is that

the semiconductor switches delivered voltage pulses of ultrashort durations, and therefore the intracavity losses were greatly reduced for a very short time per roundtrip. In contrast, conventional active mode-locking configurations involve the application of sinusoidal voltages of frequency 2L/c to the loss modulator, and the resulting opening times are significantly longer (typically $\sim$ 2ns for a 6ns roundtrip). Also, with the arrangement incorporating the solid-state devices, voltage pulses of high amplitude were switched and the large modulation depths obtained made it relatively easy to generate 100% modulated trains of pulses. Furthermore, semi-insulating GaAs or GaP devices are potentially capable of switching at a rate $\sim$ 10 times higher than the one employed in this experiment.

The large number of passes through the modulating elements is partly responsible for the pulse shortening. The effect of the multiple passes through the active modulator can be better understood from the following consideration. Assuming for simplicity that the pulse shape is solely determined by the transmission function of the modulator, which is taken to be gaussian, the intensity profile of the light pulse after n roundtrips will be given by

$$I \alpha \{A \exp - [t/\sigma]^2\}^n$$

where σ is the characteristic opening time of the Pockel's cell. Evaluating the product,

$$I \alpha \{A^n \exp - [t/(\sigma/\sqrt{n})]^2\}$$

it is found that the pulsewidth is $\sqrt{n}$ times shorter than σ. If the Pockel's cell is "on" for $\sim$ 0.5ns, after 400 passes ($\sim$ 2μs) the pulse durations would be $\sim$ 25ps, according to this simple model.

It is interesting to consider the case when the roundtrip of the two lasers is slightly different. If the cavity mismatch is T, under

the above simplifying assumptions, the pulse intensity after two round-trips can be described as

$$I \alpha \{A \exp [t/\sigma]^2\} \times \{A \exp -[(t-T)/\sigma]^2\}$$

and therefore

$$I \alpha A^2\{\exp - (T^2/2\sigma^2)\} \times \{\exp -[(t-T/2)^2/(\sigma/2)^2]\}.$$

As can be seen the shape of the pulse is still a gaussian, and no further compression is obtained in this case than when the cavities are matched exactly, since the width σ is reduced to $\sigma/\sqrt{2}$ after two passes. However, the constant term (less than unity) $\exp -(T^2/2\sigma^2)$ representing the effect of the mismatch, reduces the amplitude of the light pulse. Analogous results are obtained for larger number of roundtrips, and therefore cavity mismatch should be avoided.*

Experimentally it was also found that the cavity matching was important, and when the mismatch was greater than $\pm$ 5mm the output was not 100% modulated and the pulse quality was poor even when examined on a oscilloscope. Best results were obtained when the cavities were matched better than $\pm$0.5 mm. This fine adjustment was not very difficult to make, since it corresponded, at the end of the train, to a temporal mismatch of $\sim$ 1.5ns.

The other mechanism which is likely to play an important role in the process is gain saturation. The end part of the picosecond light pulse does not experience as much population inversion in the amplifying medium as the front part, which significantly depletes the gain [15]. As a consequence the back of the pulse is less amplified than the front edge, and is cut because of cavity losses. This should "clean up" the pulses.

---

* It is shown in [23] that provided the transmission function assumes a value 0 for $t < 0$, the light pulse is shortened until laser action finishes prematurely due to mismatch.

The results obtained for a Coumarin 6 showed that using this active mode-locking technique, 100% modulated trains of pulses of ∿30-50ps can be readily produced. In order to generate shorter pulses, a weak solution of a saturable absorber incapable of mode-locking the laser alone could be introduced inside the cavity, in a hybrid arrangement. This should reduce not only the pulse durations, but also inter-pulse noise as well.

Although other methods may produce shorter pulses in dye lasers, this simple technique can be applied for the modulation of laser systems which would be difficult to mode-lock by an alternative scheme. The shortest and the longest wavelengths for which the technique can be used are defined by the transmission of the Pockel's cell and polarizer, and can range from VUV to the infrared (∿ 0.2μm to ∿ 1.3μm [9]).

The extension of these results to an important class of UV excimer systems, the rare gas halide lasers, is discussed in the following sections of this chapter.

7.3 Active Mode-locking of Excimer lasers

7.3.1 Introduction

Picosecond UV light pulses are useful in the study of several processes that happen in an ultrafast time scale, in the fields of biology, non-linear optics, spectroscopy, photochemistry and others [16-19]. The characterization of these UV ultrashort pulses can be directly carried out using streak-cameras. As discussed in the previous chapter, streak camera systems are capable of detecting pulses of wavelength in the VUV region of the spectrum and maintain picosecond resolution.

The simplest and most widely used technique to produce ultra-

short UV pulses is the harmonic generation of mode-locked lasers, such as Rhodamine 6G dye, ruby and neodymium. The constraints imposed by the relatively low conversion efficiencies at short wavelengths, the damage of components by very intense light pulses, and the limited wavelength choice restricts to a certain extent the use of harmonic generation to produce intense pulses at various frequencies. Raman, Brillouin and other frequency conversion mechanisms introduce additional complications and losses to the system [20]. On the other hand excimer lasers, and in particular the rare gas halide family, are convenient sources of intense UV light[21,22]. They can be scaled to provide very high optical energies at high repetition rates. Because of the high efficiency achieved, excimer lasers have been considered as a viable possibility for laser fusion [20]. Like the flashlamp pumped dye laser where several different dyes are used, covering a wide range of frequencies, different rare gas halide mixtures have also been demonstrate to lase. The wavelengths obtained range from $\sim$ 175nm for ArCl to $\sim$353nm for XeF, but other excimer lasers cover the range from 124nm (Ar_2) to 558nm(KrO) [21]. The prospect of generating UV picosecond pulses with excimer lasers is attractive, and has been recently the subject of several experiments. Due to the high gains exhibited by rare gas halide systems, a few amplification studies were carried out. Single subnanosecond laser pulses obtained by slicing 10ns duration pulses from a XeCl laser were used in double-pass amplification studies[25]. This technique could alsobe extended to other excimer systems. Picosecond pulses obtained by frequency doubling a mode-locked dye laser were amplified in XeCl, and high power UV pulses were obtained [23,24]. Nanosecond pulses were obtained by injecting the sliced output from a XeF laser into another XeF oscillator [26], which had its operation thus controlled. The generation of a 100% modulated train of pulses, with individual pulse durations of <7ps was achieved by injection mode-lockinga XeCl laser [27]. This technique, however, relied on the fact that the second harmonic radiation of Rhodamine 6G could be tuned to coincide with the 308nm transition of the XeCl laser. Therefore it is

difficult to use this approach for other excimer lasers, since the second harmonic radiation of passively mode-locked dye lasers covers a limited spectral range.

Conventional excimer lasers exhibit gain for a short time, typically $\sim$ 10-50ns [21] . This is the reason why, except in the case when picosecond pulses are fed into the cavity, a mode-locked train does not have time to develop fully. A previous attempt to actively mode-lock a XeF laser using an acousto-optic modulator [28] failed to produce laser pulses with modulation depths in excess of 70%, and individual pulse durations shorter than $\lesssim$ 2ns. Passive mode-locking techniques have also been only partially successful [28,29,30], with modulation depths of 85% and pulse durations of $\lesssim$ 2ns being measured.

The high gain of excimer amplifiers renders it possible to introduce lossy modulating elements in the laser cavity. However the conventional modulation technique relies on the continuous application of a sine wave to the active element leading to the generation of nanosecond pulses. In contrast, picosecond voltage pulses switched by a semiconductor device can be applied synchronously to the Pockel's cell, as discussed in the preceeding section. In this case trains of picosecond UV pulses should be generated. The feasibility of such an experiment would confirm that the use of semiconductor switches in conjunction with active modulating systems can be applied to different types of lasers at various wavelengths, extending the results obtained for the dye lasers to the UV part of the spectrum.

7.3.2 Experimental Set-up

7.3.2.1 The Lasers

A schematic diagram of the experimental set-up used can be seen in figure 7.6. The dye laser cavity was defined by mirrors M1 (R≈100%) and M2 (R≈50%). The gain medium consisted of a 4.1mm i.d. and 7.8mm o.d. quartz cylinder, through which a 1.5×10^{-4}M water solution of Rhodamine 6G flowed. The dye cylinder was placed at the common focus of a double elliptical cavity head [13],

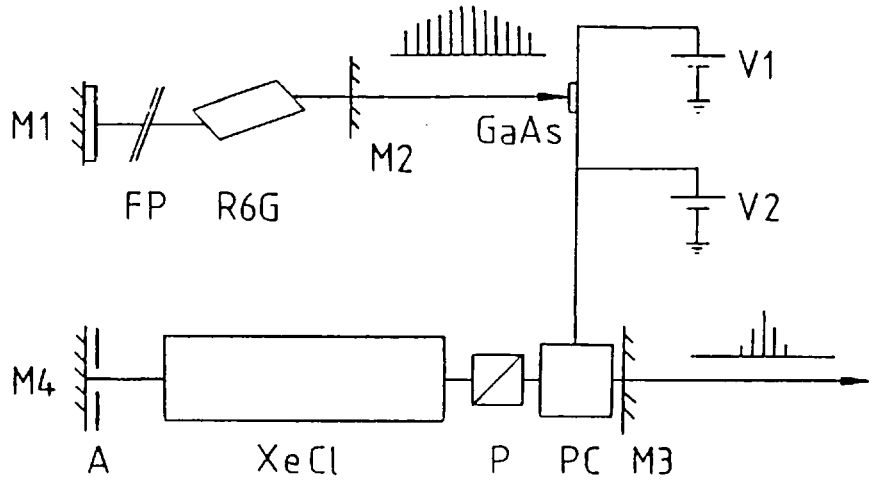

FIG 7.6 Experimental set-up

and two Xe flashlamps were placed at the other foci. The electrical energy that activated the flaslamps was typically ∿100J. The dye laser was passively mode-locked by an ethanolic solution of DODCI (∿10^{-5}M) contained in a 2mm thick cell in contact with mirror M1. A 5um Fabry-Perot (FP) allowed tuning of the laser, which was operated at ∿ 605nm. The roundtrip of the cavity was ∿ 8.3ns, or more usually ∿4.2ns. Typically the mode-locked trains had ∿ 400 pulses, lasted for ∿ 1.5μs and contained ∿ 10mJ of optical energy. The duration of the pulses used to activate the semiconductor switch was ∿ 5ps [13].

The XeCl laser cavity was defined by mirrors M4 (R ≈ 100%) and the output coupler M3 (R ≈ 40% or 80%). The roundtrip time was 8.3ns and the laser wavelength 308nm. Gain was provided by a UV preionized electric discharge produced between two 79cm long electrodes, separated by 2.3cm. The gain medium consisted of a mixture of Ne, Xe and HCl, typically in a proportion 300:15:1, at a total gas pressure in the range ∿ 1000-2000 torr. The charging voltage for the laser was adjusted between 20-30KV and the maximum output energy previously obtained with this system was 70mJ. (A detailed description of the construction and performance of the XeCl laser can be found in [31]).

The active modulation elements used were a Glan-Thompson polarizer (P) and a Pockel's cell (PC). Unlike the set-up described in section 7.2.1, the polarizer was introduced between the Pockel's cell and the XeCl amplifier. The Pockel's cell was again placed very near to the output coupler, and an aperture (A) of $\sim$ 1cm diameter was introduced in the cavity to reduce undesired feedback.

7.3.2.2 The Switch

Since the energy of the laser pulses available to activate the switching device was not very high ($\sim$ 20μJ per pulse), fairly sensitive switches had to be used. The semiconductor devices had to exhibit fast recombination time, high dark impedance, high carrier mobility and should also have a band gap of less than 2eV for efficient activation by the dye laser. The semiconductor chosen was semi-insulating Cr-doped GaAs.

The high dark impedance of S.I. GaAs allowed d.c. bias to be applied to the switch. By keeping the electric field across the gap $\lesssim$ 3KV cm^{-1}, the conduction electrons had high mobility, and also electrical breakdown problems were avoided. However, the contacts were prepared by simply depositing a layer of conductive paint (JMC 1402) on the semiconductor slab, and therefore were non-ohmic and exhibited a finite series impedance. The procedure was clearly far from ideal, but allowed the replacement of the semiconductor chip in case of electrical breakdown in few minutes.

Different gap lengths and bias voltages were used. Typically, the distance between the electrodes was $\sim$ 2mm, and the d.c. voltage drop across the device was $\sim$ 700V. Again the switch bias was the difference between the voltages V1 and V2.

The maximum amplitude of the voltage pulses switched in the experimental conditions described was obtained for a ∿ 2.5mm gap device biased to 1KV. Pulses of ∿ 350V were then detected. More typically, for 700V d.c. bias, trains of voltage pulses of ∿ 200V peak amplitude were measured on a 7834 Tektronix storage oscilloscope, where a maximum amplitude of 350V could have been obtained. However, the overall risetime of the oscilloscope and attenuators was 0.7ns and the ultra-short duration voltage pulses were integrated by the detection system. From the model developed in section 4.4.1, assuming a recombination time of ∿ 100ps, it is found that with the illumination of the gap the impedance of the switch was reduced to ∿ 1Ω.

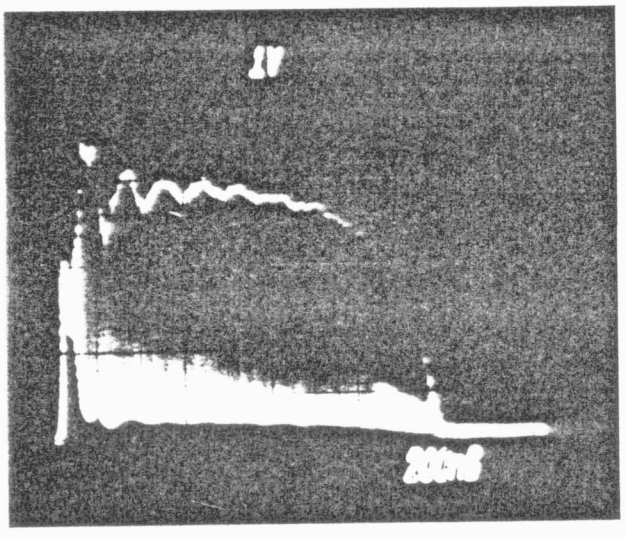

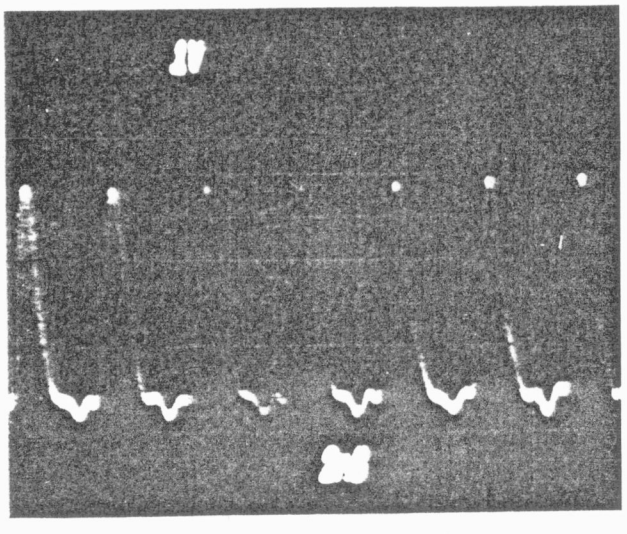

FIG 7.7 Voltage switched by GaAs device (30 times attenuated)

Figure 7.7a is an oscillogram of the train of voltage pulses (electrical attenuation ∿ 30) switched by a GaAs device biased to 700V, when activated by a mode-locked dye laser train. The oscillatory modulation observed on the envelope of the pulse train was mainly due to noise pick-up at the high voltage attenuators. On figure 7.7b the voltage pulses can be seen on an expanded

time scale.

The output from the switch was electrically connected to the Pockel's cell, which was originally not impedance matched. In spite of the 50Ω termination provided, reflections and ringing were still observed. They were mainly due to mismatch at the electrode connections and the finite capacitance of the Pockel's cell, and also due to the introduction of a further coaxial line necessary for the d.c. bias (V2 in figure 7.6). The effect of reflections is further examined in section 7.3.5.

7.3.2.3 Synchronization of the lasers.

Reliable synchronization of the two lasers had been previously achieved for the injection mode-locking experiment [23, 27]. Therefore it was not changed for the active modulation studies. Light from the flashlamps was fibre-optically coupled into a vacuum photodiode, which triggered a delay-amplifier unit (TRW 46A). A ∿ 500V pulse was then delivered to activate the XeCl laser thyratron, with a total jitter of $\lesssim$ 100ns. The long duration of the dye laser train ensured not only synchronization, but also that the excimer laser was always triggered within the same region of the dye laser train of pulses. As a consequence, the picosecond pulses used to activate the GaAs switch were reproducible in amplitude and duration, from laser shot to laser shot.

7.3.3 The Active Modulation Technique

The modulating system differed slightly from the one described in section 7.2.3, and its operation was as follows.

Initially lasing was inhibited by the application of a d.c.

voltage $V_{\lambda/4}$ to the Pockel's cell. Linearly polarized light flux entered the Pockel's cell, and reached the mirror M3 circularly polarized. The part reflected back, after passing through the Pockel's cell, had its linear polarization restored, but rotated by a total of 90^{o}. It was therefore rejected by the polarizer before re-entering the XeCl amplifier. In this case no feed back was allowed, and lasing did not take place.

When, however, a short duration voltage pulse was added to the d.c. voltage $V_{\lambda/4}$, the polarization of light travelling twice through the Pockel's cell was rotated by a total of more than 90^{o}. A short burst of light which was no longer linearly polarized then reached the polarizer. One component of the short burst was rejected, but some light was transmitted and fed-back into the amplifier, allowing laser action to develop. The arrival of the burst of light at the Pockel's cell after a roundtrip in the laser, was synchronized to the application of a subsequent short duration voltage pulse. Therefore further amplification ocurred, and mode-locking started to build-up. The synchronization was achieved by adjusting the dye laser pulse separation to be equal to or half of the roundtrip of the XeCl laser.

This modulating technique has a few advantages over the one previously described (c.f. section 7.2.2), such as: (1) The amplitude of the voltage pulse needed for maximum transmission is in this case half of that needed in the other system. (2) The Pockel's cell can be placed much nearer to the output coupler than in the previous arrangement. (3) The introduction of the polarizer between the Pockel's cell and the output coupler defined in the other case a minimum roundtrip time during which the voltage pulse should be applied to the Pockel's cell. This roundtrip time was equal to the double transit time of light through the polarizer-Pockel's cell arrangement, which was $\sim$ 350ps. In

the present configuration such minimum allowed duration for the voltage pulse does not exist. (4) The arrangement described here can be used in conjunction with non-polarized lasers, whereas in the former case Brewster angled windows were required.

7.3.4 Operation and Results

The alignment of the system was found to be important for 100% modulation to occur. The Pockel's cell was considered aligned when total extinction of a He-Ne laser beam undergoing two passes through the modulating elements was observed (for a d.c. bias V2 ≃ 2KV). This procedure was adopted for its convenience, in spite of the fact that the UV light experienced a slightly different refractive index than the 633nm radiation, when travelling inside the KDP crystal [32].

Care was taken to prevent front and back reflections from the polarizer, Pockel's cell and of both XeCl amplifier windows from giving rise to undesired feedback.

When no voltage was applied to the Pockel's cell, the XeCl laser generated unmodulated 308nm wavelength light pulses. The typical laser pulse duration was ∿ 20-35ns, as seen in figure 7.8a. Due to the severe losses introduced by the intracavity optical elements (P, PC and A), the optical pulse energy available was only a small fraction of the energy output without the active modulation system.

Typically a relatively low d.c. bias of ∿ 650V was found adequate to prevent laser action from taking place. When the voltage pulses switched by the GaAs device were applied to the Pockel's cell and added to the d.c. bias V2 100% modulated trains of pulses were

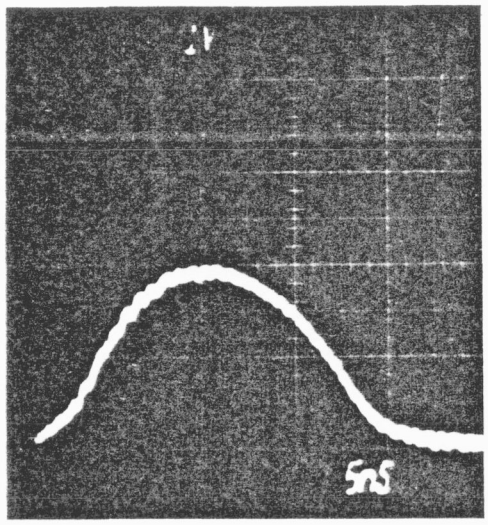

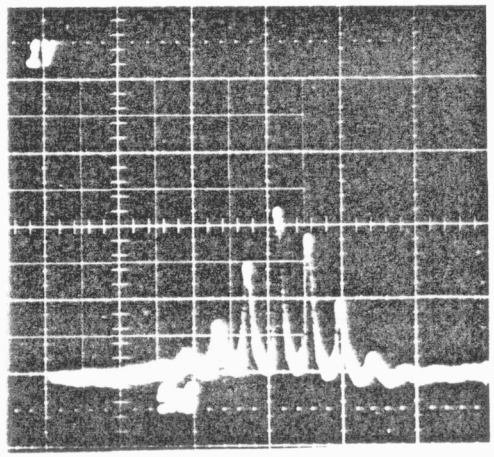

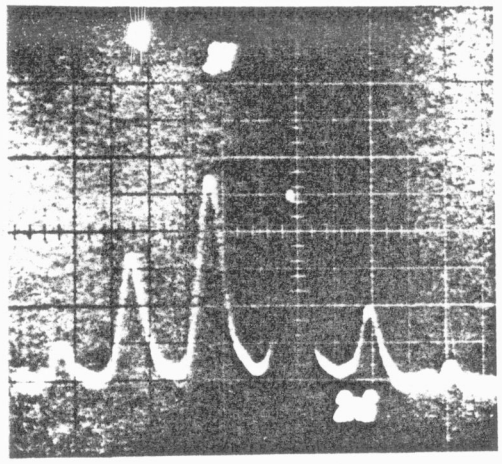

FIG 7.8
a) Oscillogram of unmodulated XeCl laser output
b) Oscilloscope trace of mode-locked XeCl laser train
c) Expanded time scale

obtained, as seen in the oscillogram of figure 7.8b. The trains usually consisted of ∿ 5-7 pulses and lasted for ∿ 20-30ns. However, fully modulated trains of up to 10 pulses were sometimes observed. When the roundtrip of the dye laser was ∿ 8ns (equal to that of the XeCl system) 100% modulation was still observed, but because the dye laser tended to double-pulse and had to be crytically operated just above threshold, the shorter cavity length was prefered.

Figure 7.8c shows the individual UV pulses in an expanded time-scale (2ns/division), and the pulsewidths seen are limited by the photodiode-oscilloscope used for monitoring.

In order to determine the actual pulse durations, and also to study the evolution of the pulses within the train, a UV sensitive Photochron II streak-camera was employed. Slow sweeping speeds were used (∿ 1.4×10^8 cms^{-1}), allowing the direct observation of series of pulses and the background (if any) contained between them. Furthermore, jitter was much less

severe, and calibration for the sweep was automatically provided by the separation between consecutive pulses of the train.

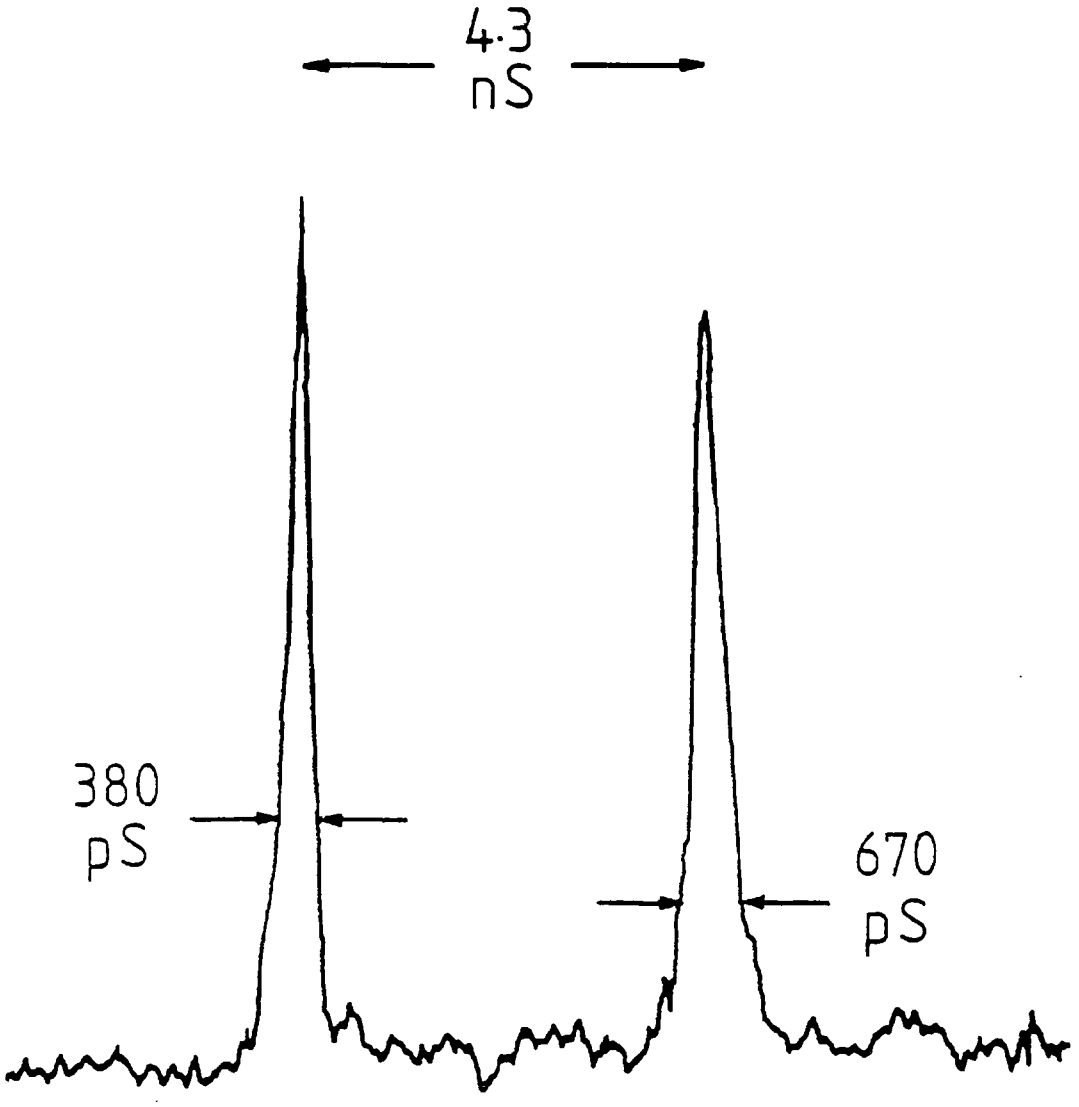

FIG 7.9 Microdensitometer trace of streak record of two consecutive pulses.

Figure 7.9 is a microdensitometer trace of a pair of pulses of the XeCl laser train, again showing 100% modulation. In this case the dye laser pulse separation was 4.3ns and the modulator opened twice per roundtrip of the excimer system. Consequently, the XeCl laser is double-pulsing, and the streaks seen correspond to different initial bursts of light. The recorded width of the pulse shown on the left is 380ps (FWHM). Assuming a dynamic spatial resolution of $\sim$ 10 lp/mm, and since the writing speed was 1 x $10^8 cms^{-1}$, the time resolution of the streak

camera was ∿ 100ps for this particular streak record. Deconvolving this value, a real pulse duration of ∿ 360ps is obtained.

A subpulse ∿ 400ps away from the main peak was observed in some cases, which could be due to undesired subcavities formed by the optical elements (P and PC) and laser windows, to mismatch between the cavities of the two lasers, or more likely due to ringing and voltage pulse reflections at the Pockel's cell.

7.3.5 Discussion

The duration of the light pulses obtained by active modulation of the XeCl laser is almost two orders of magnitude longer than those obtained by injection mode-locking. This long pulse duration implies that the phase-locking between the longitudinal modes is far from complete. Therefore the expression "mode-locked laser" is in this case, at best a rough approximation, and should only be used as such. However, it is also clear that the active modulation of rare-gas halide lasers using semiconductor switches allows the generation of 100% modulated trains of pulses of subnanosecond duration. So far this result has not been matched by other conventional active or passive modulation techniques.

In order to optimize the system and to evaluate the importance of parameters such as the number of roundtrips and the effect of ringing, a computer simulation of the experiment was carried out. As in chapter 4, the dye laser pulses were assumed to have negligible duration, the switch to exhibit prompt response (i.e., negligible risetime), and the number of free carriers was considered to decay exponentially with a (single) time constant τ = 100ps. Furthermore, because the XeCl

laser gain varied slowly compared to the opening time of the active modulator, the evolution of the gain of the excimer laser was assumed not to alter the width or shape of the individual pulses. Therefore the gain of the XeCl laser was described by a constant coefficient which, in order to make the pulse evolution more apparent from the graphs, normalized the amplitude of the pulse from roundtrip to roundtrip. Also, it was implicitely assumed that the XeCl laser did not exhibit gain saturation.

As discussed in chapter 4, the total conductance of the switch following the activation can be represented by:

$$G(t) = G_o e^{-t/\tau}$$

and its impedance is given by

$$Z(t) = Z_o e^{t/\tau}$$

where Z_o is the impedance immediatly after the activation, and τ = 100ps. The current switched is

$$i_{sw}(t) = \frac{V_{app}}{100+Z_o e^{t/\tau}} \quad (1)$$

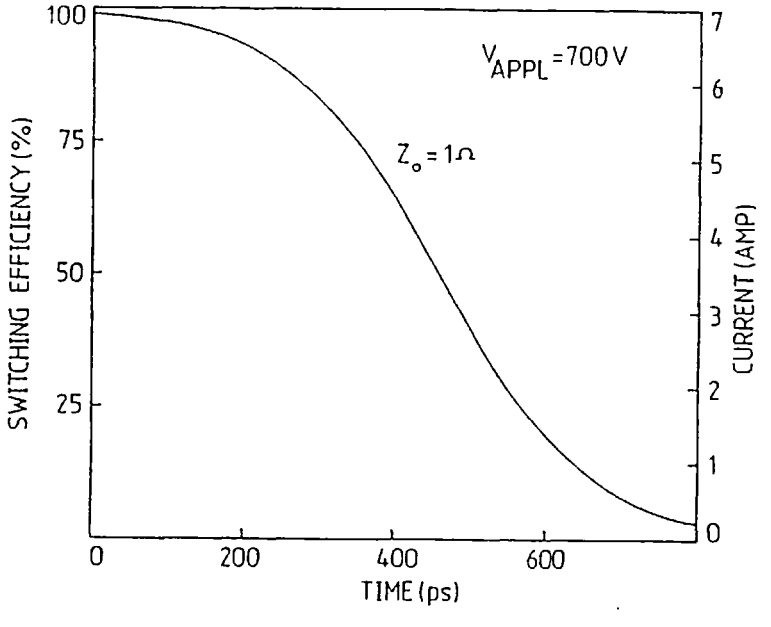

FIG 7.10 Current switched by GaAs device

A plot of $i_{sw}(t)$ can be seen in figure 7.10 for Z_o = 1Ω. Assuming that the two additional coaxial cables connected in parallel (leading to V2 and to the 50Ω termination) correspond to an impedance of 25Ω, it is possible to calculate the voltage

developed across the Pockel's cell as a function of time. Let i_r and i_t be the currents reflected and transmitted when the pulse of current

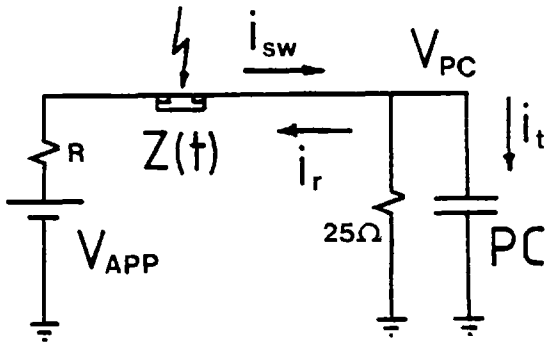

FIG 7.11

i_{sw} reaches the association in parallel of the cables and the Pockel's cell (c.f. figure 7.11). Conservation of energy and of charge can be expressed as

$$i_{sw}^2 \times 50\Omega = i_t \times V_{PC} + i_r^2 \times 50\Omega$$

$$i_{sw} = i_r + i_t$$

Solving for i_t one finds

$$i_t = 2i_{sw} - V_{PC}/50 \qquad (2)$$

The current i_t transmitted into the association of the Pockel's cell and the 25Ω load is divided, one part charging the Pockel's cell (i_{PC}) and the other the cables ($i = V_{PC}/25\Omega$).

From (2)

$$i_{PC} = (2i_{sw} - V_{PC}/50) - V_{PC}/25 \ .$$

The current flowing into a capacitor can be related to the voltage by

$$i = C dV/dt,$$

and therefore, from (1)

$$\frac{C dV_{PC}}{dt} = \frac{2 \times V_{app}}{100 + Z_o e^{t/\tau}} - \frac{3V_{PC}}{50} \ . \qquad (3)$$

This equation can be solved numerically, yielding the evolution of the voltage appearing at the Pockel's cell V_{PC} as a function of time. (V_{PC} is later added to the d.c. bias V2). Figure 7.12a shows a plot of V_{PC}, and it is apparent that due to saturation of the switch, the voltage pulse lasts for 0.5ns (FWHM), although the recombination time of the

carriers in the semiconductor is assumed to be only 100ps. The derivative of the voltage applied at t=0 is greater than zero because stray inductance was neglected, the Pockel's cell was assumed to be a perfect capacitor, and dispersion effects in the cable were not taken into account.

The build-up of a mode-locked train of pulses becomes apparent when the transmission of the active modulator is calculated, taking into account the voltage developed across the Pockel's cell. Provided the mirror M3 is sufficiently close to the crystal, the time taken for the burst of light to travel from the cell to the mirror and back again into the cell can be neglected. In this case the effect of the voltage on the Pockel's cell is to introduce a phase difference between the ordinary and extraordinary rays which is proportional to the voltage applied.

It can be shown that the relation between the intensities of the light pulse entering and leaving the modulator is then given by

$$I_{out} = I_{in} \sin^2\left(\frac{\pi V_{PC}}{V_{\lambda/2}}\right), \qquad (4)$$

where the detector is assumed to be incapable of resolving signal variations at optical frequencies. When $V_{PC} = V_{\lambda/4}$, the transmission of the modulator is maximum, and when V_{PC} is zero, all the light is rejected by the polarizer and feedback into the amplifier is not allowed.

A computer program was written to calculate the evolution of V_{PC} from equation (3), and then to simulate the intensity profile of the light pulses from equation (4) [23]. Passive losses at the elements were described by a constant coefficient of value 10^{-1}, and a laser gain of

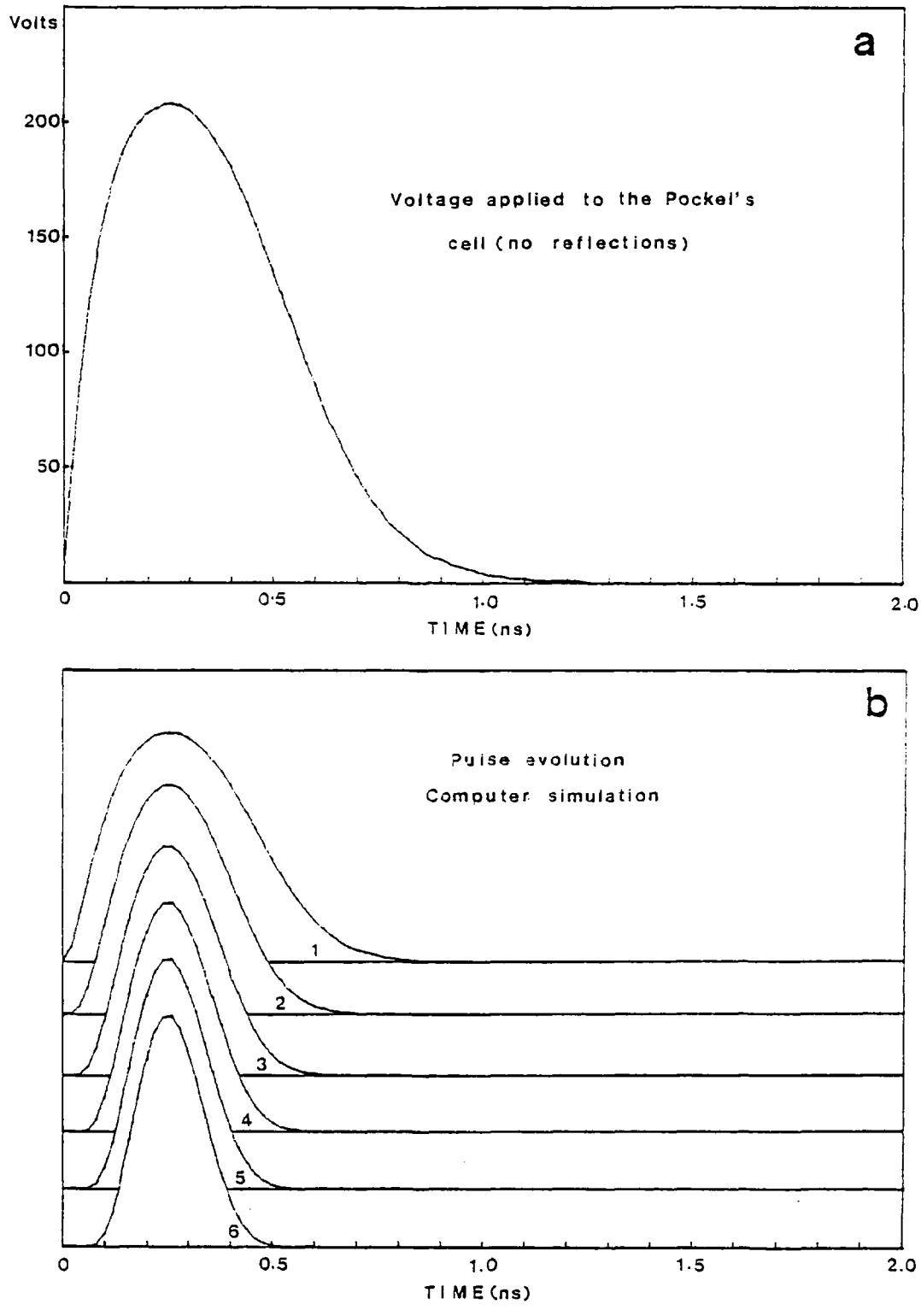

FIG 4.12 (a) Time evolution of voltage pulse applied across the Pockel's cell (b) Light pulse evolution showing shortening from ∿ 400ps to ∿ 170ps (FWHM).

$\sim$ 50 was found necessary to normalize to unity the peak amplitude of the light pulse.

A plot of the results can be seen on figure 7.12b, where the initial flux was assumed to be constant inside the cavity. After one roundtrip a short burst of light is formed, and its shape resembles that of the voltage pulse applied to the Pockel's cell. The pulse assymmetry which can be seen for low number of passes was observed experimentally in several streak records, which showed a pulse leading edge faster than the trailing edge. As the process evolves, the pulsewidth becomes shorter and its shape more symmetrical. Although it is clear from figure 7.12b that a large number of passes is desirable for the generation of shorter pulses, it is also apparent that the pulse compression becomes less significant after the first few roundtrips.

According to the results from the computer simulation, pulsewidths somewhat shorter than those measured experimentally should have been obtained($\sim$ 170ps instead of $\sim$ 360ps). Although the impedance mismatch at the Pockel's cell was taken into account, dispersion in the coaxial line, stray inductance at the electrode connections, and ringing and reflections were so far neglected. However, as mentioned in section 7.3.2.2, from oscilloscope measurements it had been established that the voltage appearing across the Pockel's cell exhibited more than one peak. The program was then modified to investigate the effect of ringing and voltage pulse reflections on the XeCl laser output, and to examine if they could be responsible for the longer pulsewidths measured and the subpulses observed. The simulated voltage appearing across the Pockel's cell was changed to that shown in figure 7.13a. This signal was obtained by adding to V_{PC} a reduced replica of the main voltage pulse (delayed by 400ps and divided by a factor of two), followed by another subpulse

which was the reflection of the reflection, and so on.

Figure 7.13b shows the evolution of the corresponding laser pulse output, and although the effect of ringing and reflections is significant for the first roundtrips, a single laser pulse is seen to develop relatively quickly. This result once more indicates that a longer laser gain duration (allowing a large number of roundtrips) is desirable, and suggests that subpulses can be observed, particularly in early stages of the pulse development. An improved version of the computer simulation can be written, taking into account the finite distance between the Pockel's cell and output coupler, to examine its role in the formation of subpulses.

The results obtained with the present computer program indicate that it would be advantageous to use e-beam sustained discharge excimer lasers, which are capable of lasing for hundreds of nanoseconds [21] and would allow $\sim$ 10 times more passes through the modulator. The use of a second Pockel's cell intracavity, activated by the same GaAs device should also lead to shorter pulse durations.

In order to increase the output energy of the system, passive losses must be reduced. This can be relatively easily accomplished, since the diameter of the Pockel's cell (1cm) wasted a significant part of the lasing area, its windows had a short wavelength cut-off at 0.3μm (nearly equal to the laser wavelength), and the thickness of the crystal (2.5 cm) was much larger than that of other commercially available cells (0.7 cm [33]).

Finally, if gain saturation can be achieved in a hybrid arrangement, further pulse shortening will occur. However, for the particular system employed, powers $\sim$700MWcm^{-2} [34] are needed, and this value is orders of magnitude

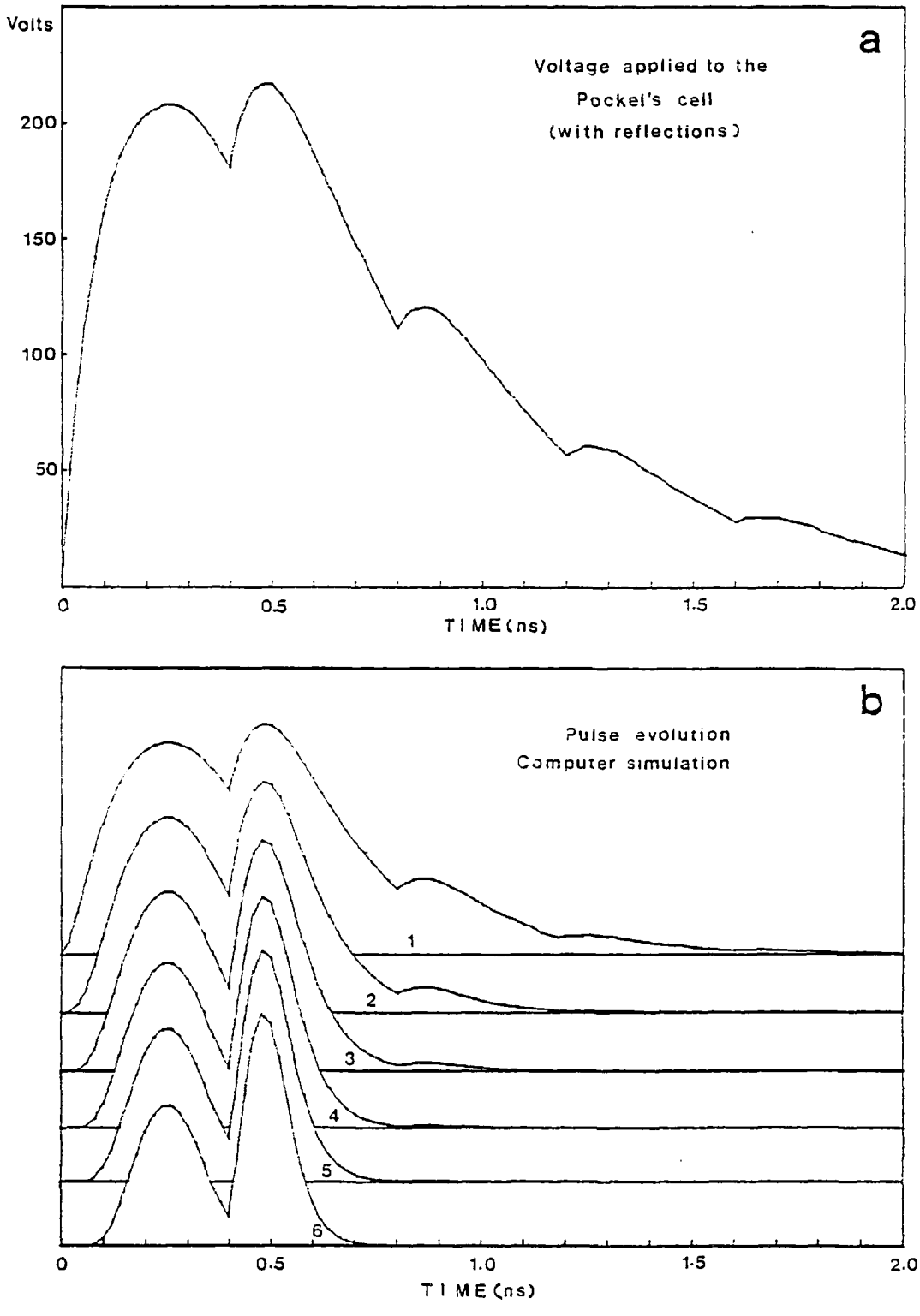

FIG 4.13 (a) Voltage applied across the Pockel's cell, taking into account reflections and ringing (b) Resulting light pulse evolution.

higher than the power densities that were available. The use of lens to reduce the beam area can help to establish those levels.

7.4 Conclusion

Semiconductor switching devices were used in conjunction with active modulators, producing 100% modulation depths and subnanosecond opening time of the loss elements. Mode-locked pulse trains at several different wavelengths were systematically obtained with a dye laser and light pulses as short as $\sim$ 30ps were recorded. When the mode-locking technique was applied to a much shorter excitation electric discharge excimer laser operating at the UV part of the spectrum, 100% modulation was still obtained, and pulses as short as 360ps were measured. The extension of these results to other dye or rare-gas halide laser systems should be straightforward. This mode-locking technique requires two synchronized lasers, one mode-locked to activate the switch, the other being the actively mode-locked one, but allows the simultaneous generation of picosecond pulses at two different wavelengths, which can be used in excite-and-probe experiments.

The results obtained also confirm the capability of ultrafast switching with III-V semiconductors, and their use to activate fast Pockel's cells. Voltage trains of kilovolts amplitude were switched in one case, and hundreds of volts in the other. The high resistivity of the switches enabled the use of d.c. bias, and their fast recovery time allowed the generation of trains of ultrashort duration voltage pulses. Picosecond synchronization existed between the voltage switched and the arrival of the mode-locked light pulse at the device. This synchronization played a vital role in the mechanism leading to build-up of a train of picosecond light pulses from the actively modulated laser.

References - Chapter 7

[1] D.J. Bradley; in Topics in Applied Physics Vol 18 ed. S.L. Shapiro (Springer Verlag 1977)

[2] C.M. Ferrar; IEEE J. Quantum Elect. QE5, 550 (1969).

[3] E. Lill, S. Schneider, F. Dörr; Optics Commun. 22, 107 (1977)

[4] E. Lill, S. Schneider, F. Dörr, S.F. Bryant, J.R.Taylor; Optics Commun. 23, 318 (1977)

[5] P. Ewart; Optics Commun. 28, 379 (1979)

[6] J. Jansy, J. Jethwa, F.P. Shäfer; Optics Commun 27, 426 (1978)

[7] J.C. Mialocq, P. Goujon; Appl. Phys. Lett. 33, 819 (1978)

[8] K. Sala, M.C. Richardson, N.C. Isenor; IEEE J. Quantum Elect. QE13, 915 (1977)

[9] Electro-Optic Developments, Technical Bulletin

[10] R. Wallenstein, in Laser Handbook vol.3, ed. M.L. Stitch (North-Holland 1979)

[11] E.G. Arthurs, D.J. Bradley, A.G. Roddie; Appl. Phys. Lett. 19, 480 (1971)

[12] E.G. Arthurs, D.J. Bradley, A.G. Roddie; Appl. Phys. Lett. 20, 125 (1972)

[13] J.R. Taylor; PhD Thesis, The Queen's Univ. of Belfast (1974)

[14] D.J. Bradley, B. Liddy, W. Sibbett, W.E. Sleat; Appl. Phys. Lett., 20, 219 (1972)

[15] G.H.C. New; IEEE, J. Quantum Elect. QE10, 115 (1974)

[16] D.J. Bradley; in Lasers in Physical Chemistry and Biology, ed. Jussot Dubrieh, Elsevier Publishing Co.,Amsterdam, 1976, p.7.

[17] W.K. Bischel,J. Bokor, D.J. Kliger, C.K. Rhodes; IEEE J Quantum Elect. QE15, 380 (1979)

[18] J. Reintjes; IEEE J. Quantum Elect. QE15, 33D (1979)

[19] See for instance Picosecond Phenomena II, Chemical Physics 14 Ed. by R.M. Hochstrasser, W. Kaiser, C.V. Shank (Springer Verlag 1980)

[20] J.R. Murray, J. Goldhar, D. Eimerl, A. Szöke; IEEE J. Quantum Elect. QE15, 342 (1979)

[21] J.J. Ewing; in Laser Handbook Vol.3, ed. M.L. Stitch (North-Holland 1979)

[22] M.H.R. Hutchinson; Appl. Phys. 21. 95 (1980)

[23] G. Reksten; PhD. Thesis, University of London (1981)

[24] M. Maeda, T. Mizunami, A. Sato, O. Uchino, Y. Miyaza; Appl. Phys. Lett. 36, 636 (1980)

[25] T.J. Pacala, J.B. Landenslager; Appl. Phys. Lett 37, 366 (1980)

[26] T.J. Pacala, C.P. Christensen, Appl. Phys. Lett 36, 620 (1980)

[27] G. Reksten, T. Varghese, D.J. Bradley; Appl. Phys. Lett. 38 513 (1981)

[28] C.P. Christensen, L.W. Brawerman, W.H. Steiner, C. Wittig; Appl. Phys. Lett 29, 424 (1976)

[29] T. Efthimiopoulos, J. Banic, B.P. Stoicheff; Can. J. Phys 57, 1437 (1979)

[30] J. Banic, T. Efthioiopoulos, B.P. Stoicheff; Appl. Phys. Lett 37, 686 (1980)

[31] Thomas Varghese; PhD Thesis, University of London 1981

[32] F. Zernike, Jr.; J. Opt. Soc. of America 54, 1215 (1964)

[33] J. Agostinelli, G. Mourou, C.W. Gabel; Appl. Phys. Lett 35, 731 (1979)

[34] M. Rokni, J.A. Mangano, J.H. Jacob, J.C. Hsia; IEEE J. Quantum Elect. QE14, 464 (1978)

CHAPTER 8

GENERAL CONCLUSION

From the studies carried out with picosecond semiconductor switches it is clear that they represent a very useful family of opto-electronic devices. It was shown that significant improvement over the performance of conventional systems can be obtained in terms of speed, high voltage capability and picosecond synchronization of the switching action to the illumination of the device (i.e.,to the light pulses).

Because of the diversified applications that such switches find, and due to the interest in ultrafast techniques motivated by the rapidly developing fields of laser communication and ultrahigh speed electronics, it is expected that further studies will be carried out and that such devices will become commercially available in a near future. It is likely that the microstrip transmission line structure will be employed, where an insulator is used as substrate and a thin semiconductor specimen is placed on the top surface, ensuring high voltage capability and large bandwidths.

In order to obtain higher switching efficiencies, and to further exploit the single and multiphoton photoconductivity processes discussed in chapter 4, other semiconductor materials should be investigated. For the applications described, higher carrier mobility and dark resistivity are desired. A semiconductor device capable of switching high voltages with low levels of light illumination and able to withstand d.c.bias at room temperature will clearly be extremely useful. The search for materials with such properties now seems to be geared towards the development of ternary and quaternary semiconductor compounds.

The high speed of the switching is ensured by the extremely fast creation of electron-hole pairs. It was mentioned earlier that if the electric field across the gap is sufficiently intense, the carriers accelerated can gain enough kinetic energy to produce secondary electron-hole pairs when colliding with electrons in the valence band. The avalanche gain which results has so far not been reported for semiconductor switches, but is a well known process on which many fast photodiodes and transistors are based. Preliminary evidence exists that avalanche multiplication might take place in nearly intrinsic Si devices at liquid nitrogen temperatures [1], where the mean free path of the electrons increases by many orders of magnitude due to the low levels of phonons in the lattice. The number of free electrons produced in the avalanche mode is a statistical quantity, and is certainly more difficult to control than when the promotion to the conduction band depends entirely on the number of photons illuminating the gap. Therefore it is likely that the synchronization between the switching action and the activation of the gap will be somewhat poorer in this case than when the light pulse fully saturates the device. However, since a low number of photons is potentially capable of generating high voltages with ultrafast risetime, the prospect of achieving avalanche gain is exciting, and certainly deserves to be studied in detail [2].

The capability of semiconductor switches to synchronize streak camera systems with picosecond precision was demonstrated in the case when relatively intense light pulses were used to illuminate the gap. As discussed earlier, section 5.8, further improvements would include the use of a d.c. biased semiconductor activated by lower optical powers, and in this case high resistivity and good carrier mobility are of particular importance.

It should be pointed out that since pulses of several kilovolts amplitude can be switched with picosecond risetime, solid-state switching devices are capable of producing voltage ramps leading to much faster writing speeds in streak cameras, provided the bandwidth of the deflection circuit can be improved. As an example, assuming that the risetime of the voltage ramp switched is $\sim$ 10ps, degrading to $\sim$ 100ps as it is applied to the deflection circuitry, and assuming that the dynamic spatial resolution of the streak tube is improved to $\sim$ 20 l.p./mm, the time taken to seep one resolution element on the phosphor screen would be $\sim$ 50fs. The photoelectron time dispersion is likely to be greater than this value for some time yet, and consequently will set the lower limit for the time resolution of the camera. Therefore, it can be said that semiconductor switches are compatible with the subpicosecond streak cameras which are being developed.

As discussed in chapter 2, framing cameras operate essentially in the same way as streak tubes, and semiconductor switching devices should be also employed to both synchronize and to ensure picosecond time resolution in the framing mode. It is relatively easy to envisage a system where a d.c.biased semi-insulating GaAs or GaP switch provides voltage pulses which are applied to the deflection and to the compensating plates, generating photographs with $\lesssim$ 10ps exposure times. Furthermore, an adequate signal can be provided to the third pair of plates, so that the voltage developed has a staircase shape and the tube is fully exploited in its multiple framing capability.

Although microwave signals have been switched with semiconductor devices [3, 4] and phase-shifting systems have been reported [5, 6], the number of applications demonstrated in conjunction with electronic circuits has so far been limited. It is expected that the activation of Gunn diodes with solid-state switches will yield a precisely controlled

high frequency generator which can be used for example in counters and modulators. Sampling circuits which have been constructed for single shot lasers with crystalling Si devices [7] should be replaced by the much more convenient and efficient sampling systems with amorphous Si switches. These devices will certainly be also employed in the detection of CW mode-locked lasers and will very likely replace the photodiodes currently in use. In spite of its importance, the use of semiconductor switching devices to activate fibre-optics light switches has so far not been demonstrated. Such application would be particularly significant because it would allow further integration of picosecond solid-state switching devices in light transmission and detection systems.

Further development of materials should lead to the extension of the techniques demonstrated for the visible and 1.06μm to the UV and NIR mode-locked lasers. These studies are especially important because of the quickly developing methods of generation of picosecond pulses in the UV, such as that described in chapter 7, and the current interest in semiconductor and colour centre IR mode-locked lasers, useful for the studies of fibres and optical processes relevant in the laser communication field.

Since the use of semiconductor switches enables one to subject materals to high electric fields in times comparable to the propagation time of photons in the media, it should be possible to investigate non-linear phenomena such as the Pockel's effect as it develops in crystals. This once more illustrates how solid-state switches can directly assist in studies of the interaction of electromagnetic waves with matter which take place in a ultrashort time-scale.

To conclude, it can be said that for virtually innaugurating the field of picosecond electronics and creating so many possibilities

of fundamental research, picosecond semiconductor switches constitute one of the most relevant family of devices which follow the invention of the laser, and open up many exciting possibilities for the future.

References - Chapter 8

[1] G. Mourou, W. Knox, M. Stavola; in Picosecond Phenomena II, Chemical Physics 14, ed. by R.M. Hochstrasser, W. Kaiser, C.V. Shank-Springer-Verlag, Berlin (1980) p.75

[2] R.A. Kiehl; IEEE Trans. Elect. Devices ED25, 1250 (1978)

[3] A.M. Johnson, D.H. Auston; IEEE J. Quantum Electr. QE11, 283 (1975)

[4] G. Mourou, C.V. Stancampiano, D. Blumenthal; Appl. Phys. Lett 38, 470 (1981)

[5] Chi H. Lee, P.S. Mak, A.P. DeFonzo; IEEE J. Quantum Elect. QE16, 277 (1980)

[6] A.G. Foyt, F.J. Leonberger, R.C. Williamson - to be published (1981)

[7] A.J. Low; PhD Thesis, Cambridge University (1978)